

U.S. Department of Commerce
National Bureau of Standards
Gaithersburg, MD 20899



TECHNICAL NOTE

451

Radiochemical Analysis Section:

Summary of Activities
July 1967 to June 1968



U.S. DEPARTMENT OF COMMERCE
National Bureau of Standards

NATIONAL BUREAU OF STANDARDS

The National Bureau of Standards¹ was established by an act of Congress March 3, 1901. Today, in addition to serving as the Nation's central measurement laboratory, the Bureau is a principal focal point in the Federal Government for assuring maximum application of the physical and engineering sciences to the advancement of technology in industry and commerce. To this end the Bureau conducts research and provides central national services in three broad program areas and provides central national services in a fourth. These are: (1) basic measurements and standards, (2) materials measurements and standards, (3) technological measurements and standards, and (4) transfer of technology.

The Bureau comprises the Institute for Basic Standards, the Institute for Materials Research, the Institute for Applied Technology, and the Center for Radiation Research.

THE INSTITUTE FOR BASIC STANDARDS provides the central basis within the United States of a complete and consistent system of physical measurement, coordinates that system with the measurement systems of other nations, and furnishes essential services leading to accurate and uniform physical measurements throughout the Nation's scientific community, industry, and commerce. The Institute consists of an Office of Standard Reference Data and a group of divisions organized by the following areas of science and engineering:

Applied Mathematics—Electricity—Metrology—Mechanics—Heat—Atomic Physics—Cryogenics²—Radio Physics²—Radio Engineering²—Astrophysics²—Time and Frequency.²

THE INSTITUTE FOR MATERIALS RESEARCH conducts materials research leading to methods, standards of measurement, and data needed by industry, commerce, educational institutions, and government. The Institute also provides advisory and research services to other government agencies. The Institute consists of an Office of Standard Reference Materials and a group of divisions organized by the following areas of materials research:

Analytical Chemistry—Polymers—Metallurgy—Inorganic Materials—Physical Chemistry.

THE INSTITUTE FOR APPLIED TECHNOLOGY provides for the creation of appropriate opportunities for the use and application of technology within the Federal Government and within the civilian sector of American industry. The primary functions of the Institute may be broadly classified as programs relating to technological measurements and standards and techniques for the transfer of technology. The Institute consists of a Clearinghouse for Scientific and Technical Information,³ a Center for Computer Sciences and Technology, and a group of technical divisions and offices organized by the following fields of technology:

Building Research—Electronic Instrumentation—Technical Analysis—Product Evaluation—Invention and Innovation—Weights and Measures—Engineering Standards—Vehicle Systems Research.

THE CENTER FOR RADIATION RESEARCH engages in research, measurement, and application of radiation to the solution of Bureau mission problems and the problems of other agencies and institutions. The Center for Radiation Research consists of the following divisions:

Reactor Radiation—Linac Radiation—Applied Radiation—Nuclear Radiation.

¹ Headquarters and Laboratories at Gaithersburg, Maryland, unless otherwise noted; mailing address Washington, D. C. 20234.

² Located at Boulder, Colorado 80302.

³ Located at 5285 Port Royal Road, Springfield, Virginia 22151.

UNITED STATES DEPARTMENT OF COMMERCE
Maurice H. Stans, Secretary
NATIONAL BUREAU OF STANDARDS • A. V. Astin, Director



TECHNICAL NOTE 451

ISSUED JANUARY 1969

Radiochemical Analysis Section:

**Summary of Activities
July 1967 to June 1968**

Edited by James R. DeVoe

Radiochemical Analysis Section
Analytical Chemistry Division
Institute for Materials Research

NBS Technical Notes are designed to supplement the Bureau's regular publications program. They provide a means for making available scientific data that are of transient or limited interest. Technical Notes may be listed or referred to in the open literature.

FOREWORD

The Analytical Chemistry Division was established as a separate division at the National Bureau of Standards on September 1, 1963, and became part of the Institute for Materials Research in the February 1, 1964 reorganization. It consists at present of nine sections and about 100 technical personnel encompassing some 45 different analytical competences from activation analysis and atomic absorption to vacuum fusion and x-ray spectroscopy. These competences, and in turn the sections which they comprise, are charged with research at the forefront of analysis as well as awareness of the practical sample, be it standard reference material or service analysis. In addition it is their responsibility to inform others of their efforts.

Formal publication in scientific periodicals is a highly important output of our laboratories. In addition, however, it has been our experience that informal, annual summaries of progress describing efforts of the past year can be very valuable in disseminating information about our programs. A word is perhaps in order about the philosophy of these yearly progress reports. In any research program a large amount of information is obtained and techniques developed which never find their way into the literature. This includes the "negative results" which are so disappointing and unspectacular but which can often save others considerable work. Of importance also are the numerous small items which are often explored in a few days and which are not important enough to warrant publication--yet can be of great interest and use to specialists in a given area. Finally there are the experimental techniques and procedures, the designs and modifications of equipment, etc., which often require months to perfect and yet all too often must be covered in only a line or two of a journal article.

Thus our progress reports endeavor to present this information which we have struggled to obtain and which we feel might be of some help to others. Certain areas which it appears will not be treated fully in regular publications are considered in some detail here. Other results which are being written up for publication in the journal literature are covered in a much more abbreviated form.

At the National Bureau of Standards publications such as these fit logically into the category of a Technical Note. In 1968 we plan to issue these summaries for all of our sections. The following is the fifth annual report on progress of the Radiochemical Analysis Section.

W. Wayne Meinke, Chief
Analytical Chemistry Division

PREFACE

The Radiochemical Analysis Section develops measurement techniques for qualitative, quantitative and structural analysis of materials through the use of radioisotopes. One of the first successful nuclear techniques for determining chemical structure is Mössbauer Spectrometry, one of the major activities in this section.

Understanding of the chemical, nuclear, and physical principles which form the foundation of a new analytical measurement technique is basic to the development of measurement techniques using radioisotopes. Consequently, nuclear instrumentation, nuclear chemistry, and statistical analysis are key activities in the section. These activities also support the Activation Analysis Section as well as the radiation and radioisotope techniques in this section.

It is essential that the methods developed be applicable in the sense that they can be used successfully for materials of interest to science and industry. Therefore, these methods are applied to the analysis of NBS Standard Reference Materials where considerable cross checking of analytical techniques is required throughout the process of certification.

A group working on radioisotope dilution techniques and tracer methods has been reactivated after a two year dormancy. Results of this group will be reported next year.

In order to define more accurately the scope of our work abstracts of publications appear in this report. Brief descriptions of studies nearing completion are included when it is our intent to submit this work elsewhere.

A roster of the groups in this section is listed in part 5. The National Bureau of Standards has several programs whereby a scientist from the United States or abroad may work in our laboratories for one or two years. It is hoped that by utilizing these programs the section will be able to perpetuate a stimulating environment.

In order to adequately specify the procedures, it has been necessary occasionally to identify commercial materials and equipment in this report. In no case does such identification imply recommendation or endorsement by the National Bureau of Standards, nor does it imply that the material or equipment identified is necessarily the best available for the purpose.

James R. DeVoe, Chief
Radiochemical Analysis Section
Analytical Chemistry Division

TABLE OF CONTENTS

| | <u>Page</u> |
|--|-------------|
| 1. INTRODUCTION | 1 |
| 2. NUCLEAR CHEMISTRY | 3 |
| A. Introduction | 3 |
| B. Nuclear Reactions | 3 |
| 1. Mass Spectrometry | 3 |
| 2. Bremsstrahlung Intensity and Composition | 4 |
| C. Statistics in Nuclear and Analytical Chemistry | 9 |
| 1. The Peak Height Method for Evaluating Nuclear Spectra | 9 |
| 2. Criteria for Reporting Trace Amounts of Radioactivity | 14 |
| 3. High Accuracy Calibration and Control in Single-Channel Gamma Spectrometry | 18 |
| 4. Counting Statistics and Standard Reference Materials | 20 |
| 5. Detection Limits | 21 |
| D. Iodine Determination by Static Mass Spectrometry | 22 |
| 3. MÖSSBAUER SPECTROMETRY | 24 |
| A. Introduction | 24 |
| B. Instrumentation | 25 |
| 1. Cryostat for Moving Absorber and Stationary Source | 25 |
| 2. Pancake Radiation Detector for Back-scattering Mode of Mössbauer Spectrometry | 28 |
| C. Backscattering Mössbauer Spectrometry | 29 |
| 1. General Description | 29 |
| 2. Spectra of Steel Samples | 30 |
| 3. Effective Penetration of Mössbauer Radiation | 38 |
| 4. Identification of Corrosion Products on the Surface of Iron by Scattering Techniques | 44 |
| D. Operator Equivalent Method for the Determination of Orbital Electric Field Gradient Tensors | 44 |

Table of Contents (Cont.)

| | <u>Page</u> |
|---|-------------|
| E. The Electric Field Gradient Tensor for Common Nickel Configurations | 51 |
| F. ^{61}Ni Theory: Nuclear Interactions | 61 |
| G. Standard Reference Material for the Chemical Shift of Tin Compounds | 65 |
| H. Fitting of Multiple Line Mössbauer Spectra Using Constraints | 68 |
| 1. Introduction | 68 |
| 2. General Theory | 69 |
| 3. Uncertainties of the Estimates | 75 |
| I. The Application of Mössbauer Spectrometry to Quantitative Analysis | 75 |
| 1. Introduction | 75 |
| 2. Experimental | 77 |
| a. Apparatus | 77 |
| b. Reagents and Preparation of $\text{SnO}_2\text{-Al}_2\text{O}_3$ Mixtures | 77 |
| c. Mössbauer Experiments | 78 |
| d. Analysis of Copper-base Alloys | 78 |
| e. Tin Ores | 79 |
| 3. Results and Discussion | 79 |
| J. Tin Mössbauer Spectrometry Following the Decay of ^{119}Sb | 90 |
| K. Abstracts of Publications | 93 |
| 4. NUCLEAR INSTRUMENTATION | 96 |
| A. Introduction | 96 |
| B. Overflow Counter | 96 |
| 1. Introduction | 96 |
| 2. Description of Logic | 97 |
| C. Sequential Scanner to Control Frequency Synthesizer | 99 |
| 1. Introduction | 99 |
| 2. Description of System | 101 |
| D. Circuit Change to Improve Reliability of Interface Units | 102 |

Table of Contents (Cont.)

| | <u>Page</u> |
|---|-------------|
| E. Time of Year (TOY) System | 105 |
| 1. Time of Year Clock | 105 |
| 2. Time of Year (TOY) Clock Controller | 105 |
| F. Maintenance of Teletypes and Paper Tape Punches | 107 |
| G. Interface Between Mass Spectrometer and Small Electronic Computer | 109 |
| 5. PERSONNEL AND ACTIVITIES | 110 |
| A. Personnel Listing | 110 |
| B. Publications | 111 |
| C. List of Talks | 111 |
| 6. ACKNOWLEDGMENTS | 114 |
| 7. REFERENCES | 115 |
| APPENDIX I. OMNITAB PROGRAM FOR ANALYSIS OF MOSSBAUER SPECTRA | 117 |

LIST OF FIGURES

| <u>Figure</u> | | <u>Page</u> |
|---------------|---|-------------|
| 1 | Gold foil - NaI spectrum | 7 |
| 2 | Gold foil - Ge(Li) spectrum | 8 |
| 3 | Cadmium-wrapped gold foil - Ge(Li) spectrum | 8 |
| 4 | ^{137}Cs photopeak | 10 |
| 5 | Maximum ratio, base line/peak (B/N) vs peak counts (N) | 11 |
| 6 | ^{54}Mn with ^{22}Na baseline | 12 |
| 7 | Mössbauer cryostat | 25 |
| 8 | Photograph of pancake proportional detector source side | 26 |
| 9 | Photograph of pancake proportional detector back side | 27 |
| 10 | Diagram of pancake proportional detector | 29 |
| 11 | Pulse height spectrum of ^{57}Co source for pancake detector, operating at 1400 volts, with 10% CH_4 90% A flow gas | 31 |
| 12 | Pulse height spectrum of ^{57}Co source for conversion electrons | 31 |
| 13 | Iron block scattering spectrum | 32 |
| 14 | SRM #1174 - white cast iron | 33 |
| 15 | Tool steel (collimated source) | 34 |

List of Figures (Cont.)

| <u>Figure</u> | | <u>Page</u> |
|---------------|--|-------------|
| 16 | Tool steel (transmission geometry) | 35 |
| 17 | Photograph of pancake detector used for backscattering at 45° angle | 36 |
| 18 | Mössbauer spectrum of steel plate taken by conversion electron detection | 37 |
| 19 | Schematic showing geometry for scattering experiment | 39 |
| 20 | Amount of backscatter as a function of thickness of the scatterers | 40 |
| 21 | Scattering spectrum of stainless steel with overlay of 0.22 mil iron foil | 41 |
| 22 | Scattering spectrum of stainless steel with overlay of 0.5 mil iron foil | 42 |
| 23 | Scattering spectrum of stainless steel with overlay of 0.72 mil iron foil | 43 |
| 24 | Three common electron configurations for Ni^{2+} , using a one-electron Hamiltonian | 52 |
| 25 | Two common electron configurations for Ni^{2+} , using a many electron Hamiltonian | 53 |
| 26 | The effect of magnetic, quadrupole, and mixed perturbations of the Mössbauer levels of the ^{61}Ni nucleus | 62 |
| 27 | Quadrupole spectrum as a function of η | 66 |
| 28 | Transmission spectrum of $BaSnO_3$ | 67 |
| 29 | Percent effect and attenuation as a function of sample thickness | 68 |
| 30 | Typical Mössbauer spectrum of SnO_2 in Al_2O_3 | 80 |
| 31 | Plot of height of peak to baseline ratio vs mg of SnO_2 | 83 |
| 32 | Plot of area of peak to baseline ratio vs mg of SnO_2 | 84 |
| 33 | Pulse height spectrum of ^{119m}Sn with lithium drifted silicon detector | 88 |
| 34 | ^{119}Sb vs $BaSnO_3$ (thickness is 150 mg/cm^2) | 91 |
| 35 | $^{119}Sn_2O_5$ vs $BaSnO_3$ (thickness is 150 mg/cm^2) | 92 |
| 36 | Diagram depicting overflow of memory for pulse height analyzer | 97 |
| 37 | Timing of logic pulses in pulse height analyzer | 98 |

List of Figures (Cont.)

| <u>Figure</u> | | <u>Page</u> |
|---------------|--|-------------|
| 38 | Logic diagram of overflow counter | 99 |
| 39 | Binary scalers for counting overflows | 100 |
| 40 | Block diagram of sequential scanner | 102 |
| 41 | Logic diagram and schematic for interface of pulse height analyzer and frequency synthesizer | 103 |
| 42 | Board No. 6 of pulse height analyzer interface | 104 |
| 43 | Time of year clock | 106 |
| 44 | Time of year clock controller | 108 |

LIST OF TABLES

| <u>Table</u> | | <u>Page</u> |
|--------------|--|-------------|
| 1 | Absolute nuclear reaction rates and relative yields | 5 |
| 2 | Advantages and limitations of the peak height method | 13 |
| 3 | Trace level reporting | 15 |
| 4 | Minimum upper limits ($\alpha=.05$) | 16 |
| 5 | Value of upper limits based upon zero counts | 17 |
| 6 | Observed counting precision | 20 |
| 7 | 3d electron contribution to the EFG elements | 52 |
| 8 | Hamiltonian matrix for the $\lambda L \cdot S$ perturbation on 3T_1 | 58 |
| 9 | Spin-orbit perturbation results for the 3T_1 level of 3F in T_d symmetry | 59 |
| 10 | EFG elements for the low lying states of Ni with T_d coordination | 60 |
| 11 | Quadrupole Hamiltonian matrix for the spin 5/2 state | 63 |
| 12 | Partial derivatives for linear approximation | 74 |
| 13 | Variation of spectral parameters with the amount of SnO_2 | 82 |
| 14 | Comparison of calculated values with the observed values of H/B | 85 |
| 15 | Analysis of Sn in copper-base alloys | 86 |
| 16 | Effect of geometry on spectral parameters | 86 |
| 17 | Effect of Pd filter on spectral parameters | 87 |

RADIOCHEMICAL ANALYSIS: MÖSSBAUER EFFECT, NUCLEAR
CHEMISTRY, NUCLEAR INSTRUMENTATION, STATISTICAL ANALYSIS

July 1967 to June 1968

Edited by James R. DeVoe

ABSTRACT

This is the fifth summary of progress of the Radiochemical Analysis Section of the Analytical Chemistry Division at the National Bureau of Standards.

The sections' effort comprises four major areas:

Mössbauer spectrometry, nuclear chemistry, nuclear instrumentation and the application of statistics in nuclear and analytical chemistry.

Studies in nuclear reactions have centered around measurement by time of flight mass spectrometry of helium-4 produced from reactions such as ${}^7\text{Li}(\gamma, \alpha){}^3\text{H}$.

Statistical methods have been applied to the measurement of peaks in radiation spectra, to reporting trace amounts of radioactivity, to the calibration of Standard Reference materials, and to the reporting of detection limits of a system of measurement.

A procedure for cooling a moving absorber with a stationary source for Mössbauer spectrometry is described. A system for taking spectra using the scattering mode is described along with a large "pancake" shaped proportional counter that is used in the system. Theoretical interpretations of Mössbauer spectra of nickel compounds are given. Computer programs which incorporate constraints such as field intensity and quadrupole moments have been written. Several applications of Mössbauer spectrometry, such as surface corrosion studies are described. Preliminary data are given on the charge states of ${}^{119\text{m}}\text{Sn}$ after nuclear recoil. A technique for resolving some of the difficulties in quantitative analysis of chemical structures is also described.

An overflow counter for collecting more counts than the memory capacity of a pulse height analyzer is described. A sequential scanner for a frequency synthesizer has adapted the NBS Optical Interferometric Mössbauer Spectrometer from a constant velocity to a constant acceleration mode.

James R. DeVoe, Chief
Radiochemical Analysis Section
Analytical Chemistry Division

Key Words:

NBS Linac, computers, standard reference materials, photonuclear reactions, cross sections, flux monitors, nickel-61, Mössbauer spectrometry, computer programs for Mössbauer spectrometry, backscatter geometry, proportional counter, Mössbauer instrumentation, detection limits for analysis, counting statistics, corrosion products, electric field gradient tensors, nuclear recoil, quantitative Mössbauer spectrometry, overflow counter, interferometric Mössbauer spectrometer.

1. INTRODUCTION

The effort of this section has centered around four main areas, Mössbauer spectrometry, nuclear chemistry, nuclear instrumentation, and the statistical interpretation of experimental data. An additional project called "Radioisotopic Methods of Analysis" will use radioisotopic dilution techniques for high precision quantitative analysis for macro constituents in materials.

Systems of instrumentation continue to be the area of major effort in Mössbauer spectrometry. This is evidenced by the continued effort in scattering techniques. This system provides a capability for measuring bulk samples and should increase the overall applicability of this spectrometry. Significant effort has been placed in the area of understanding the fundamental processes of the hyperfine interaction. Particular attention has centered about measurement of the sign of the electric field gradient tensor.

Applications of the Mössbauer effect are beginning to become commonplace. Scattering techniques have been used to measure corrosion products on surfaces. The structure of iron in various ferrites used in magnetic tapes or as memory cores of computers has proven interesting. The structure of iron in cements and of tin in glasses has been measured.

It would be highly desirable to be able to measure the amount of various structures in a material. Even though formidable problems exist, it is clear that in many cases a meaningful result can be obtained. It appears more probable than ever before that the use of calibrated standards will allow quantitative measurement of structures by Mössbauer spectrometry.

While the standards program for "bench marking" chemical shift has progressed nicely, it is evident that its usage by scientists must increase. This system of standards has been endorsed by an ASTM committee, and it is apparent that infor-

mation on these standards must be given greater publicity.

The effort in nuclear chemistry has been related in the past year mostly to the statistical interpretation of counting data. Considerable progress has been made in this area, culminating in a manuscript describing techniques for reporting limits of detection of a measurement system. It is anticipated that the impact of this work will have a considerable induction period after which greater efficiency in communication of analytical results is anticipated. It is expected that greater effort in photonuclear reaction mechanisms will be possible in the coming year.

The effort in nuclear instrumentation has been directed toward repair and upkeep of a variety of electronic instruments for several sections in the division. Emphasis has been placed, however, on special systems of instrumentation in Mössbauer spectrometry. In particular, the sequential scanner with a frequency synthesizer adapts the optical interferometer from constant velocity to constant acceleration. A part of our effort in instrumentation has been for the mass spectrometry section.

2. NUCLEAR CHEMISTRY

A. Introduction

The program has continued in its binary form in which nuclear reaction studies have served as input for statistical investigations and statistical problems have been attacked in order to find better methods for treating nuclear data and to improve the accuracy of the resulting conclusions. Generally, both aspects of the program have contributed to the solution of problems arising in other research groups at NBS.

A particularly important product of the work is a manuscript (abstract presented below) which concisely describes the principles of and standardizes the nomenclature for limits of detection of a measurement system.

B. Nuclear Reactions

1. Mass Spectrometry

Research reported in the previous Progress Report [2] has continued on a part-time basis in collaboration with the Photonuclear Physics Section. The initial aim of the project is to demonstrate detectability and measure yields for the photonuclear production of helium-3,4 from stable isotopes of lithium. The most significant progress during the past year has been successful absolute calibration of the sample analysis system and the setting of approximate (experimental) detection limits for helium-4. A calibration curve was determined over a range of several orders of magnitude by means of multiple expansions of pure ^4He in a system of calibrated volumes, "packaging" in copper capsules (as described in Ref. [2]) and puncturing in the "static" Mass Spectrometry analysis system. Significant nonlinearity set in at about a pressure of 10^{-5} torr, while background was limiting at the low pressure end. The system is presently believed reliable down to approximately 10^{10} to 10^{11} atoms of helium.

Two independent measurements of the $\text{Li}(\gamma, \alpha)$ yield were made by irradiating samples at the Activation Analysis termi-

nal [2] using bremsstrahlung from 90 MeV electrons and copper foil monitors. The yields obtained relative to that of the reaction, $^{65}\text{Cu}(\gamma, n)$, were 0.174 and 0.176, respectively. The "agreement" is fortuitous, for random errors were estimated to be approximately $\pm 15\%$ (relative standard deviation). Before proceeding with additional quantitative studies, however, it has become desirable to gather information on the beam composition--particularly with respect to bremsstrahlung, and fast thermal neutrons. Such studies are discussed below.

2. Bremsstrahlung Intensity and Composition

A considerable effort has gone into the study of bremsstrahlung foil monitoring accuracy and precision; spatial and intensity comparisons of various available bremsstrahlung beams; the related absolute yields of radioactivity monitors; the use of reliability of relative monitor yields as beam characteristic indices; and a determination of beam composition by means of a number of activation and absorption foils. The attainable precision using the reactions $^{12}\text{C}(\gamma, n)$ and $^{65}\text{Cu}(\gamma, n)$ has been evaluated by the methods outlined in Reference [2] and section C of this report. In the absence of source repositioning the "true" standard deviation is approximately 0.1%, whereas it appears to be limited to about 0.5% when repositioning is involved.

A program, FYLD, has been written to deal with a number of aspects involved with absolute beam intensities and fluxes, absolute stable and radioactivity monitor yields, responses of the various detectors involved, relative reaction yields, and predicted yields--all with the associated corrections and standard error estimates.

A comparison of the relative nuclear reaction rates available from different sources of bremsstrahlung at NBS appears in Table 1. Absolute rates are given for the reaction, $^{65}\text{Cu}(\gamma, n)$, as determined by detecting the radioactive product, ^{64}Cu . The relative reaction rates, which are directly pro-

Table 1. Absolute nuclear reaction rates and relative yields

| | Electron Energy (MeV) | Reaction Rate (min ⁻¹) ^{a,b} | Relative Yield ^c |
|------------------------------------|-----------------------|---|-----------------------------|
| <u>Synchrotron</u> | 90 | 3×10^{-16} ^d | .094±.002 |
| <u>Linac-45° Room</u> ^e | 60 | 4×10^{-15} | .095±.003 |
| <u>Linac-Pneumatic Tube</u> | 60 | 5×10^{-13} | .074±.002 |
| | 90 | 2×10^{-12} | .076±.002 |

^a"Typical" maximum absolute rates for the nuclear reaction, $^{65}\text{Cu}(\gamma, n)^{64}\text{Cu}$.

^bReaction rates are given to only one significant figure because significant variations occur in both time and space.

^cThe relative yield represents the observed rate for the reaction $^{63}\text{Cu}(\gamma, 2n)$ divided by that for $^{65}\text{Cu}(\gamma, n)$. Errors are standard deviations.

^dThe reaction rate, $3 \times 10^{-16} \text{ min}^{-1}$ is equal to an "equivalent quantum" flux of about $6 \times 10^9 \text{ cm}^{-2} \cdot \text{min}^{-1}$.

^eSee acknowledgments.

portional to bremsstrahlung flux, indicate that - of the presently available irradiation positions - the pneumatic tube position is the most effective for producing a reaction whose maximum cross section is in the region of the Giant Resonance. For purposes of isotope production or "uncomplicated" photon activation analysis, it is thus clear that the best results will occur in this position, using a reasonably high electron energy. On the other hand, for the study of excitation functions or for activation with minimal neutron interference or electron irradiation, the first two locations may be preferable. They differ from the third location in that the bremsstrahlung-producing target is considerably thinner and the transmitted electrons are magnetically "dumped" rather than being partially absorbed in water.

Since in the reaction, $^{63}\text{Cu}(\gamma,2n)^{61}\text{Cu}$ accompanies the reaction, $^{65}\text{Cu}(\gamma,n)^{64}\text{Cu}$, it has been convenient to examine the relative yields of the two (Table 1) as a "index" for bremsstrahlung purity and energy distribution. The relative yields (61/64) appearing in the last column of Table 1 reinforce the "suspicion" of the pneumatic tube irradiation location, as the 20% decrease in relative yield may have been brought about by a combination of (n, γ) production of ^{64}Cu and a degraded bremsstrahlung energy distribution, which would also favor ^{64}Cu .

Further study of the beam composition has been undertaken by means of the neutron-induced reactions:

- (1) $^{27}\text{Al}(n,\gamma)^{28}\text{Al}$
- (2) $^{197}\text{Au}(n,\gamma)^{198}\text{Au}$
- (3) $^{27}\text{Al}(n,p)^{27}\text{Mg}$

The first reaction serves as an indicator for thermal neutrons, the second for thermal and resonance neutrons, while the third requires neutrons whose energies exceed about 3 MeV. Besides those listed above, additional reactions include those from the monitors (Cu-foils, as well as $^{27}\text{Al}(n,\alpha)^{24}\text{Na}$, and $^{197}\text{Au}(\gamma,n)^{196}\text{Au}$). A combination of spectroscopy (NaI) and decay curve analysis permitted the resolution of all products except those resulting from ^{197}Au . Here, the γ -energy difference is only 14 keV, the ^{198}Au activity is small compared that of ^{196}Au , and the half lives (2.7 days and 6.2 days, respectively) are not convenient for resolution by means of decay. Therefore, one must resort either to isotope separation or high resolution (Ge) spectroscopy. The latter method was applied in this case, and preliminary information is given in Figures 1, 2, and 3. The first figure depicts the NaI spectrum from an irradiated (uncovered) gold foil, while Figure 2 shows the spectrum obtained with Ge(Li) using the same foil. The



Figure 1. Gold foil - NaI spectrum

peaks observed correspond to gamma rays of energies:
333 keV (^{196}Au), 356 keV (^{196}Au), 412 keV (^{198}Au), and 426 keV
(^{196}Au). The excess of ^{196}Au over ^{198}Au may be appreciated
by remembering that the abundance of the 412 keV gamma ray is
95%, while that of the 426 keV gamma ray is only 6%. A small
(~30%) but significant decrease in the ratio of the 412 keV
peak to those arising from ^{196}Au is seen in Figure 3. In this
case the foil was wrapped in "thick" cadmium, and one there-
fore concludes that significant amounts of both thermal and
resonance neutrons were present in the bremsstrahlung beam.

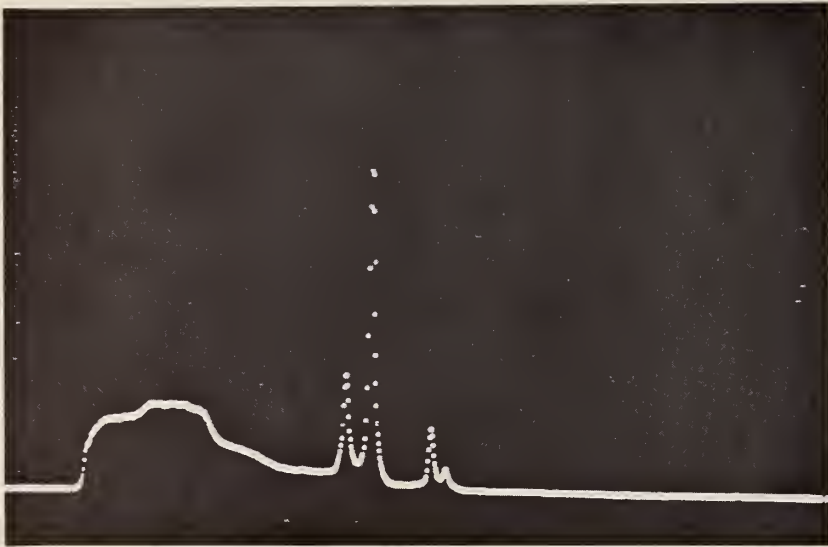


Figure 2. Gold foil - Ge(Li) spectrum

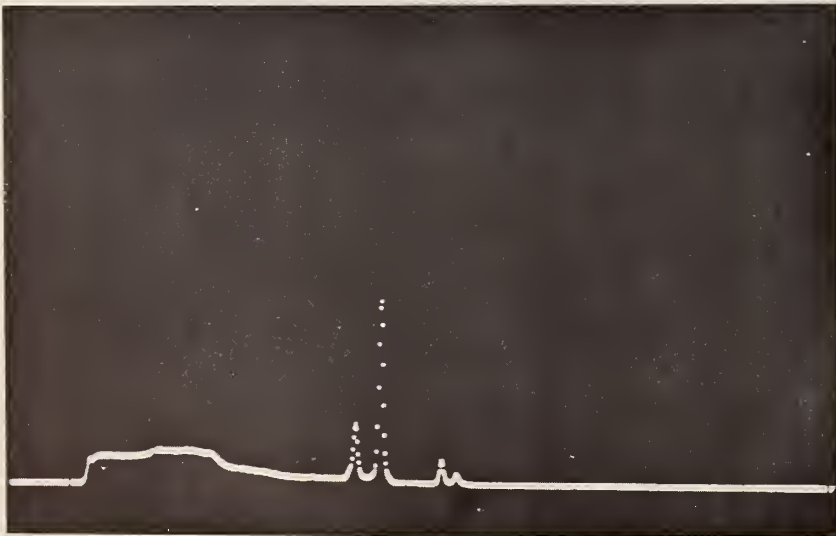


Figure 3. Cadmium-wrapped gold foil - Ge(Li) spectrum

C. Statistics in Nuclear and Analytical Chemistry

1. The Peak Height Method for Evaluating Nuclear Spectra

Peak heights are commonly used for quantitative measurement when output signals are presented in the form of continuous traces, as in mass spectrometry or gas chromatography. A similar approach has been examined for the analysis of nuclear spectra--where results appear as digital histograms--as a possible alternative to peak integration (with base line subtraction). The method has been thoroughly evaluated for non-overlapping peaks; it has been found to be completely reliable, relatively free from systematic error, nearly independent of peak shape assumptions, and extremely simple and rapid. The principal sources of error in the method include uncertainty in the peak location, gain variation, and base line (Compton) corrections.

Details of the method may be conveniently developed by reference to Figure 4. The .662 MeV photopeak of ^{137}Cs is depicted there for two different channel "densities". The essence of the method involves taking the number of counts in the peak channel, corrected for the base line contribution, as a measure of intensity. At the lower channel density (left-hand peak in Figure 4) the selected channel is less likely to lay symmetrically about the "true" peak position. For both densities the gross number of counts in the peak channel is characterized by Poisson fluctuations; as a result, the peak channel may not even contain the maximum number of counts. It is in this digital structure of both coordinates that the nuclear spectral data differ from the continuous spectra which are observed in many other disciplines. The digital structure both adds limitations to the use of peak heights and modifies the rules for determining peak heights, as compared to continuous spectra.

Considering first the coarse structure of the abscissa, if the peak is not centered in a channel, an error arises

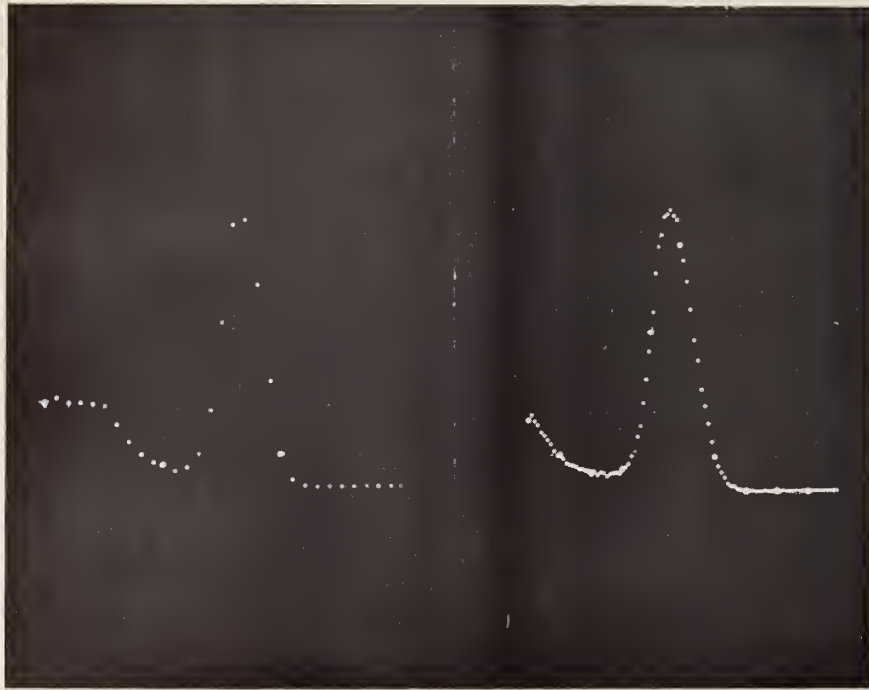


Figure 4. ^{137}Cs photopeak

from this lack of symmetry; the magnitude of this error depends upon the channel density. For a peak whose shape is approximately Normal, the maximum error due to the symmetry effect is less than 1% for densities exceeding 8.2 channels/FWHM. Symmetry changes can be readily corrected for, with an inaccuracy of less than 1% for a density as low as 4.2 channels/FWHM. Information (count) loss--compared to counts resulting from peak integration--between these two limiting densities, varies from about 55% to 89%.

Numerous approximate methods exist for base line correction. One which has been applied here is especially simple: one estimates the base line contribution to the peak channel as the average of the numbers of counts at the minimum (on the low-energy side) and those in the channel which is equally distant from the peak on the high energy side. (The rule must

be modified in the case of interfering spectra and for Ge(Li) detectors, but such modifications will not be discussed here). An estimate of the standard deviation of the net number of peak counts may then be made on the basis of the counts in the three channels in question. There are two limitations to the above procedure, however. (1) If the ratio Base Line/Peak counts (B/N) is large, but gross counts (N) are small; one may not be certain that a peak is, in fact, present. (2) On the other hand, if N is very large, the error estimate (based upon counting statistics) may be vitiated by a systematic error in the baseline correction. Detailed treatment of these two limitations has led to maximum values of B/N as a function of the number of peak counts, N , and the (estimated) relative (systematic) error, f_B , in the base line due to nonlinearity. Results of the calculations are plotted in Figure 5. The purpose of the plot is to serve as a guide

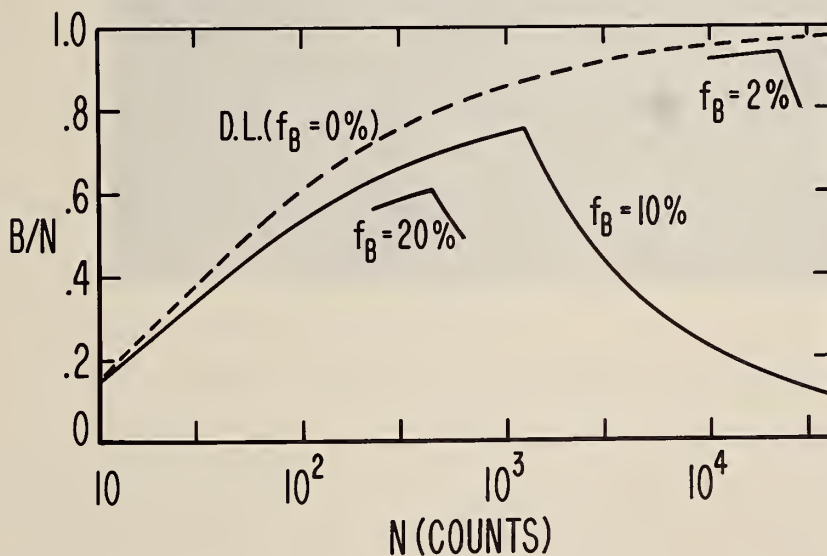


Figure 5. Maximum ratio, base line/peak (B/N) vs peak counts (N)

in deciding--for a given ratio, B/N , and "reasonable" estimate, f_B --whether there are sufficient peak counts, N , to be detectable, and whether there are few enough so that the Poisson counting error represents the principal source of uncertainty. Figure 6 displays a "real" base line resulting from ^{22}Na in the region of .84 MeV (^{54}Mn) taken with NaI. The relative base line error (+12%) is perhaps typical for non-overlapping peaks with such a detector.

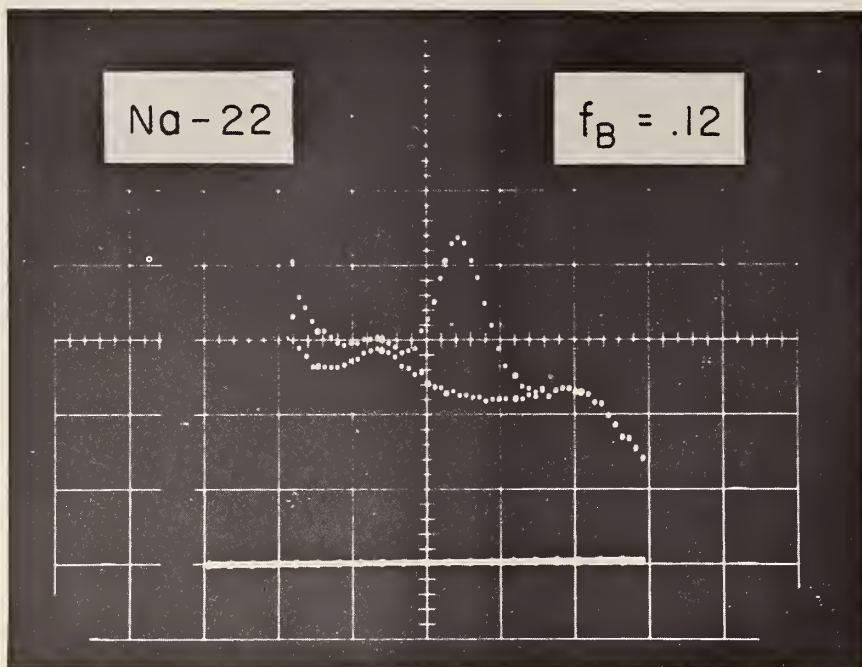


Figure 6. ^{54}Mn with ^{22}Na baseline

In addition to the symmetry error, which may be made negligible (density >8) or well-corrected (density >4), there may exist errors due to shifts in gain. A very simple first-order gain correction may be made by multiplying the net peak height by the relative change in gain. Assuming that the peak location may be estimated (by inspection) to $1/2$ channel and that the peak is approximately Normal, it can be shown that gain shifts as large as 10% or 80% (depending

upon the details of the method) may be thus corrected, with an inaccuracy in the correction of less than 1%. Such calculated correction accuracy has been confirmed experimentally.

An overall investigation of the accuracy of the peak height approach has been carried out by means of a factorial experiment [5] in five dimensions. The four abscissae (independent variables) were: interference level, symmetry changes, channel density, and gain shifts. The design used was a $1/2 \times 2^4$ balanced factorial. Results of the analysis confirmed that high levels of interference do affect the peak height estimate and that a factor of two change in channel density (conversion gain) may be significant (for 1% "counting statistics") while the remaining factors and all interactions among factors are not significant, at least in the region of hyperspace which was spanned. An additional result of the analysis was an internal variance estimate, which was found to be quite consistent with that derived from counting statistics.

A summary of the advantages and limitations of the peak height method is presented in Table 2.

Table 2. Advantages and limitations of the peak height method

ADVANTAGES

1. Simplicity and speed.
2. Relatively insensitive to gain shifts.
3. Accuracy may be somewhat better than that of "peak area".
4. Little knowledge of other components or "shape" required.

LIMITATIONS

1. Some loss in Poisson precision.
2. Resolution fluctuations must be absent.
3. $\text{FWHM} > 4$ channels.
4. $(B/N) < (B/N)_{\text{crit}}$. and f_B estimate (limited required).

The author is grateful to Brian Joiner for suggesting and outlining the factorial approach. The analytical method was based upon the Yates algorithm as described in Chapter 12 in Reference [7].

2. Criteria for Reporting Trace Amounts of Radio-activity [3]

Radiochemical observations which are not clearly "positive" deserve special attention in order to prevent ambiguity in reporting. Frequently such results are given as zero, or as an estimated mean (positive or negative) and its standard deviation. In order to better interpret such borderline results, possibly for legal purposes, it is suggested that they be considered as "detected" or "not detected" according to definite statistical criteria for detection and detectability. If "not detected" -- the case of particular interest here -- one may either report the associated "detection limit", or an upper limit may be given. The upper limit should relate to a one-sided confidence interval, and occasional negative values should be expected.

By way of illustration, consider an experiment in which three samples yielded 144, 95, and 115 counts in a given period of time, where the mean detector background was known to be 100 counts in that same time interval. The results of applying to this problem the principles developed previously [3] are given in Table 3. Only in the first case may the signal be considered "detected", and one may report this conclusion together with the detection limit, L_D . Both of the latter two results are reasonable statistically, and they should be reported as "not detected" together with the corresponding upper limits.

When one encounters extremely low levels of activity and background, however, the method applied above is not adequate, for it is based upon the assumption of normality. The detector referred to above is one which employs β - γ - γ coincidence

Table 3. Trace level reporting^{a,b}

| <u>Net Counts$\pm\sigma$</u> | <u>Detection</u> | <u>L_C</u> | <u>L_D</u> | <u>Upper Limit ($\alpha=.05$)</u> |
|---|------------------|----------------------|----------------------|--|
| 44 \pm 12 | D | 16.4 | 35.6 | --- |
| - 5 \pm 10 | ND | | | 11.0 |
| 15 \pm 11 | ND | | | 32.7 |

^aAll units are counts

^bNotation is that of Ref.

and has a measured background of about 1 count per hour. Hence, the time for the experiment described is 100 hours. Thus, if one is dealing with somewhat shorter periods -- as may be necessitated by short-lived activity -- it may be necessary to consider in detail the Poisson distribution in setting confidence intervals and upper limits. The special situation arising when zero counts are observed is particularly straightforward, and it has been examined in some detail.

Two questions are of primary importance in the extreme low level (zero count) situation: (1) in planning an experiment, what is the minimum counting time in order to set a given upper limit; (2) having observed zero (or some other small number of) counts, what is the corresponding upper limit (or confidence interval, if "detected"). Table 4 lists the upper limits ($\alpha=.05$) which would result if zero counts are observed where the counting "time" is expressed in terms of the mean number of background counts. The third column in the table lists the probability of observing zero counts, under the null hypothesis. Thus, in order to establish an upper limit equal to the background equivalent activity (BEA) with the β - γ - γ detector (BG=1 cph) one need only count for 1.5 hours. The "chance" of doing so, however, is only 22% [=exp (-1.5)]. On the other hand, if one wished to establish

Table 4. Minimum upper limits ($\alpha=.05$)

| $(\rho_M)_{\min}(a)$ | Mean BG counts (τ) | $W(0) = e^{-\tau}$ |
|----------------------|------------------------------|--------------------|
| ∞ | 0 | 1 |
| 6.20 | .417 | .65 |
| 2.76 | .818 | .44 |
| 1.00 | 1.50 | .22 |

(a) Sample activity/background equivalent activity

a detection limit (as defined in Ref. [4]) equal to the background equivalent activity, a counting period of 16 hours would be required! In order to make the example more explicit, consider ^{60}Co whose BEA is 37.5 fCi. If the desired upper limit were 1 pCi, the time required would be 6.5 min, where the probability of "success" (observing zero counts) would be 89%. The second facet of the problem may be illustrated by assuming that the result of a 25 min observation is zero counts. Here, the upper limit may be deduced from Table 4: the "reduced time" equals 25 min/60 min = 0.417; hence the upper limit equals $6.20 \times \text{BEA} = 6.20 \times 37.5 \text{ fCi} = 233 \text{ fCi}$: the *a priori* probability of observing zero counts is 65%.

The foregoing principles have been tested experimentally and also applied to a problem in activation analysis. In the "control" experiment, one thousand observations were found to be consistent with an upper limit estimate based upon the Poisson distribution. For the "experiment" the mean rate was adjusted to be just 3 counts/channel. (A multichannel scaler was used having a "dwell time" of .1 sec/channel). If zero counts were observed in any given channel the calculated upper limit ($\alpha=.05$) would likewise be 3 counts. The expected number of zeroes equals 50, with

a 95% confidence interval extending from 37 to 63. The number of zeros observed was 61. The activation analysis problem involved low level activity of moderate half life (~hours). A number of samples resulting from isotope separation had to be examined within the time limit set by this half life, and therefore it was necessary to plan the counting interval per sample such that there would be a good chance of setting an "acceptable" upper limit. The result of the planning led to an interval of 25 min--as with ^{60}Co , above--and the corresponding upper limit was, similarly, 233 fCi. As the probability of observing zero counts was only 65%, however, it was necessary to consider the limit which would result if one were "unlucky" enough to observe 1 count. In such a case, the gross upper limit (as deduced from the Poisson distribution) becomes 4.74 counts instead of 3.00 counts. Correcting for background (.42 counts) one arrives at the net upper limit of 4.32 counts which is equivalent to 390 fCi.

The principal advantages of applying the "zero-count" approach are listed in Table 5.

Table 5. Value of upper limits based upon zero counts

1. Good chance (22%) of establishing U.L. = BEA by means of "brief" counting (zero counts).
2. Usefulness of such limits with "low level" counters (BEA < 1 pCi) which employ extensive shielding, spectroscopy, or coincidence.
3. Considerable saving of time for samples having negligible activity, and for rapid surveys.
4. Possible necessity when short lived nuclides are counted with low background counters.

3. High Accuracy Calibration and Control in Single-Channel Gamma Spectrometry [6]

A single-channel analyzer is especially appropriate for counting samples having controlled mixtures of radionuclides. Such is the case, for example, for foil monitors of reactor or accelerator beams. Since activation monitors for photo-nuclear reactions must be counted with especially good precision, an investigation has been made of precision and accuracy in the analysis of the photodisintegration products of copper using the single channel approach.

Selection of discriminator settings was originally attempted by means of an associated multichannel analyzer and pulser, but serious inconsistencies were encountered. As a result, a simple mathematical approach was adopted, in which three or four differential observations in the vicinity of the photopeak are combined with an appropriate analytic expression for the peak shape. If one assumes that a photopeak may be described by the Normal distribution, the number of counts (N) within a "small" window of a single channel analyzer may be represented as in Equation 1.

$$N \approx \exp \left(-(x-x_0)^2 / 2\sigma^2 \right) \quad (1)$$

where x_0 is the centroid of the distribution, x is this center of the (differential) window, and σ is the standard deviation of the distribution. If two additional differential observations are made, displaced from the first observation by discriminator (base line) charges of $+D$, $-D$, respectively, one may calculate the peak centroid as shown in Equations 2 and 3,

$$\rho \equiv \frac{1_n(N/N_-)}{1_n(N/N_+)} = \frac{D[2x-x_0]-D}{D[-2(x-x_0)-D]} \quad (2)$$

$$x_0 = x + \frac{D}{2} \left(\frac{\rho-1}{\rho+1} \right) \quad (3)$$

where the numbers of counts corresponding to the displacements $+D$ and $-D$ are represented by N_+ and N_- , respectively. Accuracy of the approach for peak location and "control" using a single channel analyzer was checked by collecting counts from a ^{22}Na source with both a single- and a multi-channel analyzer. Selecting a region extending $\pm\text{FWHM}$ from the peak center in each case, approximately 1.52×10^5 counts were obtained. The difference between the two results was 0.54%, while the standard deviation of the difference was 0.36%.

A computer program has been written for calculating the peak parameters as outlined above, along with estimates of the FWHM and peak amplitude and area. If only peak location is desired, it has been found more convenient to use a nomogram which was constructed on the basis of Equation 3.

A principal application in our laboratory is the counting of β^+ -emitters (samples and monitor foils) which result from photonuclear activation. In order to establish and check "control" in counting the resulting annihilation quanta, we have used a standard source of ^{22}Na . Using the scheme outlined above, we have determined a relative standard deviation for peak location of approximately 0.2%. The real precision for peak amplitude, however, was found to depend upon the width of the window, as well as the condition and location of the source. Estimates of reproducibility based on the shape of the ^{22}Na spectrum indicated that the optimum window setting was approximately $\pm 2 \times \text{FWHM}$. Experimental estimates of "excess" random error, σ_{XS} , were deduced by the methods described in the previous report Reference [2]; they are given below in Table 6.

The results in Table 6 relay the importance of window width and source positioning, and they show that a reproducibility (standard deviation) of approximately 0.1% is attainable with the present system.

Table 6. Observed counting precision^a

| <u>Position</u> ^b | <u>Discrim.</u> | <u>Sample</u> ^c | <u>v</u> | <u>σ_{xs}</u> | <u>Limits (.95 C.L.)</u> |
|------------------------------|-----------------|----------------------------|----------|---------------------------------|--------------------------|
| Fixed | 2*FWHM | ²² Na | 11 | .09% | (.03%, .19%) |
| Fixed | Integral | Cu-5 | 9 | .06% | (0%, .19%) |
| Fixed | FWHM | Cu-1 | 4 | .19% | (0%, .75%) |
| Varied | 2*FWHM | Cu-8 | 6 | .44% | (.25%, 1.1%) |

^aPoisson counting precision (standard relative deviation) was equal to 0.1% for each observation.

^b"Fixed"=source untouched between observations;
"Varied"=source removed and replaced.

^c²²Na is the standard source; Cu's are bremsstrahlung monitors.

4. Counting Statistics and Standard Reference Materials

Standard Reference Materials (SRMs) which are determined by nuclear methods are characterized by uncertainties depending, at least in part, upon the (approximately) Poisson distribution of radioactive decay. Generally, the final estimates (mean and standard error) for a given SRM are based upon a number of independent observations. Such observations frequently will be characterized by differing (Poisson) standard deviations and sometimes by an additional (non-Poisson) component of variance--due to instrument instability, heterogeneity, etc. The statistical treatment of such sets of observations has been referred to by S. S. Nargolwalla in a discussion of fast neutron activation analysis (program: NGEN, Ref. [1]); the principles of the treatment have been outlined in a discussion of the precision of radioactivity measurements (program: XESS, Ref. [2]). In essence, the method of treating the data included first calculating a weighted mean and standard error, based upon "counting statistics". Second, χ^2 is evaluated to test for the presence of additional sources of variation. If the test is

negative, the (Poisson) results may be used to set a confidence interval. Otherwise, an iterative calculation is carried out to set limits for the additional variance.

The foregoing approach was recently applied in deducing average results for oxygen-in-steel SRM's (#1090, #1091, #1092) determined by fast neutron activation--for comparison with results obtained by vacuum- and inert gas fusion. Data sets for these three SRMs were submitted by S. S. Nargolwalla of the Activation Analysis Section. The direct, weighted means and standard errors found for the three standards were: 492 ± 12 ppm (#1090), 132.7 ± 1.7 ppm (#1091), 26.6 ± 1.6 ppm (#1092). Only in the case of #1091 was the computed χ^2 significant at the 5% level. The resulting 95% confidence interval for σ_{xs} (Ref. [2]) ranged from .7% to 12.6% (R.S.D.), the best estimate being 4.5%. The very wide confidence interval resulted from the facts that there were relatively few observations and that σ_{xs} was comparable to the standard deviation due to counting statistics. The problem of setting exact confidence intervals when both sources of variation are important has not yet been solved.

Helpful discussions with S. S. Nargolwalla and B. L. Joiner are gratefully acknowledged.

5. Detection Limits

LIMITS FOR QUALITATIVE DETECTION AND QUANTITATIVE DETERMINATION

by Lloyd A. Currie published in Analytical Chemistry 40, 1968

The occurrence in the literature of numerous, inconsistent and limited definitions of a detection limit has led to a re-examination of the questions of signal detection and signal extraction in analytical chemistry and nuclear chemistry. Three limiting levels have been defined: L_C -the net signal level (instrument response) above which an *observed* signal may be reliably recognized as "detected"; L_D -the "true" net signal level which may

be *a priori* expected to lead to detection; and L_Q -the level at which the measurement precision will be satisfactory for quantitative determination. Exact defining equations as well as series of working formulae are presented both for the general analytical case and for radioactivity. The latter, assumed to be governed by the Poisson distribution, is treated in such a manner that accurate limits may be derived for both short- and long-lived radionuclides either in the presence or absence of interference. The principles are illustrated by simple examples of spectrophotometry and radioactivity, and by a more complicated example of activation analysis in which a choice must be made between alternative nuclear reactions.

D. Iodine Determination by Static Mass Spectrometry

In order to assess the feasibility of determining "trace levels" of iodine isotopes by means of conversion to a suitable volatile compound and "static" mass spectrometry, samples of ethyl iodide (vapor) were prepared and analyzed. (Ethyl iodide was selected because of its relatively high vapor pressure and because it should be relatively straightforward to synthesize and purify by gas chromatography.) Starting with the pure compound, using calibrated volumes of a vacuum line for multiple expansions, two samples were prepared in copper capsules for subsequent analysis. Nominal pressures were 1.1×10^{-3} torr and 2.4×10^{-9} torr, respectively.

Upon puncturing the capsules, only the one containing the higher pressure gave a measureable signal with the E.A.I. quadrupole mass spectrometer (see acknowledgments). Mass peaks observed corresponded to $(C_2H_5I)^+$ and I^+ ; the former gave a signal of about 40 mV, and the latter about 20 mV. Both signals decreased approximately exponentially with a halftime of about 1.5 min. Decomposition of C_2H_5I continued

with time, but the I^+ signal reached a steady-state value of about 1.9 mV. Taking the above results together with the initial number of molecules placed in the capsule and the observed background (≈ 0.01 mV), one concludes that about 5×10^9 molecules of ethyl iodide would give a signal equivalent to that of the background. It seems very likely, however, that the true "sensitivity" for the ethyl iodide is greater by a factor of about 105, considering calibration factors observed with other gases and those given in the instruction manual. Probably physical or chemical reaction of the ethyl iodide with the wall of the capsule took place during its unfortunately long storage period. Although the sensitivity of the E.A.I. spectrometer is quite satisfactory, and the "gas" chemistry approach is feasible, there are significant limitations to the method. One is the fact that the instrument is not characterized by extremely high resolution; this would limit the isotope ratios which might be examined. (One may "trade-off" sensitivity for resolution, however. We have, for example, been able to measure the natural abundance of deuterium). A second limitation, which would have to be explored for the particular molecular species to be used, is the interference from fragments of the parent molecule or from impurities.

(L. A. Currie)

3. MÖSSBAUER SPECTROMETRY

A. Introduction

The majority of the studies in this project continues to emphasize instrumentation and in particular new systems. The method of backscattering measurements for bulk samples has been in operation for well over 18 months. More recent developments of a scattering detector and a spectrometer with interferometric velocity sensing in the constant acceleration mode have provided continuing stimulus in this area.

Increasing emphasis has been placed on studying new Mossbauer nuclides, and this year's efforts provide data which indicate that nickel compounds can be studied by Mossbauer Spectrometry.

Several new standards are in the final stages of production and calibration. The most important of these is a pure iron foil whose six peak positions will be determined for spectrometer calibration.

Continuous modifications are made to the mathematical methods for resolving complex spectra and a new approach is described.

Quantitative measurements using Mössbauer spectrometry have been continued. This report describes some preliminary attempts on the determination of tin in tin bearing materials. Recent advances in instrumentation may help, but the technique is limited in its ability for quantitative measures of this sort because of complex solid state properties of the matrix.

Considerable effort has been expended in compiling the current literature in the field. If interest is sufficient, an effort may be made to publish a computer listing of current titles, to supplement the "Mössbauer Effect Data Index" by A. H. Muir [8].

B. Instrumentation

1. Cryostat for Moving Absorber and Stationary Source

The simple liquid nitrogen cryostat described in Reference [2] has been redesigned to accommodate a moving absorber. This configuration has the advantage of optimum utilization of the source-detector geometry without large inverse square law distortion, cooling of the source, and rapid changing of sources. Furthermore, the moving absorber configuration eliminates the problem of iron impurities in the counter window causing interference. In this cryostat, the source is mounted on a brass tee, which slides into the heat sink, as shown in Figure 7. The absorber is supported by a 5 mil silver flexure plate connected to the drive pushrod by means of a yoke. Cooling is provided by a bottom-feeding permanently

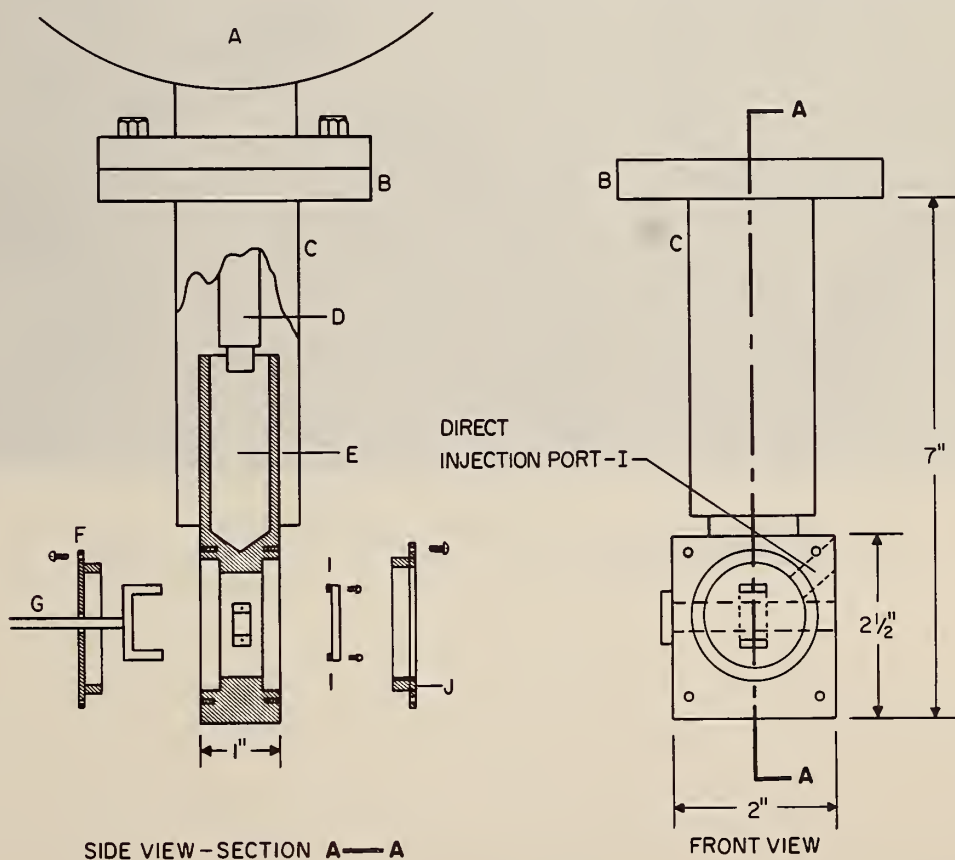


Figure 7. Mössbauer cryostat

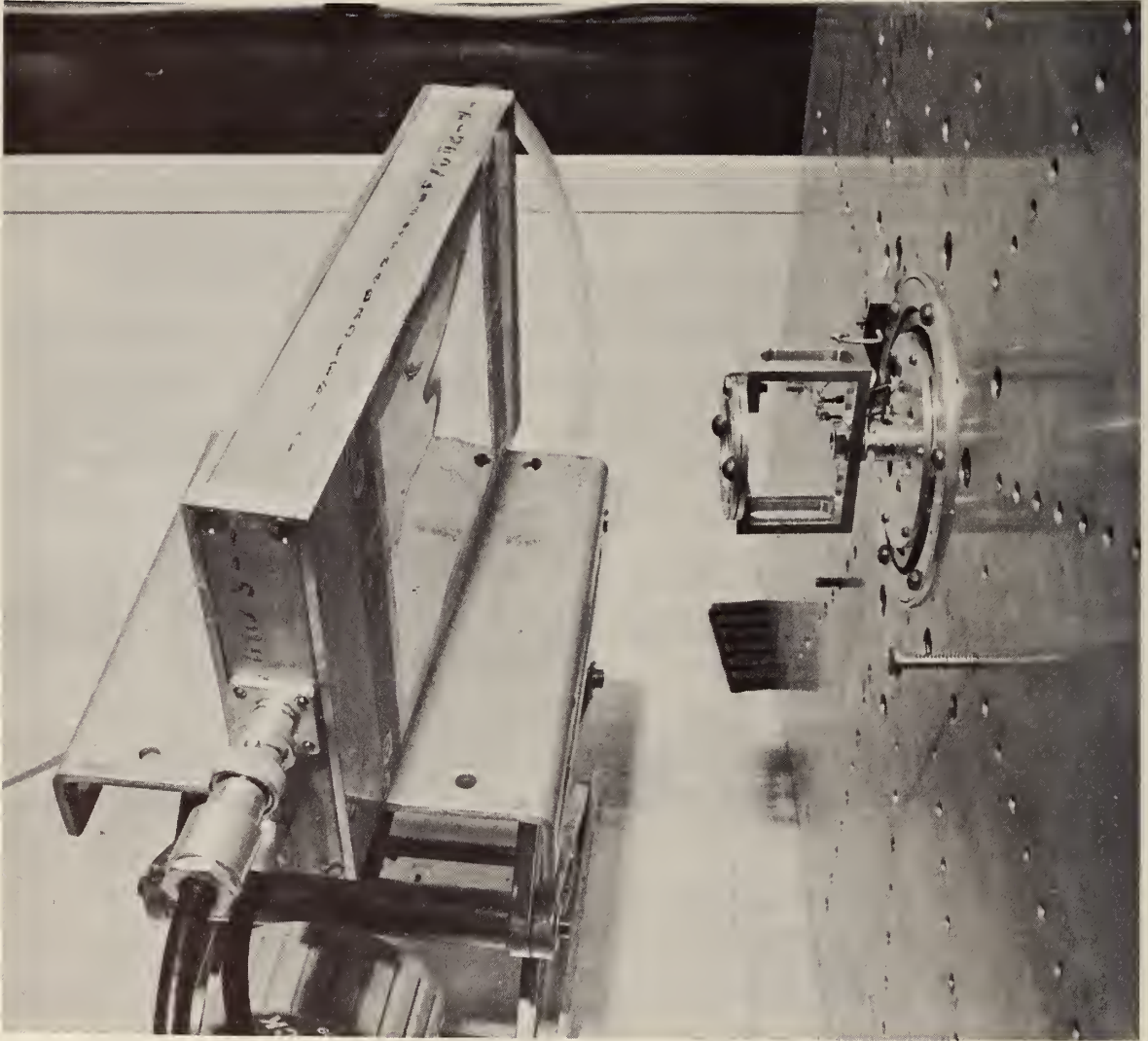


Figure 8. Photograph of pancake proportional detector source side.

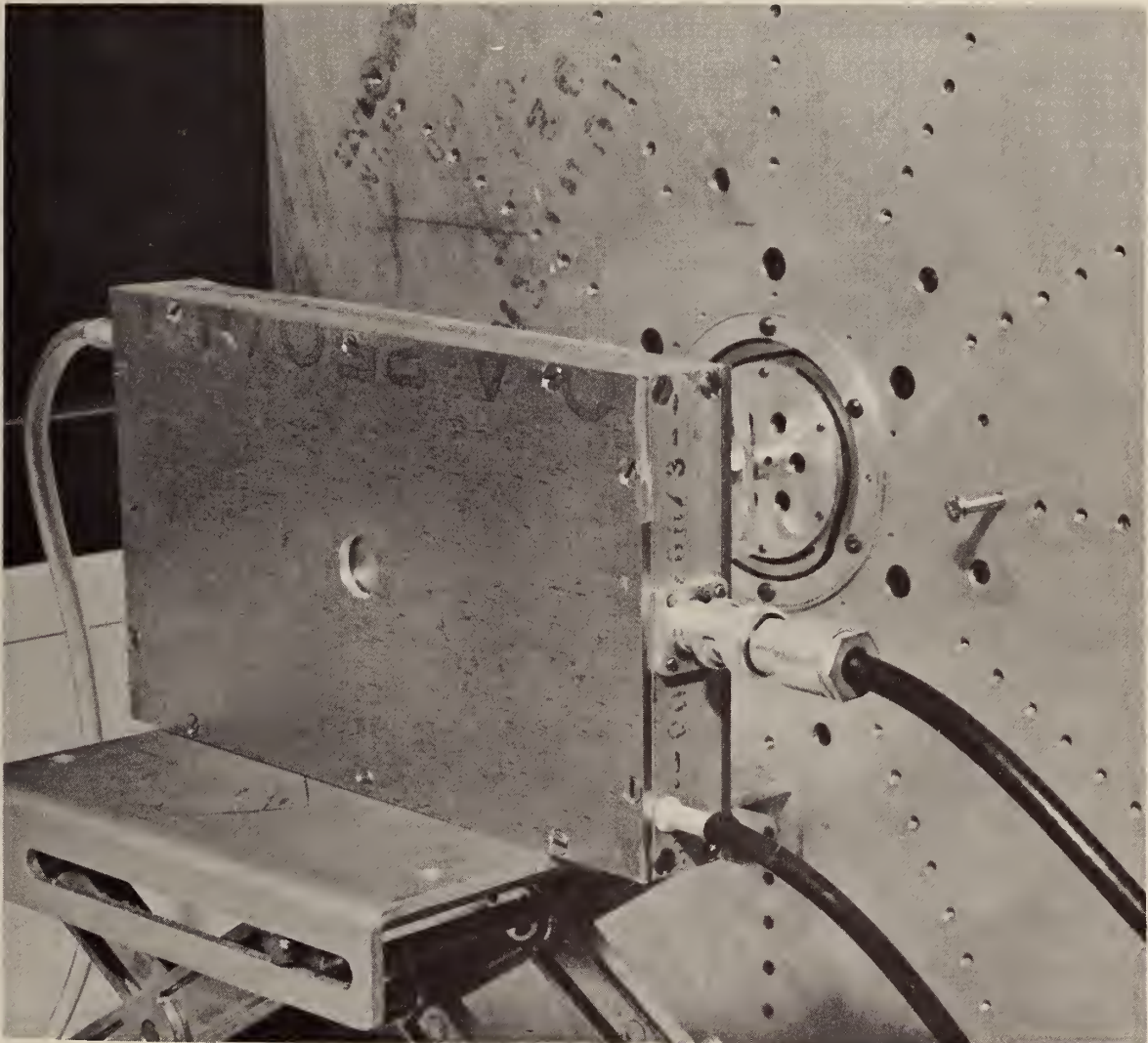


Figure 9. Photograph of pancake proportional detector back side.

evacuated dewar (A), which maintains a constant nitrogen level in contact with the heat sink (E). For a discussion of other parts indicated see Reference [2]. The heat sink is insulated with polyurethane foam and an aluminum coated Mylar radiation shield. The insulation is cast around the heat sink using Armstrong expando foam; 1/2 inch of foam is sufficient for nitrogen temperature insulation.

2. Pancake Radiation Detector for Backscattering Mode of Mössbauer Spectrometry

The conventional transmission technique used in Mössbauer spectrometry does not lend itself well for the analysis of bulk materials. To solve this problem, a scattering technique has been developed. This method has the disadvantage of poor geometry. To improve the geometry factor, a pancake proportional detector has been developed, see photographs in Figures 8 and 9. The detector has an effective area of 12 square inches; its detection efficiency is 65% and its resolution is 20% (FWHM) for 6.3 keV x-ray radiation. Prototype detectors were constructed with wires spaced 1/2 inch apart in the detector. Although the efficiency of the detector was good, the pulse height resolution was very poor. The efficiency of the detector was not a critical function of the wire spacing, and in the final design only two wires were used, spaced symmetrically 3/8 inch from the wall. A detector diagram is shown in Figure 10, and is made from aluminum (A), with aluminized Mylar windows (H). The 1 mil stainless steel wires (C) are supported by 1/4 inch plexiglass strips (B) and are connected in parallel to a H.V. supply (E), at approximately +1400 volts. A conventional charge sensitive preamplifier and double delay line clipped amplifier are used. The pulse height spectrum of a 4 mCi ^{57}Co source is shown in Figure 11. The detector gas is 10% CH_4 and 90% Ar at atmospheric pressure, with a 0.1 cc/min flow rate (inlet and outlet, D).

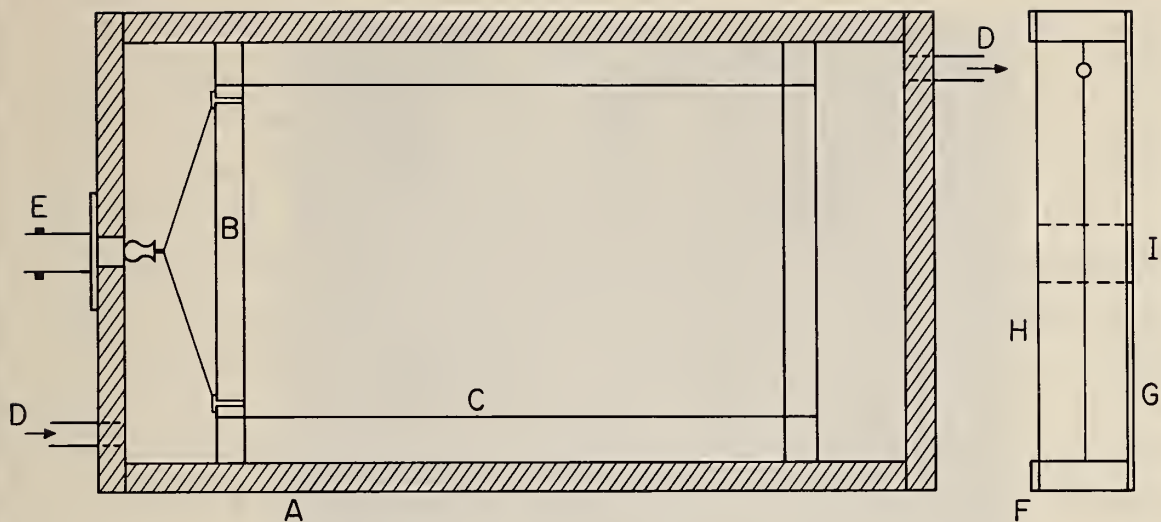


Figure 10. Diagram of pancake proportional detector

The detector has also been used for the detection of conversion electrons. In this case, the Mössbauer absorber was placed in contact with a 10% CH₄-90% He flow gas by putting it in place of the detector window. The pulse height spectrum is shown in Figure 12, with the detector operated at +1200 volts.

The pancake detector increases the detection efficiency by a factor of about four as compared to the previously used 2 inch diameter Reuter Stokes detector and can be used for conversion electron detection.

(K. R. Swanson and J. J. Spijkerman)

C. Backscattering Mössbauer Spectrometry

1. General Description

For Mössbauer analyses of bulk materials, such as gauge blocks, SRM steel samples, and steel plate, the transmission geometry is not applicable. A backscattering technique has been used successfully for this analysis and it represents a nondestructive technique.

For ⁵⁷Fe the backscattering technique can detect the Mössbauer effect by the 14.4 keV gamma radiation, 6.3 keV

x-ray radiation or 8 keV conversion electrons. Since the internal conversion coefficient for the 14.4 keV level is 9.4, detection of the 6.3 keV x-rays or the conversion electrons is very efficient. Both methods have been used.

The maximum geometrical efficiency for the detection of the backscattered radiation correspond to a 2π steradian solid angle (50%). The earlier "through the detector technique", described in Analytical Chemistry 38, 382R(1966) has this theoretical geometrical efficiency, but the intrinsic detection of the 14.4 keV gamma radiation by the detector greatly lowers its ability to provide good spectra in a short time period. With the commercially available detectors, and using a 45° angle between the incident and scattered radiation, a geometrical efficiency of 10% can be obtained. The spectra of Figures 13 and 14 were obtained using this technique. The cosine effect is large in this configuration, and Figure 15 shows the spectrum of tool steel with a well collimated source. Figure 16 shows the spectrum of the same material in transmission.

The pancake detector described in Section B-2 greatly improved the geometrical efficiency. A photograph of this detector used for scattering is shown in Figure 17. Furthermore, it was possible to insert a 1/2 inch O.D. tube through the detector, without affecting the resolution (see Figure 10). This eliminated the counting of the 14.4 keV gamma radiation as in the "through the detector technique". A point source would be highly desirable for this method and the recently developed ^{57}CoO source [9] will allow this.

The conversion electron detector has 50% geometrical efficiency. Figure 18 shows the spectrum of a steel plate placed inside the pancake detector.

2. Spectra of Steel Samples

Mössbauer spectra of several Standard Reference Material steel samples were obtained to determine whether this method

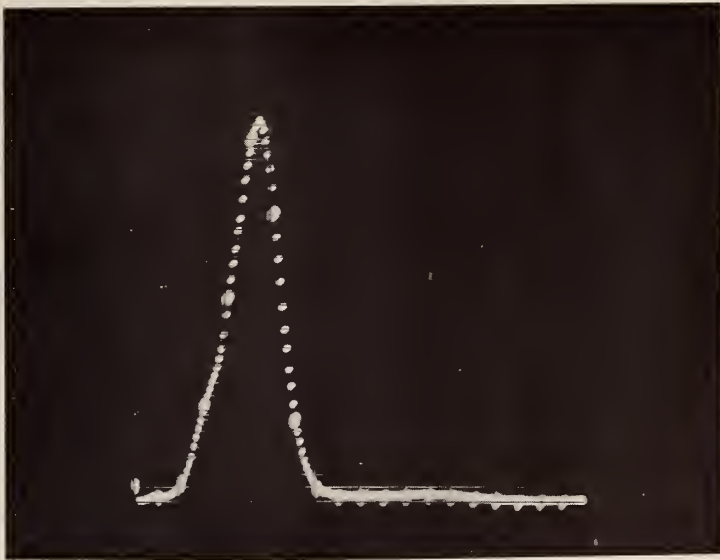


Figure 11. Pulse height spectrum of ^{57}Co source for pancake detector, operating at 1400 volts, with 10% CH_4 90% A flow gas.

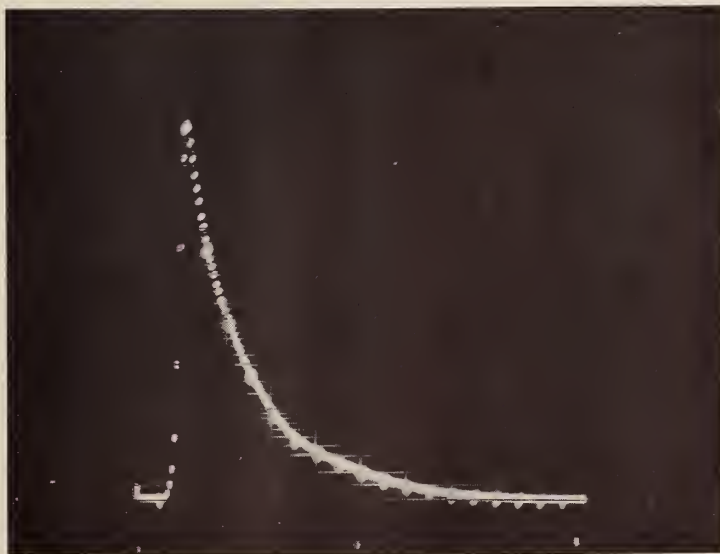


Figure 12. Pulse height spectrum of ^{57}Co source for conversion electrons

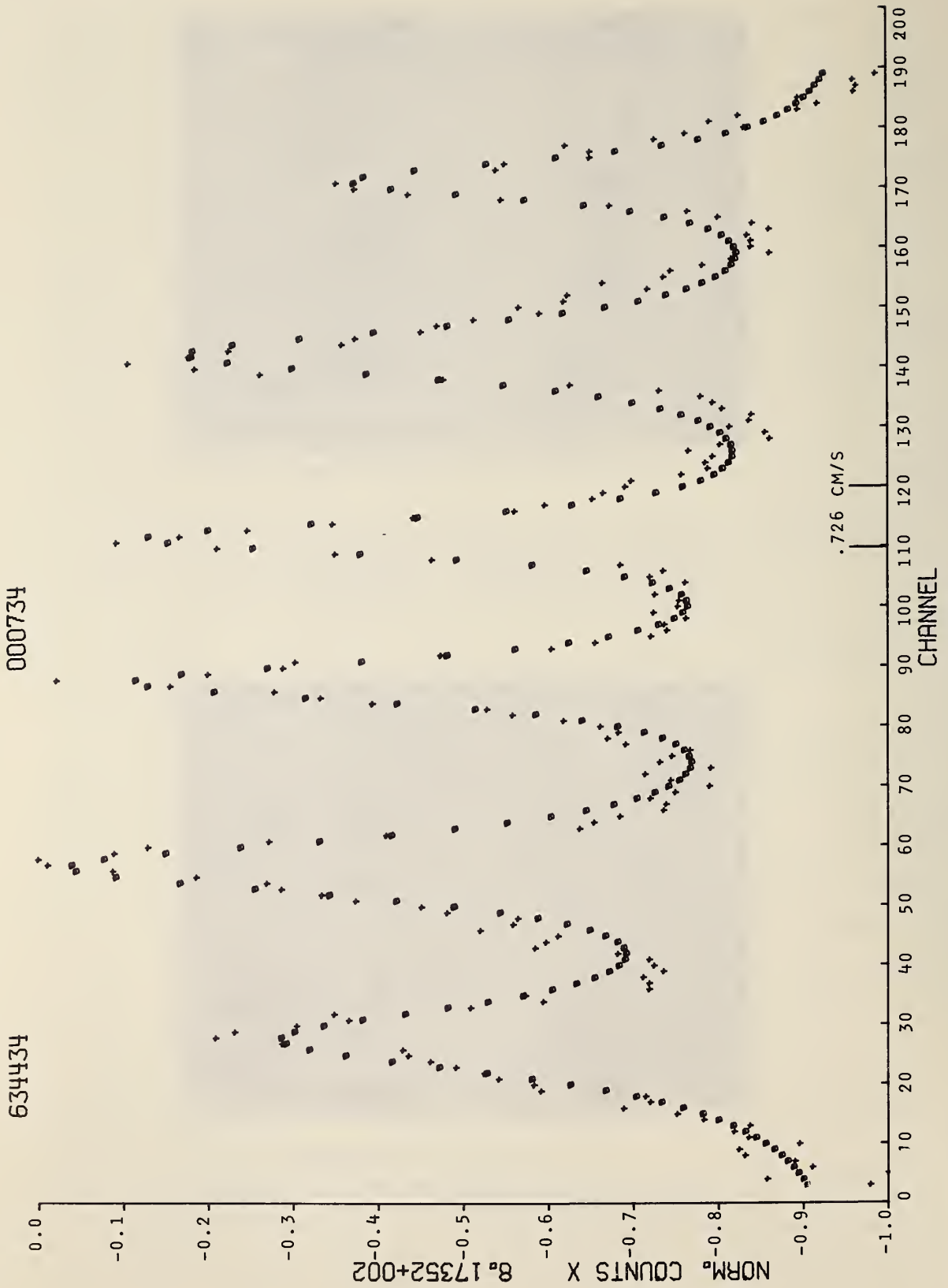


Figure 13. Iron block scattering spectrum

000737

3744228

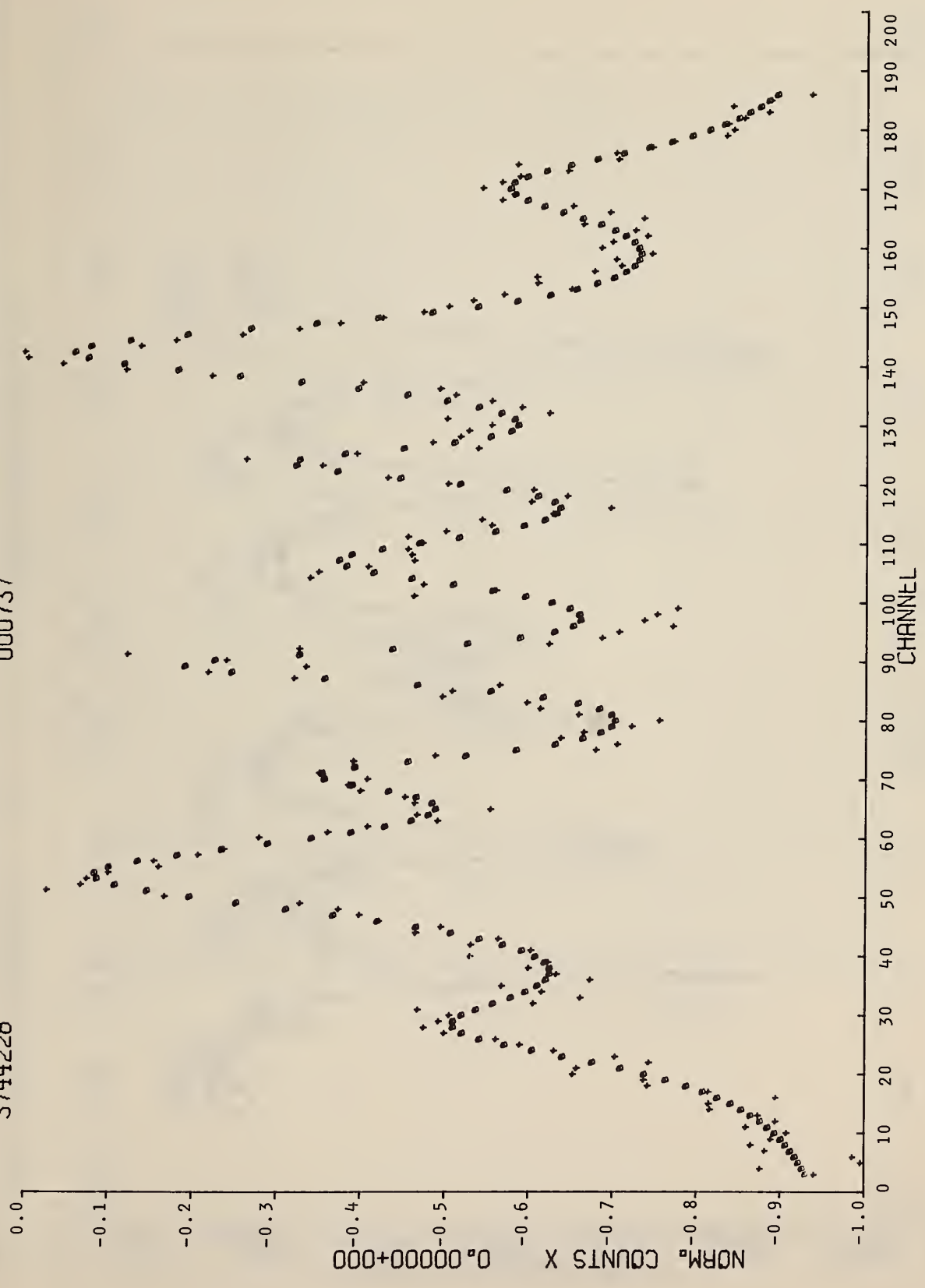


Figure 14. SRM #1174 - white cast iron

BASELINE= 129403

SPECTRUM NO. KS 961

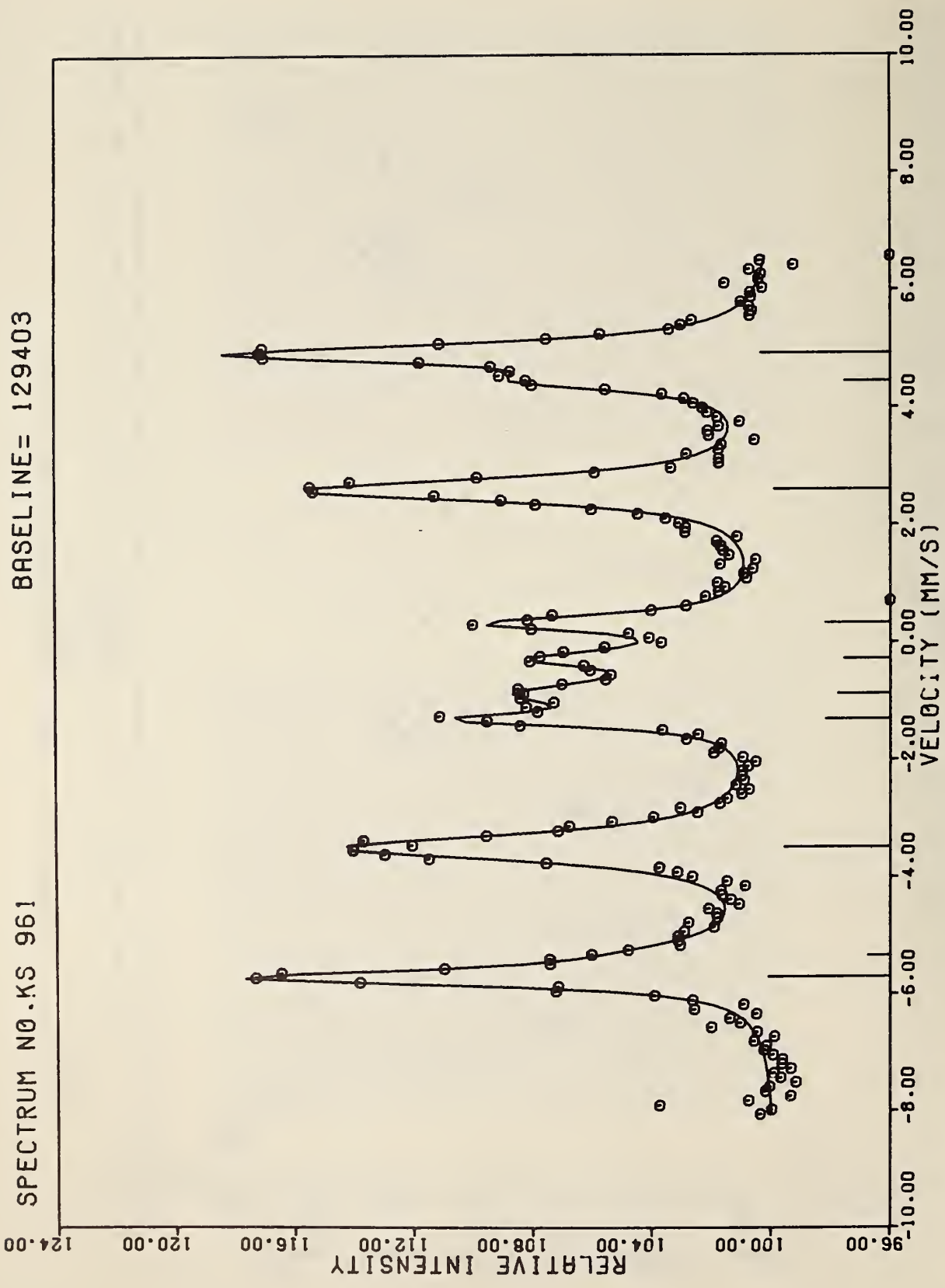


Figure 15. Tool steel (collimated source)

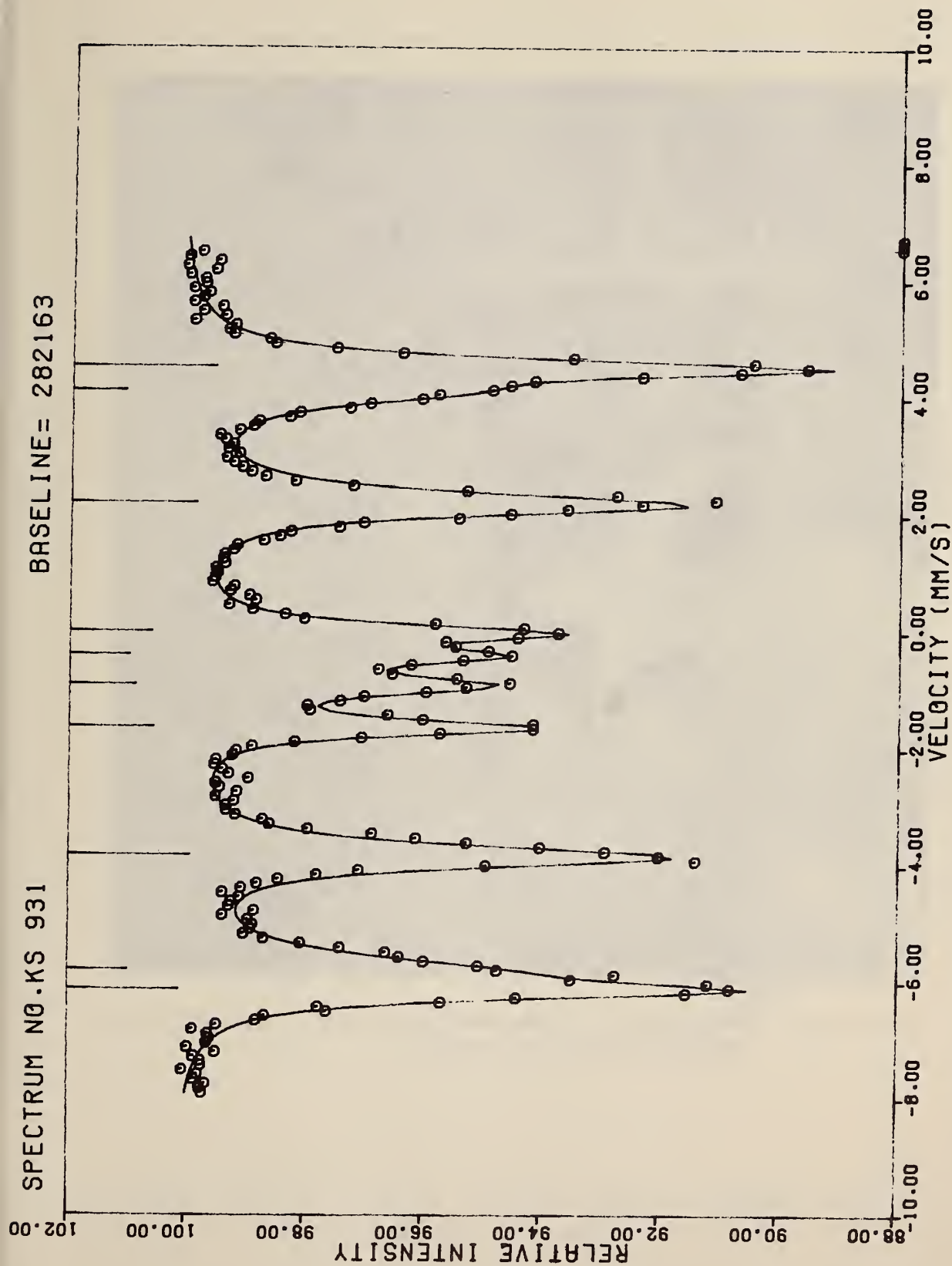


Figure 16. Tool steel (transmission geometry)

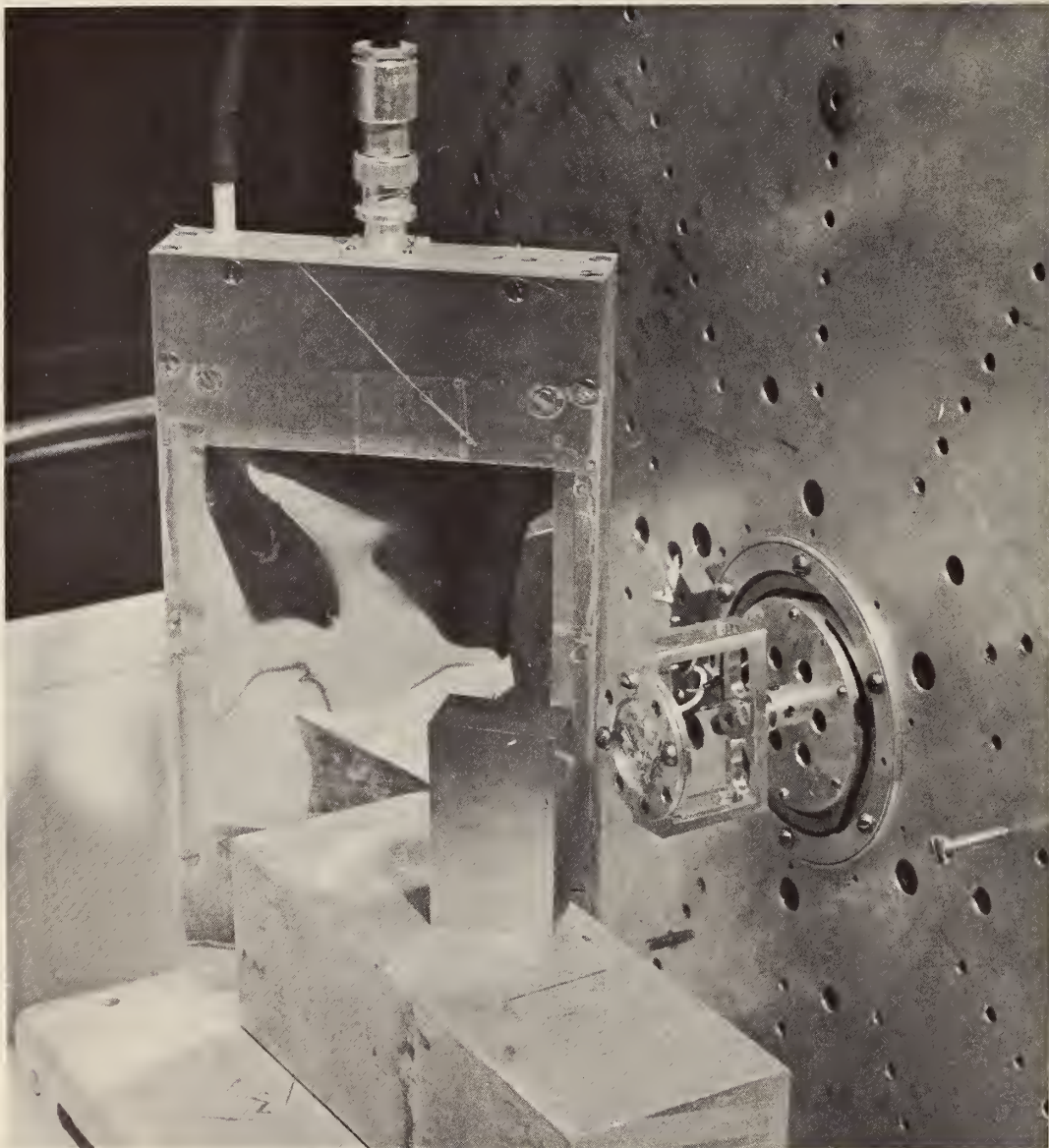


Figure 17. Photograph of pancake detector used for back-scattering at 45° angle.

BASELINE= 404108

SPECTRUM NO. PP 241

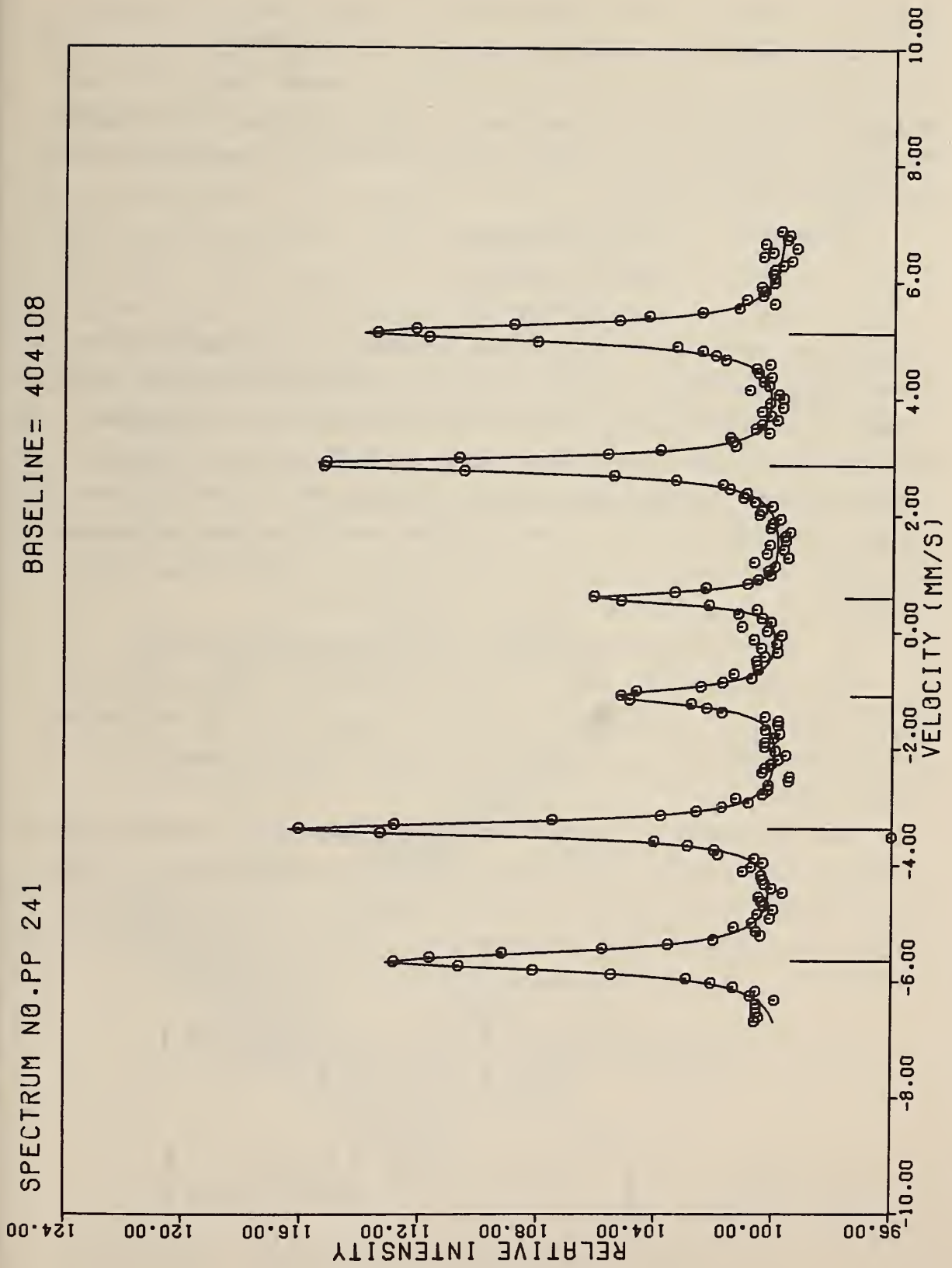


Figure 18. Mössbauer spectrum of steel plate taken by conversion electron detection

could be used to check uniformity of a particular Standard Reference Material. Indications are that it may be an excellent method to check reproducibility of some types of steel. Further studies are in progress. Three samples of Standard Reference Material 1174 were analyzed for the cementite content with the results:

| | |
|----------|-----------------|
| 1174-(a) | 28±6% cementite |
| (b) | 33±6% cementite |
| (c) | 31±6% cementite |

(error is standard deviation of a single determination derived from a least squares analysis of the particular spectrum). The cementite content was obtained from the area peak ratio of the cementite peaks to that of the ferrite peaks, and no correction for the respective f-factors was made. The resolution of the spectra was poor due to cosine smearing and inverse square law effects. Additional applications of this nature will be studied.

3. Effective Penetration of Mössbauer Radiation

The penetration depth of the Mössbauer radiation in a solid sample is critical since it is important to determine whether a surface or a bulk measurement of the sample is being made.

The amplitude of the backscatter Mössbauer signal can be computed in order to evaluate the penetration depth. Ignoring details of the source and the sample to detector solid-angle, the backscatter intensity at zero velocity for a given distance, y , into the sample ($T(y)$) is given as

$$T(y) = \text{Const.} \exp \left\{ \frac{\mu_{14} y}{\sin \phi} \right\} \int_{-\infty}^{\infty} dE \exp \left\{ \frac{-n_a f_a \sigma_{14} y}{\sin \phi} \right\} \cdot$$

$$\frac{1}{E^2 + \Gamma_s^2/4} \int_0^{\pi/2} d\theta \sin \theta \exp \left\{ \frac{-\mu_6 y}{\cos \theta \sin \phi} \right\}$$

where $\sigma_{14} = \frac{\sigma_o \Gamma_s^2}{E^3 + \Gamma_s^2}$ is the corrected cross-section for

resonant absorption and μ_{14} and μ_6 are mass absorption coefficients for 14.4 and 6.3 keV photons, respectively. σ_o is the cross-section for resonant absorption, Γ_s is the full width at half height of the source and E is the energy of transition. The angles are defined in Figure 19. The 14.4 keV gamma rays are collimated to be incident at angle ϕ with respect to the sample surface while the 6.3 keV internal conversion x-rays are emitted in directions making an angle θ with respect to the normal of the sample surface. A similar calculation has recently been carried out by Hershkowitz and Walker [10] in the transmission geometry for studying thin films which are a part of the detector window. The integral

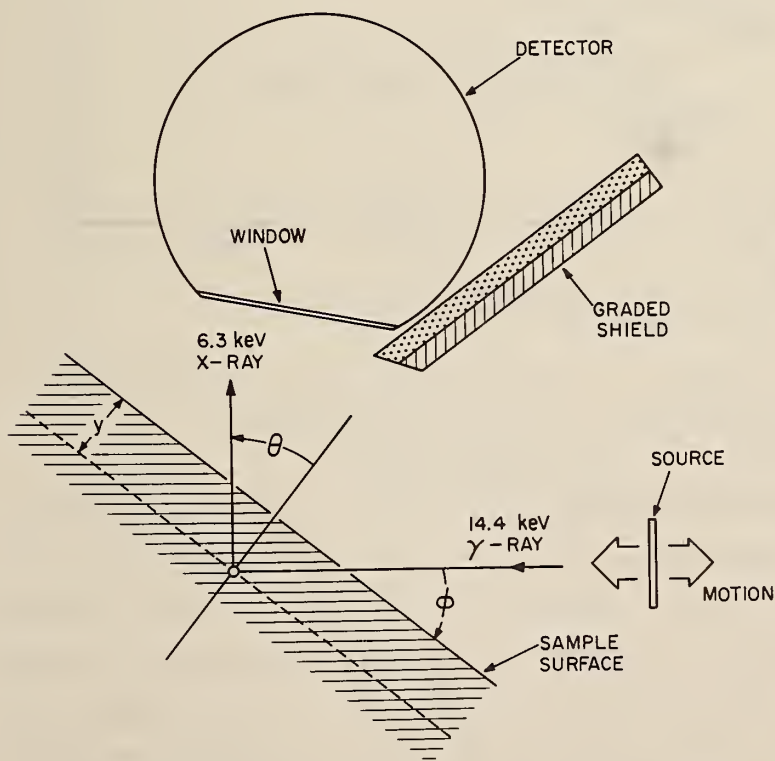


Figure 19. Schematic showing geometry for scattering experiment.

of $T(y)$ e.g. $\int_0^{y_m} T(y)dy$ gives the intensity of 6.3 keV x-rays detected as a function of maximum penetration depth, y_m , into the surface. The results of the calculation are shown in Figure 20. To check the validity of the assumptions, spectra of a stainless steel plate were taken, with 0.22, 0.50 and 0.72 mil thick iron foil placed over the stainless steel plate.

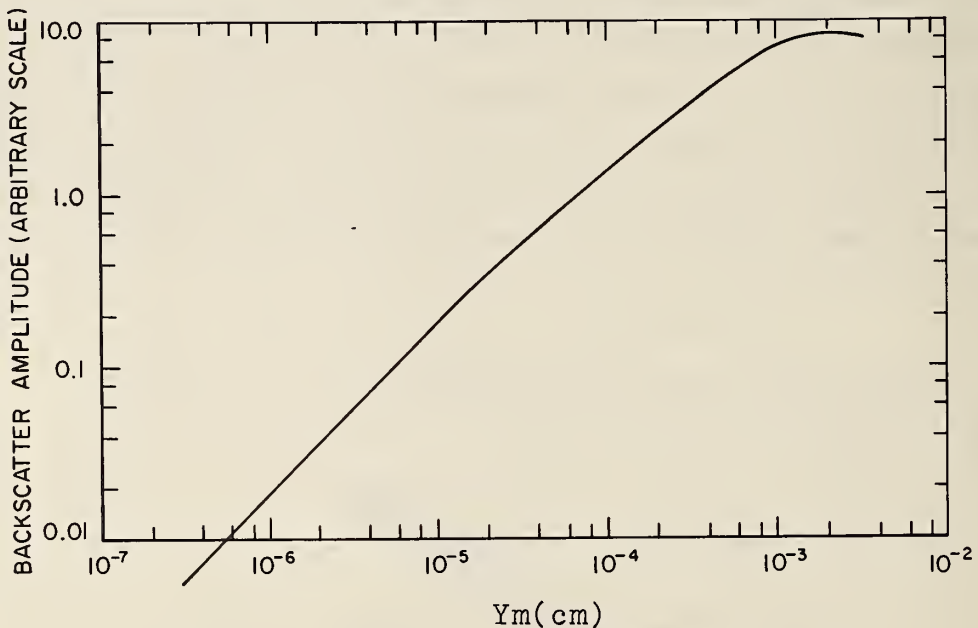


Figure 20. Amount of backscatter as a function of thickness of the scatterers.

Spectra shown in Figures 21, 22 and 23 show $77.8 \pm 2\%$, $93.0 \pm 2\%$, $98 \pm 2\%$ reflection intensity of the stainless steel peak through the 0.22, 0.50 and 0.72 mil iron foil, respectively. The uncertainty reported is approximately two standard deviations. The standard deviation was estimated from the last iteration of a non-linear fitting procedure based on a Taylor series expansion about the estimated values. Agreement with the theoretical calculation for these limited data is satisfactory.

SPECTRUM NO. KS 953

BASELINE= 454781

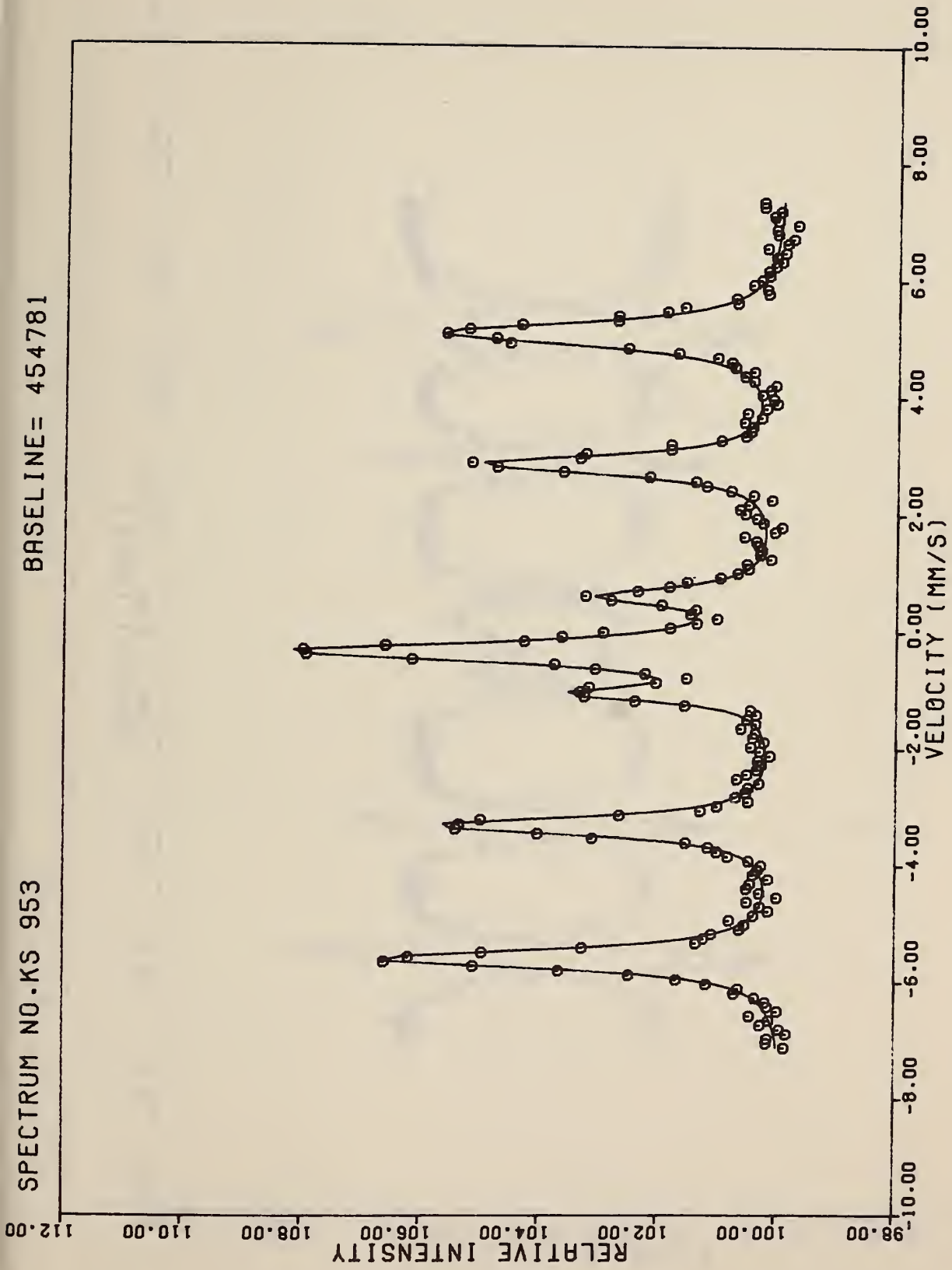


Figure 21. Scattering spectrum of stainless steel with overlay of 0.22 mil iron foil

SPECTRUM NO. KS 950

BASELINE= 637314

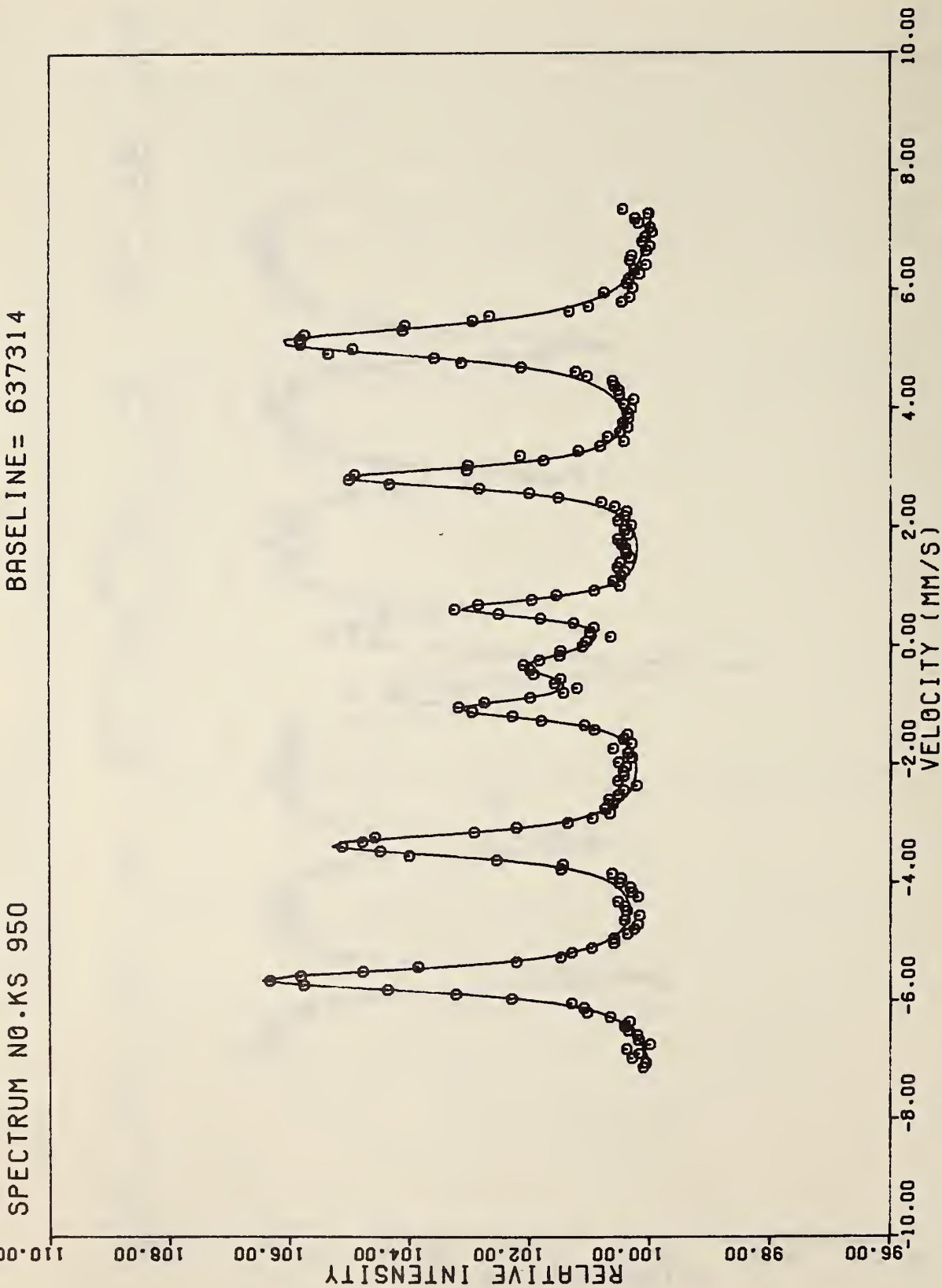


Figure 22. Scattering spectrum of stainless steel with overlay of 0.5 mil iron foil

SPECTRUM NO. KS 952

BASELINE= 647257

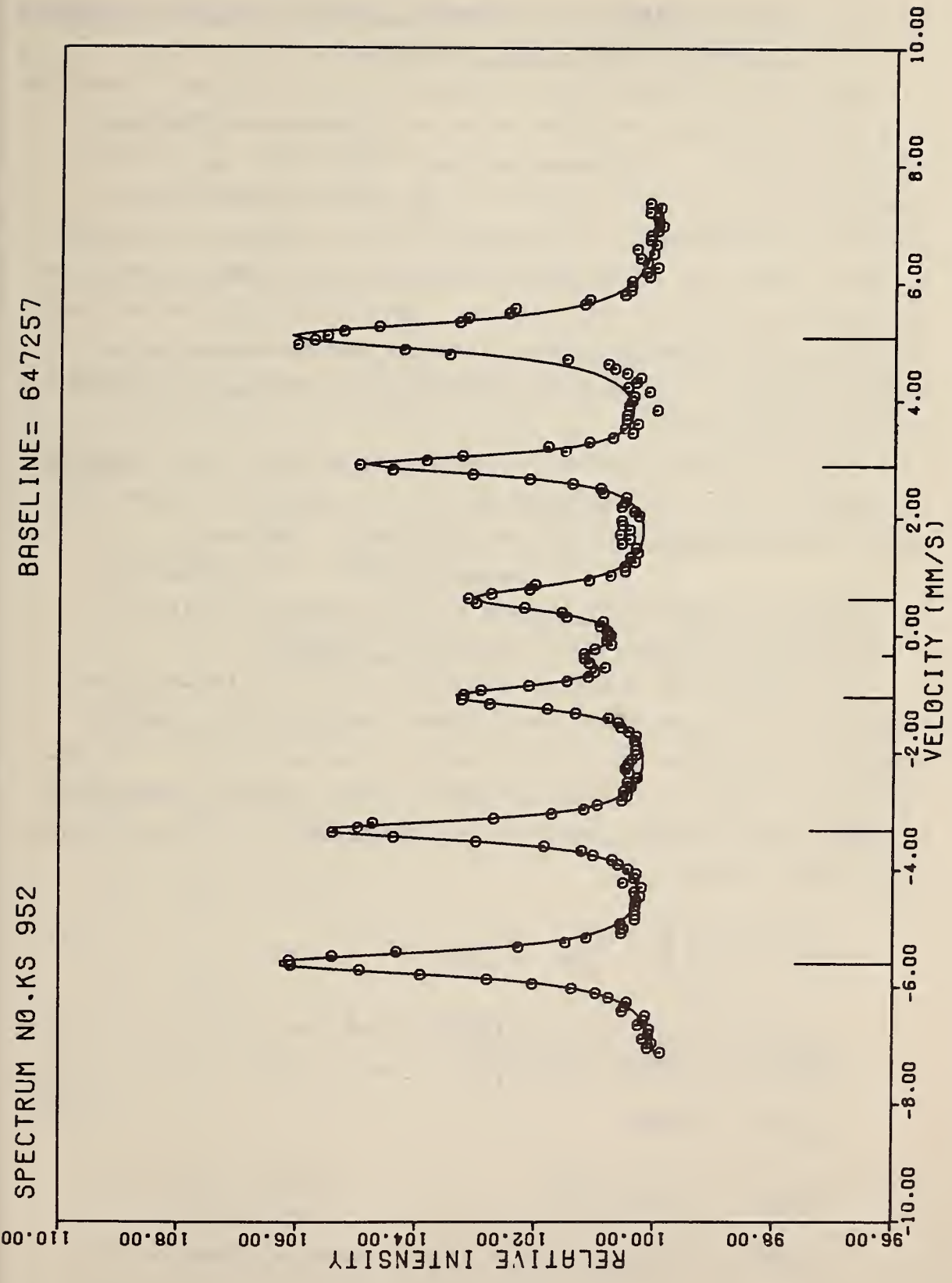


Figure 23. Scattering spectrum of stainless steel with overlay of 0.72 mil iron foil

4. Identification of Corrosion Products on the Surface of Iron by Scattering Techniques

The detection and identification of a compound formation on a steel surface was made using a backscatter Mössbauer effect technique. The compound was identified as β -FeOOH from Mössbauer effect parameters of iron oxide and oxy-hydroxide compounds. An estimate of the compound thickness is given based on a calculation of the backscatter amplitude versus distance into the sample. This technique can be used to identify corrosion products on the surface of iron bearing materials. (To be published in the "Journal of Applied Physics Letters").

Special appreciation is expressed to Dr. J. H. Terrell of Mithras, Inc. for working on the mathematical expression and for providing some of the calibrated samples.

(K. R. Swanson and J. J. Spijkerman)

D. Operator Equivalent Method for the Determination of Orbital Electric Field Gradient Tensors

The method of operator equivalents is a time-honored technique for converting real space operators to angular momentum operators compatible with Dirac notation. The advantage of Dirac notation is that common quantum mechanical integrals may be evaluated by the application of the following relationships:

$$\langle LM' | \hat{O} | LM \rangle \equiv \int_{\tau} \psi_{LM'}^* \hat{O} \psi_{LM} d\tau \quad (1)$$

$$\langle LM' | LM \rangle = \delta_{MM'}, \quad \delta_{ij} = \begin{cases} 0 & \text{if } i \neq j \\ 1 & \text{if } i = j \end{cases} \quad (2)$$

$$\hat{L}_z | LM \rangle = M | LM \rangle \quad (3)$$

$$\hat{L}^2 | LM \rangle = L(L+1) | LM \rangle$$

$$\hat{L}_{\pm} | LM \rangle = (\hat{L}_x \pm i\hat{L}_y) | LM \rangle = \sqrt{(L \mp M)(L \pm M + 1)} | L M \pm 1 \rangle$$

where the operator \hat{O} is a general polynomial in the operators \hat{L}_z , \hat{L}^2 , \hat{L}_+ , and \hat{L}_- . Combining (2) and (3) yields:

$$\langle LM' | \hat{L}_z | LM \rangle = M \delta_{MM'} \quad (4)$$

$$\langle LM' | \hat{L}^2 | LM \rangle = L(L+1) \delta_{MM'}$$

$$\langle LM' | \hat{L}_{\pm} | LM \rangle = \sqrt{(L \mp M)(L \pm M + 1)} \delta_{M'(M \pm 1)}$$

The elements of the electric field gradient (EFG) tensor at the origin due to a charge 'q' located at a point 'x,y,z' are given by the various second partial derivatives of the potential due to the charge.

$$V_{xx} \quad \frac{\partial^2 V}{\partial x^2} = \frac{\partial^2}{\partial x^2} \left(\frac{q}{\sqrt{x^2+y^2+z^2}} \right) = q \left(\frac{3x^2-r^2}{r^5} \right); r = \sqrt{x^2+y^2+z^2}$$

$$V_{yy} = q(3y^2-r^2)/r^5 \quad (5)$$

$$V_{zz} = q(3z^2-r^2)/r^5$$

$$V_{xy} = V_{yx} = 3qxy/r^5$$

$$V_{xz} = V_{zx} = 3qxz/r^5$$

$$V_{yz} = V_{zy} = 3qyz/r^5$$

The more commonly written spherical polar form, e.g.

$V_{zz} = q r^{-3} (3 \cos^2 \theta - 1)$, is readily obtained by substituting

$$x = r \sin \theta \cos \phi \quad (6)$$

$$y = r \sin \theta \sin \phi$$

$$z = r \cos \theta$$

into (5).

When the charge in question is distributed over a wave function, Ψ , the elements of the EFG tensor are given by the expectation values of the point charge expressions.

$$V_{ab} = \int_{\tau} \Psi^* V_{ab} \Psi d\tau \quad a, b = x, y, z$$

$$V_{aa} = q(3 \hat{a}^2 - \hat{r}^2)/r^5 \quad (7)$$

$$V_{ab} = q(3 \hat{a} \hat{b})/r^5$$

In many cases of interest, the wave function is expressed as a linear combination of angular momentum eigenfunctions, having the form

$$\Psi = N \sum_{M=-L}^L C_M \Psi_{LM} \quad (8)$$

$$N = \left(\sum_{M=-L}^L |C_M|^2 \right)^{-1/2}$$

Thus, evaluation of each EFG tensor element may require the performance of as many as L^2 integrations if all of the C_M are non-zero:

$$V_{ab} = |N|^2 \sum_{M'=-L}^L \sum_{M=-L}^L C_{M'}^* C_M \int_{\tau} \Psi_{LM'}^* V_{ab} \Psi_{LM} d\tau \quad (9)$$

For such a case, the desirability of expressing the V_{ab} in terms compatible with Dirac notation is clear.

Stevens [11] and others have shown that, within a manifold of states for which L is constant, [a]

$$\begin{aligned} \hat{x} &= k' \hat{L}_x \\ \hat{y} &= k' \hat{L}_y \\ \hat{z} &= k' \hat{L}_z \\ \hat{r}^2 &= k' \hat{L}^2 \end{aligned} \quad (10)$$

^aThe method is not valid for hybrid orbitals such as sp^3 , since two values of L are involved.

subject to the constraint that the commutation properties of the real space operators be imposed upon their angular momentum counterparts, e.g.,

$$\hat{x} \hat{y} = 1/2k' (\hat{L}_x \hat{L}_y + \hat{L}_y \hat{L}_x) \quad (11)$$

With these substitutions, the EFG operators become

$$\hat{V}_{aa} = k (3 \hat{L}_a^2 - \hat{L}^2), \quad k = k'q\langle r^{-5} \rangle, \quad a,b = x,y,z \quad (12)$$

$$\hat{V}_{ab} = 3 k(\hat{L}_a \hat{L}_b + \hat{L}_b \hat{L}_a)/2.$$

The spherically symmetric r^{-5} may be lumped with the constant without loss of generality. The final form of the operators is obtained with the substitutions

$$\hat{L}_x = (\hat{L}_+ + \hat{L}_-)/2 \quad (13)$$

$$\hat{L}_y = (\hat{L}_+ - \hat{L}_-)/2i$$

to yield

$$\hat{V}_{xx} = k \left[3(\hat{L}_+^2 + \hat{L}_+ \hat{L}_- + \hat{L}_- \hat{L}_+ + \hat{L}_-^2)/4 - \hat{L}^2 \right] \quad (14)$$

$$\hat{V}_{yy} = k \left[-3(\hat{L}_+^2 - \hat{L}_+ \hat{L}_- - \hat{L}_- \hat{L}_+ + \hat{L}_-^2)/4 - \hat{L}^2 \right]$$

$$\hat{V}_{zz} = k \left[3 \hat{L}_z^2 - \hat{L}^2 \right]$$

$$\hat{V}_{xy} = 3k(\hat{L}_+^2 - \hat{L}_-^2)/4i$$

$$\hat{V}_{xz} = 3k(\hat{L}_+ \hat{L}_z + \hat{L}_- \hat{L}_z + \hat{L}_z \hat{L}_+ + \hat{L}_z \hat{L}_-)/4$$

$$\hat{V}_{yz} = 3k(\hat{L}_+ \hat{L}_z - \hat{L}_- \hat{L}_z - \hat{L}_z \hat{L}_+ - \hat{L}_z \hat{L}_-)/4i$$

In order to apply (14) easily, it is convenient to have an additional set of relationships which may be obtained from (3):

$$\hat{L}_{\pm}^2 |LM\rangle = \left[(L \mp M - 1)(L \mp M)(L \pm M + 1)(L \pm M + 2) \right]^{1/2} |LM \pm 2\rangle \quad (15)$$

$$\hat{L}_{\pm} \hat{L}_{\mp} |LM\rangle = (L \pm M)(L \mp M + 1) |LM\rangle = (\hat{L}^2 - \hat{L}_Z^2) |LM\rangle$$

$$\hat{L}_{\pm} \hat{L}_Z |LM\rangle = \left[M (L \mp M)(L \pm M + 1) \right]^{1/2} |L M \pm 1\rangle$$

$$\hat{L}_Z \hat{L}_{\pm} |LM\rangle = (M \pm 1) \left[(L \mp M)(L \pm M + 1) \right]^{1/2} |L M \pm 1\rangle$$

The simplest applications of (14) involve pure hydrogenic orbitals such as d_0 , $d_{\pm 1}$, $d_{\pm 2}$. For instance, the element V_{yy} of EFG tensor for d_0 is given by

$$\begin{aligned} V_{yy} &= \langle 20 | \hat{V}_{yy} | 20 \rangle \quad (16) \\ &= -3k (\langle 20 | \hat{L}_+^2 | 20 \rangle - \langle 20 | \hat{L}_+ \hat{L}_- | 20 \rangle - \langle 20 | \hat{L}_- \hat{L}_+ | 20 \rangle + \\ &\quad \langle 20 | \hat{L}_-^2 | 20 \rangle) / 4 - k (\langle 20 | \hat{L}^2 | 20 \rangle) \\ &= -3k (0 - 6 - 6 + 0) / 4 - k(6) = 3k \end{aligned}$$

In a similar manner, it may be shown that $V_{xx} = 3k$, $V_{zz} = -6k$, and all of the others are zero.

The constant 'k' may best be evaluated by performing one (preferably the simplest) of the integrations. The constant may be found most easily for the d manifold using $\hat{V}_{zz} = q r^{-3} (3 \cos^2 \theta - 1)$ and $d_0 = \sqrt{\frac{5}{16\pi}} (3 \cos^2 \theta - 1)$.

$$\begin{aligned}
\langle 20 | V_{zz} | 20 \rangle &= -\frac{5}{16\pi} \int_0^{2\pi} \int_0^\pi (3 \cos^2 \theta - 1)^3 \sin \theta d\theta d\phi \langle q r^{-3} \rangle \quad (17) \\
&= -(5/8) \langle q r^{-3} \rangle \int_0^\pi (27 \cos^6 \theta - 27 \cos^4 \theta + 9 \cos^2 \theta - 1) \\
&\quad d(\cos \theta) \\
&= (4/7) \langle q r^{-3} \rangle = -6k
\end{aligned}$$

or

$$k = -(2/21) \langle q r^{-3} \rangle \quad (18)$$

The evaluation of 'k' in (18) applies for both one electron 'd' orbitals or many electron 'D' orbitals, since they have the same angular dependence. The difference lies in the radial part of the wave function used for the evaluation of $\langle r^{-3} \rangle$.

In general, the orbitals of interest may be linear combinations of hydrogenic orbitals due to the presence of crystal fields, spin-orbit coupling, or other interactions. It is useful to demonstrate the use of the operator equivalent method for such a case with the "stationary" 'd' orbitals which are 'd' manifold eigenfunctions in the presence of an octahedral, tetrahedral, or square planar field.

$$d_z^2 = d_0 = |20\rangle \quad (19)$$

$$d_{x^2-y^2} = (d_{22} - d_{2-2}) / (i\sqrt{2}) = (|22\rangle - |2-2\rangle) / (i\sqrt{2})$$

$$d_{xy} = (d_{22} + d_{2-2}) / \sqrt{2} = (|22\rangle + |2-2\rangle) / \sqrt{2}$$

$$d_{xz} = (d_{21} - d_{2-1}) / (i\sqrt{2}) = (|21\rangle - |2-1\rangle) / (i\sqrt{2})$$

$$d_{yz} = (d_{21} + d_{2-1}) / \sqrt{2} = (|21\rangle + |2-1\rangle) / \sqrt{2}$$

As a random example, the EFG element V_{xx} for the orbital d_{xz} is given by:

$$\begin{aligned} V_{xx} &= |1/(i\sqrt{2})|^2 (\langle 2\ 1| - \langle 2\ -1|) V_{xx} (|2\ 1\rangle - |2\ -1\rangle) \quad (20) \\ &= 1/2 \left[\langle 2\ 1| V_{xx} |2\ 1\rangle - \langle 2\ 1| V_{xx} |2\ -1\rangle \right. \\ &\quad \left. - \langle 2\ -1| V_{xx} |2\ 1\rangle + \langle 2\ -1| V_{xx} |2\ -1\rangle \right] \end{aligned}$$

Since V_{xx} is a sum of five operators, (20) may be thought of as a sum of twenty terms. However, many terms, such as $\langle 2\ 1| \hat{L}_-^2 |2\ 1\rangle$, may be seen to be zero by inspection, since the 'M' values in the bra and ket must match after the application of the operator. The non-zero terms in (20) are

$$\begin{aligned} V_{xx} &= (k/2) \langle 2\ 1| \left[3(L_+L_- + L_-L_+)/4 - L^2 \right] |2\ 1\rangle - \quad (21) \\ &\quad - \langle 2\ 1| 3L_+^2/4 |2\ -1\rangle - \langle 2\ -1| 3L_-^2/4 |2\ 1\rangle + \langle 2\ -1| \\ &\quad \left[3(L_+L_- + L_-L_+)/4 - L^2 \right] |2\ -1\rangle \\ &= (k/2) \left[3(6+4)/4 - 6 - 3(6)/4 - 3(6)/4 + 3(4+6)/4 - 6 \right] \\ &= -6(k/2) = (2/7) \langle q\ r^{-3} \rangle \end{aligned}$$

In many actual cases, neither the "rotating" orbitals, d_0 , $d_{\pm 1}$, $d_{\pm 2}$, nor the stationary orbitals given in (19) are the eigenfunctions of the Hamiltonian. In such cases, the tabulated values of the EFG tensor elements for the common 'd' orbitals are of no value, and the operator equivalent method is extremely useful in the necessary evaluation.

The operator equivalent method is also convenient for manifolds other than 'd', and for cases in which many electron basis functions should be used. An example of the

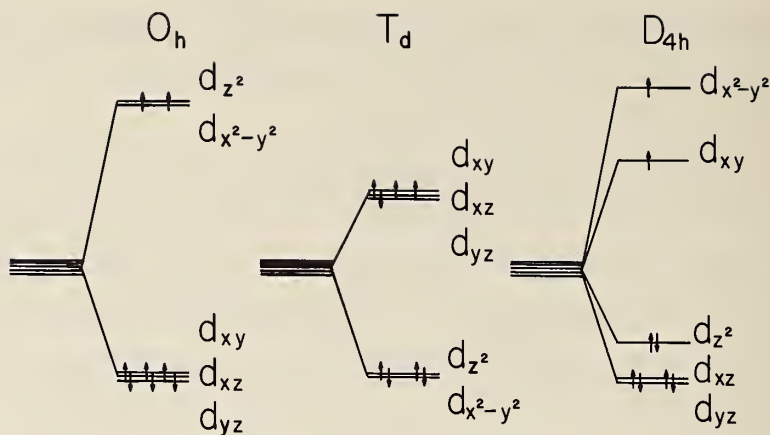
latter is included in the section "⁶¹Ni Theory: EFG Tensor" for an eight-electron problem in which F wave functions (L = 3) are used as a basis set.

In concluding, it is worthwhile to note that the EFG tensor obtained by the method of operator equivalents, as with any other method, is at best a 'first guess'. Before relating the calculations to experimental results, it is necessary to put the EFG tensor into 'standard form', in which the tensor is diagonal, and the elements are ordered such that $|V_{zz}| \geq |V_{yy}| \geq |V_{xx}|$.

E. The Electric Field Gradient Tensor for Common Nickel Configurations

The interpretation of nickel spectra exhibiting a quadrupole interaction requires an understanding of the origin of the electric field gradient tensor. Of the two contributions to the EFG tensor, ligand and 'd' electron, only the latter requires special consideration for ⁶¹Ni. The study presented here concerns only the most common oxidation state of nickel, Ni⁺², and the most common nickel complex configurations, octahedral and tetrahedral. The effect of distortions is considered only qualitatively.

The one electron approximation technique for predicting the EFG tensor has proven quite satisfactory for ⁵⁷Fe Mossbauer spectrometry, and may be extended to nickel by inclusion of the additional electrons. Ni⁺² has a total of eight 3d electrons, whereas Fe⁺² and Fe⁺³ have six and five, respectively. The one electron approximation yields expected EFG elements of zero for Ni⁺² in both octahedral and tetrahedral symmetries, and $V_{zz} = 8/7 \langle q/r^3 \rangle$ (where q is negative), $\eta = 0$ for square planar symmetry. The orbital populations are illustrated in Figure 24 and the EFG contributions are given in Table 7. The presence of a small distortion from tetrahedral symmetry to slightly lift the t_{2g} degeneracy would be expected to produce a non-zero value for V_{zz} .



Electron configuration in Ni²⁺ (3d⁸)

Figure 24. Three common electron configurations for Ni²⁺, using a one-electron Hamiltonian.

Table 7. 3d electron contribution to the EFG elements.

| Orbital | $V_{xx}/\langle qr^{-3} \rangle_d$ | $V_{yy}/\langle qr^{-3} \rangle_d$ | $V_{zz}/\langle qr^{-3} \rangle_d$ |
|---------------|------------------------------------|------------------------------------|------------------------------------|
| d_z^2 | -2/7 | -2/7 | +4/7 |
| $d_x^2 - y^2$ | +2/7 | +2/7 | -4/7 |
| d_{xy} | +2/7 | +2/7 | -4/7 |
| d_{xz} | +2/7 | -4/7 | +2/7 |
| d_{yz} | -4/7 | +2/7 | +2/7 |

The eight electron problem has been solved for the two simpler symmetries for the purposes of comparison with one electron results and the inclusion of spin-orbit coupling. The crystal field theory-energy-level-diagrams for d^8 in octahedral and tetrahedral symmetries with spin-orbit coupling are well documented and are reproduced in Figure 25. However, energy level diagrams alone are not sufficient for

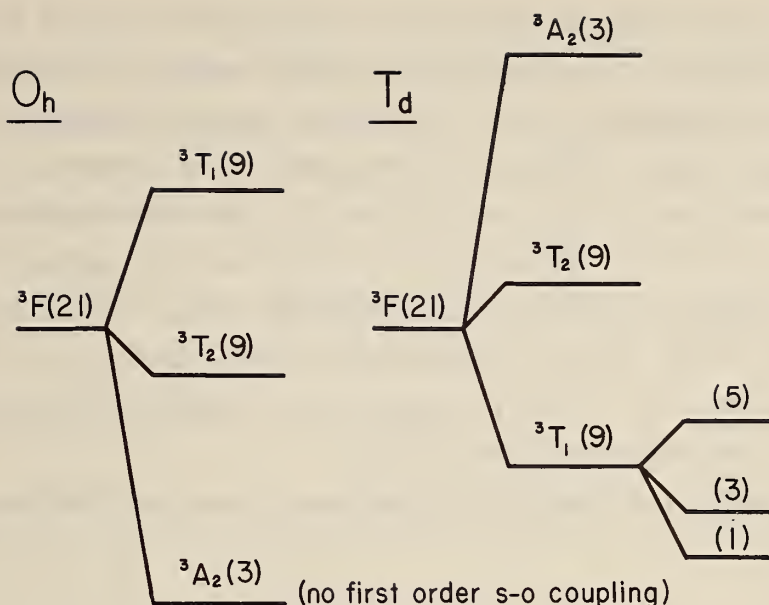


Figure 25. Two common electron configurations for Ni^{2+} , using a many electron Hamiltonian.

the computation of the EFG tensor, and the needed wave functions are less well documented. It is often simpler to perform the calculation than to conduct the necessary literature search. In the present case, the wave functions for octahedral and tetrahedral symmetries in the absence of spin-orbit coupling were easily located in Reference [12]. The calculation of the wave functions with the inclusion of the spin-orbit perturbation is sketched below, as well as the operator equivalent method (Section D) for obtaining the EFG elements once the wave functions are known.

The results of d^2 calculations may be applied to the d^8 problem by recognizing that two "holes" in the 'd' manifold is equivalent to eight electrons, since ten 'd' electrons constitute a full shell. The energy level diagram must be inverted, however, since the holes act like positive electrons. The change from an octahedral to a tetrahedral crystal field results in another inversion of the energy level

diagram, as well as a change in the magnitude of the crystal field splitting. The free ion ground state is known from atomic spectroscopy to be 3F , where the superscript is the spin multiplicity, $2S+1$, and the letter F denotes a total angular momentum of $L=3$ according to spectroscopic notation. The total orbital degeneracy of the free ion ground state is $2L+1=7$, to give a total degeneracy of $3 \times 7 = 21$. The crystal field lifts only orbital degeneracy and yields for the present symmetries two triply degenerate levels (T_1 and T_2) and one singly degenerate level (A_2).

The orbital eigenfunctions are given in Reference [22], p. 393) as:

$$|A_2 0\rangle = \frac{1}{\sqrt{2}} |32\rangle - |3-2\rangle \quad (1)$$

$$|T_1 1\rangle = \frac{1}{2\sqrt{2}} \left[-\sqrt{5}|3-3\rangle - \sqrt{3}|31\rangle \right]$$

$$|T_1 0\rangle = |30\rangle$$

$$|T_1 -1\rangle = \frac{1}{2\sqrt{2}} \left\{ -\sqrt{5}|33\rangle - \sqrt{3}|3-1\rangle \right\}$$

$$|T_2 1\rangle = \frac{1}{2\sqrt{2}} \left\{ \sqrt{3}|33\rangle + \sqrt{5}|3-1\rangle \right\}$$

$$|T_2 0\rangle = \frac{1}{2\sqrt{2}} \left\{ |32\rangle + |3-2\rangle \right\}$$

$$|T_2 -1\rangle = \frac{1}{2\sqrt{2}} \left\{ \sqrt{3}|3-3\rangle + \sqrt{5}|31\rangle \right\}$$

where the numbers in the kets on the right denote the values of L and M_L , respectively. Spin-orbit coupling may be included rigorously by adding the spin-orbit interaction term to the crystal field term of the Hamiltonian and diagonalizing the 21×21 matrix obtained with the set of product basis functions, $LM_L SM_S$. A much simpler way is to consider the effect of a spin-orbit perturbation on the lowest crystal

field level alone. This approach is justified by first order perturbation theory for cases in which the crystal field splitting is much larger than the spin-orbit splitting.

For the case of an octahedral crystal field, the ground state orbitals are:

$$|A_2 0, S M_S\rangle \equiv |A_2 0\rangle |S M_S\rangle = \frac{1}{\sqrt{2}} \{ |3 2\rangle - |3 -2\rangle \} |S M_S\rangle = 1, \quad (2)$$

$$M_S = -1, 0, 1.$$

The spin-orbit term of the Hamiltonian may be expressed as:

$$\lambda \hat{L} \cdot \hat{S} = \lambda \hat{L}_Z \hat{S}_Z + 1/2 (\hat{L}_+ \hat{S}_- + \hat{L}_- \hat{S}_+) \quad (3)$$

where the operators \hat{S}^2 , \hat{S}_Z , \hat{S}_+ , and \hat{S}_- obey the same rules with respect to the kets $|S M_S\rangle$ as do the operators \hat{L}^2 , etc., with respect to the kets $|L M_L\rangle$. (See Equation 3, Section D). Adopting the simplified notation

$$|M_L, M_S\rangle \equiv |L M_L\rangle |S M_S\rangle \quad (4)$$

(since $L = 3$ and $S = 1$ throughout the problem), it may easily be verified that

$$\hat{L}_Z \hat{S}_Z |M_L, M_S\rangle = M_L M_S |M_L, M_S\rangle \quad (5)$$

$$\hat{L}_\pm \hat{S}_\mp |M_L, S\rangle = \left[(L_\mp M_L) (L_\pm M_L + 1) (S_\pm M_L) (S_\mp M_L + 1) \right]^{1/2} |M_L \pm 1, M_S \mp 1\rangle$$

The matrix elements of the spin-orbit Hamiltonian over the ground state orbitals are then given by:

$$\begin{aligned}
\lambda \langle A_2 0, 1 M_S' | \hat{L} \cdot \hat{S} | A_2 0, 1 M_S \rangle &= \quad (6) \\
&= 1/2 \lambda \langle 2, M_S | \hat{L} \cdot \hat{S} | 2, M_S \rangle - \langle 2, M_S | \hat{L} \cdot \hat{S} | -2, M_S \rangle \\
&\quad - \langle -2, M_S | \hat{L} \cdot \hat{S} | 2, M_S \rangle + \langle -2, M_S | \hat{L} \cdot \hat{S} | -2, M_S \rangle \\
&= 1/2 \lambda \begin{bmatrix} 2M_S & -0 & -0 & -2M_S \end{bmatrix} = 0
\end{aligned}$$

In other words, the low lying level for octahedral symmetry experiences no spin-orbit coupling, to first order.

The spin-orbit problem need not be repeated for the higher lying energy levels before computing the EFG tensor elements because kT is much smaller than the crystal field splitting in general. Thus the relative Boltzmann population of the higher levels is negligibly small. The EFG tensor for the system is then the Boltzmann average of the EFG tensors for the three states of the low lying level, and, since the states are degenerate, the Boltzmann weighting factors are equal.

The EFG tensors for the three states may be found by using the method of operator equivalents discussed in Section D. Thus, the element V_{zz} for the state $|A_2 0, 1 1\rangle$ is given by:

$$\begin{aligned}
V_{zz} &= \langle A_2 0, 1 1 | \hat{V}_{zz} | A_2 0, 1 1 \rangle \quad (7) \\
&= 1/2 \langle 2, 1 | \hat{V}_{zz} | 2, 1 \rangle - \langle -2, 1 | \hat{V}_{zz} | 2, 1 \rangle - \langle 2, 1 | \hat{V}_{zz} | -2, 1 \rangle + \\
&\quad \langle -2, 1 | \hat{V}_{zz} | -2, 1 \rangle \} \\
&= 1/2 \{ 3(2)^2 - 3 \times 4 - 0 - 0 + 3(2)^2 - 3 \times 4 \} = 0
\end{aligned}$$

Since the orbital portion of the wave function is the same for all three states, the same result obtains for $|A_2 0, 1 -1\rangle$

and $|A_{20,1} 0\rangle$. In a similar manner, the other EFG elements may also be shown to be zero, and the elements of the total EFG tensor are thus zero as well, in agreement with the one-electron result.

The spin-orbit coupling problem is considerably lengthier for the case of tetrahedral symmetry, since the low lying 3T_1 level is nine-fold degenerate. The Hamiltonian matrix, obtained in a manner similar to Equation (6), is given in Table 8, with the states arranged so as to make "blocking" of the matrix convenient. Upon diagonalizing the five submatrices, the eigenvalues and eigenvectors indicated in Table 9 are determined.

The EFG elements for the system are given by the Boltzmann average of the EFG elements for the nine states. Before taking the Boltzmann average, however, it is convenient to compute the EFG elements for each of the spin-orbit energy levels, since the Boltzmann factor is the same for each state within an energy level. The EFG elements for each state may be easily obtained by the method of operator equivalents, and the resulting diagonal elements are shown in Table 10; the off-diagonal elements were all zero. It is obvious from the table that the total values of the diagonal EFG elements for each of the three energy levels are all zero. Thus the Boltzmann average is zero also for each element, in accord again with the one electron result.

It is interesting to note that the individual states within the three-fold and five-fold degenerate levels have non-zero EFG elements. This means that a small distortion to lift the degeneracies would be expected to yield a non-zero Boltzmann average, again consistent with the one electron result. Such is not the case for octahedral symmetry, since the individual states have zero EFG elements.

(John C. Travis)

Table 8. Hamiltonian Matrix for the $\lambda L \cdot S$ Perturbation on 3T_1

| | $ A\rangle$ | $ B\rangle$ | $ C\rangle$ | $ D\rangle$ | $ E\rangle$ | $ F\rangle$ | $ G\rangle$ | $ H\rangle$ | $ I\rangle$ |
|--------------|---------------|---------------|---------------|---------------|---------------|---------------|---------------|---------------|---------------|
| $\langle A $ | $-3\lambda/2$ | 0 | 0 | 0 | 0 | 0 | 0 | 0 | 0 |
| $\langle B $ | 0 | 0 | $-3\lambda/2$ | 0 | 0 | 0 | 0 | 0 | 0 |
| $\langle C $ | 0 | $-3\lambda/2$ | 0 | 0 | 0 | 0 | 0 | 0 | 0 |
| $\langle D $ | 0 | 0 | 0 | $3\lambda/2$ | $-3\lambda/2$ | 0 | 0 | 0 | 0 |
| $\langle E $ | 0 | 0 | 0 | $-3\lambda/2$ | 0 | $-3\lambda/2$ | 0 | 0 | 0 |
| $\langle F $ | 0 | 0 | 0 | 0 | $-3\lambda/2$ | $3\lambda/2$ | 0 | 0 | 0 |
| $\langle G $ | 0 | 0 | 0 | 0 | 0 | 0 | 0 | $-3\lambda/2$ | 0 |
| $\langle H $ | 0 | 0 | 0 | 0 | 0 | 0 | $-3\lambda/2$ | 0 | 0 |
| $\langle I $ | 0 | 0 | 0 | 0 | 0 | 0 | 0 | 0 | $-3\lambda/2$ |

$$\begin{aligned}
 |A\rangle &= |T_1^1, 1, 1\rangle & |D\rangle &= |T_1^1, 1, -1\rangle & |G\rangle &= |T_1^0, -1, 1\rangle \\
 |B\rangle &= |T_1^1, 1, 0\rangle & |E\rangle &= |T_1^0, 1, 0\rangle & |H\rangle &= |T_1^{-1}, 1, 0\rangle \\
 |C\rangle &= |T_1^0, 1, 1\rangle & |F\rangle &= |T_1^{-1}, 1, 1\rangle & |I\rangle &= |T_1^{-1}, 1, -1\rangle
 \end{aligned}$$

Table 9. Spin-orbit perturbation results for the 3T_1 level of 3F in T_d symmetry

| | | Eigenvector Coefficients** | | | | | | | | | | | | | | | | | | | | | |
|-------|---------------|--|-------------|-------------|-------------|----|----|--------------|------------|--------------|---|--------------|------------|--------------|------------|---|---|-------------|---|-------------|---|-------------|--------------|
| | | eigenvector = $\sum_{M_L, M_S} A(M_L, M_S) M_L, M_S$ | | | | | | | | | | | | | | | | | | | | | |
| State | Eigenvalue | $M_L=-3$ | $M_S=-1$ | -3 | -3 | -1 | -1 | -1 | -1 | 0 | 0 | 0 | 0 | 1 | 1 | 1 | 1 | 1 | 3 | 3 | 3 | 3 | |
| a1 | 3λ | $\sqrt{10}$ | 0 | 0 | 0 | 0 | 0 | 0 | $\sqrt{6}$ | 0 | 4 | 0 | $\sqrt{6}$ | 0 | 0 | 0 | 0 | 0 | 0 | 0 | 0 | 0 | $\sqrt{10}$ |
| b1 | $3\lambda/2$ | 0 | $\sqrt{15}$ | 0 | 0 | 0 | 0 | 0 | 0 | 0 | 0 | $\sqrt{24}$ | 0 | $\sqrt{24}$ | 0 | 3 | 0 | 0 | 0 | 0 | 0 | 0 | 0 |
| b2 | $3\lambda/2$ | 0 | 0 | 0 | 0 | 3 | 0 | $\sqrt{24}$ | 0 | $\sqrt{24}$ | 0 | 0 | 0 | 0 | 0 | 0 | 0 | 0 | 0 | 0 | 0 | $\sqrt{15}$ | 0 |
| b3 | $3\lambda/2$ | $\sqrt{15}$ | 0 | 0 | 0 | 0 | -3 | 0 | 0 | 0 | 0 | 0 | 0 | 0 | 3 | 0 | 0 | 0 | 0 | 0 | 0 | 0 | $-\sqrt{15}$ |
| c1 | $-3\lambda/2$ | 0 | 0 | $\sqrt{30}$ | 0 | 0 | 0 | 0 | 0 | 0 | 0 | 0 | 0 | 0 | 0 | 0 | 0 | $\sqrt{18}$ | 0 | 0 | 0 | 0 | 0 |
| c2 | $-3\lambda/2$ | 0 | 0 | 0 | $\sqrt{18}$ | 0 | 0 | 0 | 0 | 0 | 0 | 0 | 0 | 0 | 0 | 0 | 0 | 0 | 0 | $\sqrt{30}$ | 0 | 0 | 0 |
| c3 | $-3\lambda/2$ | 0 | $\sqrt{15}$ | 0 | 0 | 0 | 0 | 0 | 0 | 0 | 0 | $-\sqrt{24}$ | 0 | $-\sqrt{24}$ | 0 | 3 | 0 | 0 | 0 | 0 | 0 | 0 | 0 |
| c4 | $-3\lambda/2$ | 0 | 0 | 0 | 0 | 3 | 0 | $-\sqrt{24}$ | 0 | $-\sqrt{24}$ | 0 | 0 | 0 | 0 | 0 | 0 | 0 | 0 | 0 | 0 | 0 | $\sqrt{15}$ | 0 |
| c5 | $-3\lambda/2$ | $\sqrt{5}$ | 0 | 0 | 0 | 0 | 0 | $\sqrt{3}$ | 0 | $-\sqrt{32}$ | 0 | $-\sqrt{32}$ | 0 | 0 | $\sqrt{3}$ | 0 | 0 | 0 | 0 | 0 | 0 | 0 | $\sqrt{5}$ |

* λ is negative, since the shell is more than half full.

** The functions for $M_L=\pm 2$ are not present in 3T_1 . The eigenvectors may be normalized by dividing the coefficients by $\sqrt{48}$.

Table 10. EFG elements for the low lying states of Ni with T_d coordination

| State | $V_{xx} / \langle qr^{-3} \rangle F$ | $V_{yy} / \langle qr^{-3} \rangle F$ | $V_{zz} / \langle qr^{-3} \rangle F$ |
|-------|--------------------------------------|--------------------------------------|--------------------------------------|
| a1 | 0 | 0 | 0 |
| b1 | -1/15 | -1/15 | 2/15 |
| b2 | -1/15 | -1/15 | 2/15 |
| b3 | 2/15 | 2/15 | -4/15 |
| c1 | 2/15 | 2/15 | -4/15 |
| c2 | 2/15 | 2/15 | -4/15 |
| c3 | -1/15 | -1/15 | 2/15 |
| c4 | -1/15 | -1/15 | 2/15 |
| c5 | -2/15 | -2/15 | 4/15 |

F. ^{61}Ni Theory: Nuclear Interactions

The calculation of the nuclear interactions for ^{61}Ni is straightforward and proceeds in exactly the same manner as the corresponding calculations for ^{57}Fe with the single exception that the excited and ground nuclear states have spins 5/2 and 3/2, respectively. The familiar interaction Hamiltonians are recorded here for correlation with Figure 26 which shows the energy level diagrams:

$$\hat{H}_M = -g\beta_n \hat{H} \hat{I}_z \quad (1)$$

$$\hat{H}_Q = A(3\hat{I}_z^2 - \hat{I}^2), \quad A = eQV_{zz}/40$$

$$\hat{H}'_M = \hat{H}_M \cos \theta$$

$$\hat{H}'_Q = \hat{H}_Q(3 \cos^2 \theta - 1)/2$$

where g is the magnetogyric (gyromagnetic) ratio, β_n is the nuclear magneton, Q is the nuclear quadrupole moment, and V_{zz} is an element of the electric field gradient (EFG) tensor (discussed in Section E). The primed Hamiltonians are perturbation Hamiltonians, with θ being the angle between the principal quantization axes of the zeroth order and the perturbing interactions. The quadrupolar Hamiltonians in (1) and Figure 26 are for the special case in which the EFG elements V_{xx} and V_{yy} are equal.

The determination of the relative magnitudes of the magnetic and quadrupolar interactions in the ground and excited states is best done experimentally. The determination of the magnetic moment ratio was discussed in NBS Technical Note 421 [2]. The latest value determined at NBS for this ratio is $\mu_e/\mu_g = -0.56 \pm 0.082$.* As for the quadrupolar interactions,

*The uncertainty reported is approximately two standard deviations. The standard deviation was estimated from the last iteration of a non-linear fitting procedure on a Taylor series expansion about the estimated values.

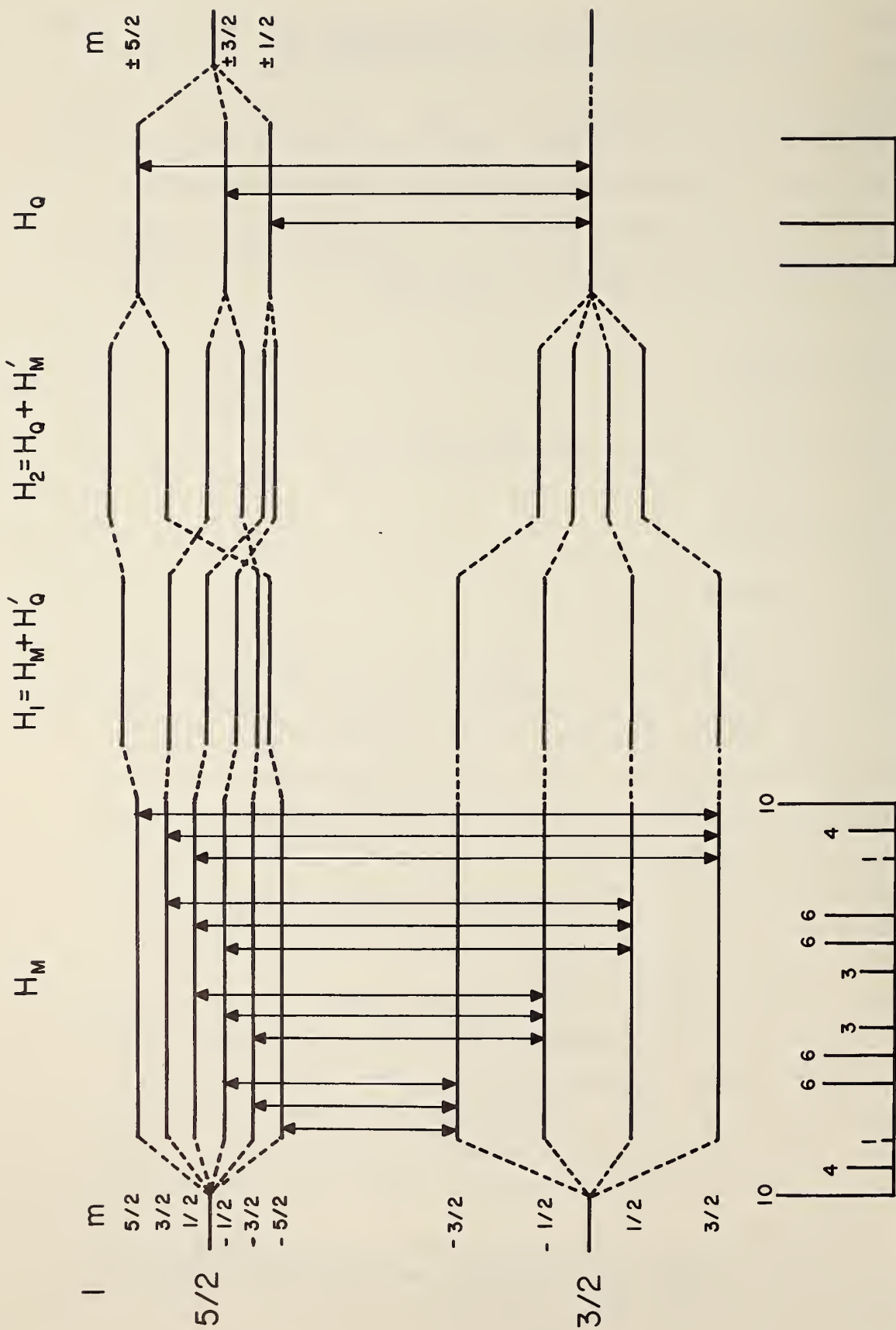


Figure 26. The effect of magnetic, quadrupole, and mixed perturbations of the Mössbauer levels of the ^{61}Ni nucleus

Table 11. Quadrupole Hamiltonian matrix for the spin 5/2 state

| | $ \frac{5}{2} \frac{5}{2}\rangle$ | $ \frac{5}{2} \frac{-5}{2}\rangle$ | $ \frac{5}{2} \frac{3}{2}\rangle$ | $ \frac{5}{2} \frac{-1}{2}\rangle$ | $ \frac{5}{2} \frac{-3}{2}\rangle$ | $ \frac{5}{2} \frac{1}{2}\rangle$ |
|--------------------------------------|-----------------------------------|------------------------------------|-----------------------------------|------------------------------------|------------------------------------|-----------------------------------|
| $\langle \frac{5}{2} \frac{5}{2} $ | 10 A | 0 | 0 | 0 | 0 | $\sqrt{10}\eta A$ |
| $\langle \frac{5}{2} \frac{3}{2} $ | 0 | 10 A | 0 | $\sqrt{10}\eta A$ | 0 | 0 |
| $\langle \frac{5}{2} \frac{-1}{2} $ | 0 | 0 | -2 A | $\sqrt{18}\eta A$ | 0 | 0 |
| $\langle \frac{5}{2} \frac{-3}{2} $ | 0 | $\sqrt{10}\eta A$ | $\sqrt{18}\eta A$ | -8 A | 0 | 0 |
| $\langle \frac{5}{2} \frac{1}{2} $ | $\sqrt{10}\eta A$ | 0 | 0 | 0 | -2 A | $\sqrt{18}\eta A$ |
| | | | | | $\sqrt{18}\eta A$ | -8 A |

preliminary results confirm the indication from NMR work [13] that the ground state quadrupole moment is essentially zero for purposes of Mössbauer spectroscopy.

The indicated intensities shown in the line spectra in Figure 26 are for a powdered sample, and are obtained from the squares of appropriate Clebsch-Gordon coefficients, as discussed in Technical Note 421 [2]. The intensity calculations are much more complicated for the Hamiltonians H_1 and H_2 , as well as for the quadrupolar Hamiltonian for the case in which $V_{xx} \neq V_{yy}$, but may be performed by the method of Reference [14] once the eigenvectors are known.

For the general quadrupolar interaction case of $V_{xx} \neq V_{yy}$, the Hamiltonian becomes

$$H_A = A \left[3I_z^2 - I^2 + \eta(I_+^2 + I_-^2)/2 \right], \quad \eta = \frac{V_{xx} - V_{yy}}{V_{zz}} \quad (2)$$

The Hamiltonian matrix for the spin 5/2 excited state is shown in Table 11. The reason for the arbitrary ordering of rows and columns will become evident. The elements of value $\sqrt{10}\eta A$ tend to mix the $\pm 1/2$ states with the $\pm 5/2$ states, while the elements of value $\sqrt{18}\eta A$ tend to mix $\pm 3/2$ with $\pm 1/2$ states. According to second order perturbation theory, the latter mixing has the most influence on the energy levels by a factor of roughly $(\sqrt{18/10})(18A/6A)$, or approximately 5.4. Therefore, a crude approximation to the η -dependence of the energy levels may be obtained by ignoring the smaller mixing terms and diagonalizing only the blocked out sub-matrices of Table 11. This procedure yields the approximate eigenvalues and eigenvectors:

$$E(\pm 5/2) = 10 A, \quad |\pm 5/2\rangle' = |\pm 5/2\rangle$$

$$E(\pm 3/2) = A(-5 + 3\sqrt{1+2\eta^2}), \quad |\pm 3/2\rangle' = N_+ [|1/2\rangle - \lambda_+ |\pm 3/2\rangle]$$

$$E(\pm 1/2) = A(-5 - 3\sqrt{1+2\eta^2}), \quad |\pm 1/2\rangle' = N_- [|\pm 1/2\rangle - \lambda_- |\pm 3/2\rangle]$$

$$\lambda_{\pm} = \frac{\sqrt{1+2\eta^2} \pm 1}{2\eta}, \quad N_{\pm} = [1 + \lambda_{\pm}^2]^{-1/2}$$

The accuracy of the approximation may be checked by noting that the three lines approach a very nearly symmetrical arrangement for $\eta=1$, as expected.

The behavior of the quadrupole spectrum as a function of asymmetry parameter is illustrated in Figure 27 for a more accurate, although less convenient, set of eigenvalues than given in (3). As of the present, only small quadrupolar interactions have been observed (see Ref. [15]), and no asymmetry parameters effects have been observed.

(J. C. Travis and J. J. Spijkerman)

G. Standard Reference Material for the Chemical Shift of Tin Compounds

Work in progress to develop a Mössbauer chemical shift standard for ^{119}Sn , described in Technical Note 421 [2] has been primarily focused on BaSnO_3 . This material is stable in air, and exhibits no long term chemical and physical changes which affect the Mössbauer spectrum. The spectrum shown in Figure 28 shows a narrow, well defined singlet, with a large Mössbauer effect. Several attempts to obtain single crystals of this material failed. Encapsulation of BaSnO_3 in plastic did not affect the spectrum, and a 2% uniform distribution could be obtained. Several absorbers with BaSnO_3 concentration from 5.0 mg/cm² up to 250 mg/cm² were analyzed, using a 3 mCi Pd_3Sn source, for percent effect, line width and γ radiation attenuation. The percent effect and attenuation are shown in Figure 29. These results in-

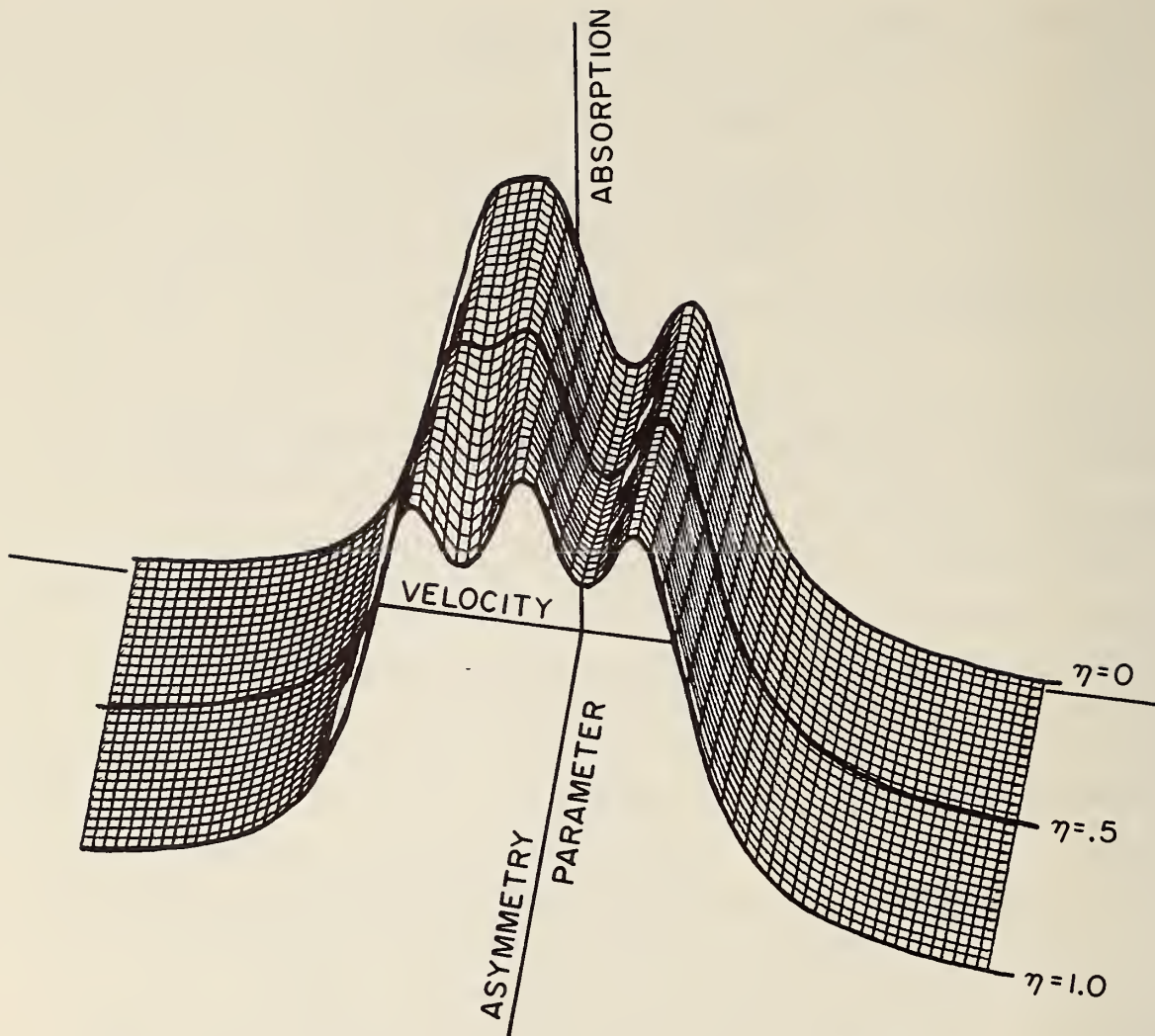


Figure 27. Quadrupole spectrum as a function of η

indicate that a 100 mg/cm^2 concentration is most desirable, for a maximum Mössbauer resonance absorption without excessive attenuation. Extrapolation to zero thickness gave a line width of $0.79 \pm 4\%$ mm/sec and $0.85 \pm 4\%$ mm/sec* for a

*The uncertainty reported is approximately two standard deviations. The standard deviation was estimated from the last iteration of a non-linear fitting procedure on a Taylor series expansion about the estimated values.

BASELINE= 793613

SPECTRUM NO. PP0214

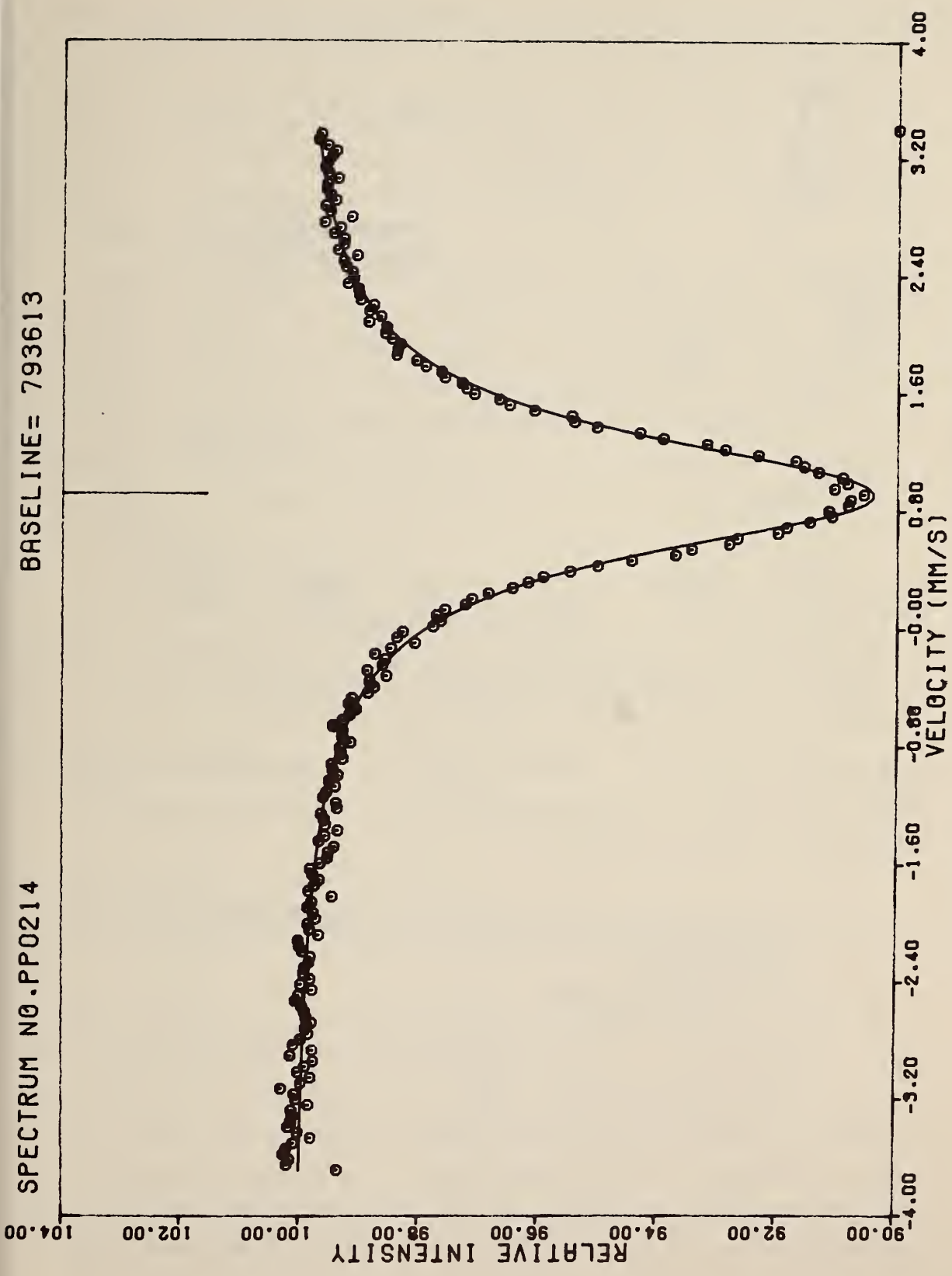


Figure 28. Transmission spectrum of BaSnO₃

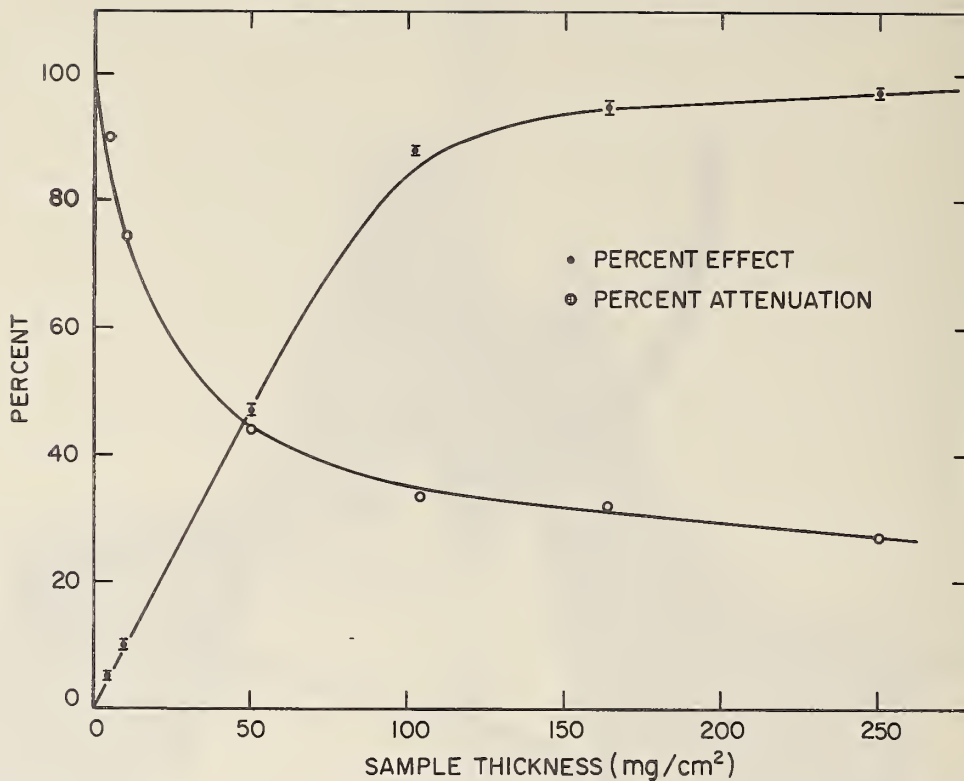


Figure 29. Percent effect and attenuation as a function of sample thickness

100 mg/cm² absorber. Further work is in progress to determine uniformity and reproducibility of absorbers prepared by plastic encapsulation.

(J. J. Spijkerman)

H. Fitting of Multiple Line Mössbauer Spectra Using Constraints

1. Introduction

Most of the commonly used programs for computer processing of Mössbauer spectra, such as NBS's own PARLORS [2], fit the sum of an appropriate number of "independent" Lorentzian curves to the data. In these programs the positions, heights, and half-widths of the Lorentzian's are varied independently until a best fit is obtained. The lack of prejudice of such programs with respect to the relative positions and intensi-

ties of such lines is desirable in most cases. However, at other times, the extraction of useful experimental results requires the use of known theoretical relations between the relative positions, heights and half-widths. Such theoretical relations may be employed as constraints to reduce the number of variables and thereby provide better estimates of the remaining parameters.

Spectra for which a constrained fit program is necessary are characterized by the presence of one or more sets of unresolved lines, low signal-to-noise ratios, or both. The programs described in the following sections were written because all multiple-line nickel spectra fall in the first category, and many in the second as well. Work is currently underway on a program for iron spectra with more than one site present.

2. General Theory

In the analysis of a spectrum, it is first necessary to assume a theoretical model for the spectrum in question. Such a model will ordinarily depend on the velocity (v) and on a set of (θ) of n (unknown) physical parameters (R_i) as indicated in (1).

$$Y = f(v, \theta), \quad \theta = (R_1, R_2, \dots, R_n) \quad (1)$$

The parameters reflect the height of the base line, the curvature and position of the parabola, the isomer shift, the magnetic field, etc. When the function is observed at N discrete points in velocity, its value at the i 'th velocity may then be theoretically described by

$$Y_i = f(v_i, \theta) + e_i, \quad \theta = (R_1, R_s, \dots, R_n), \quad i = 1, 2, \dots, N \quad (2)$$

where the e_i are random variations due to counting statistics. The problem then is to obtain estimates for the unknown

parameters (θ), and the method of nonlinear least-squares is usually selected as a means of obtaining these estimates, (see, for example, Draper and Smith, [16]).

If "good" initial estimates, $\theta^{(0)}$, of the unknown parameters are available, the following method iteratively improves the initial estimates until the true least-squares estimates of the parameters have been obtained, and it usually works quite well. The mathematical model is first approximated by the first order terms of a Taylor series expansion about the initial estimates, the expansion being carried out in terms of the unknown parameters as in (3).

$$Y_i = f(v_i, \theta^{(0)}) + \sum_{k=1}^n (R_k - R_k^{(0)}) \left. \frac{\partial f(v_i, \theta)}{\partial R_k} \right|_{\theta = \theta^{(0)}}$$

This may be rewritten as

$$\Delta Y_i^{(0)} = \sum_{k=1}^n \Delta R_k^{(0)} F_{k,i}^{(0)}$$

where

$$\Delta Y_i^{(0)} = Y_i - f(v_i, \theta^{(0)}),$$

$$\Delta R_k^{(0)} = R_k - R_k^{(0)},$$

and

$$F_{k,i}^{(0)} = \left. \frac{\partial f(v_i, \theta)}{\partial R_k} \right|_{\theta = \theta^{(0)}}$$

Equation (4) is then fitted to the experimental data, which in the present case consist of roughly 200 data points, and the n unknowns, $\Delta R_k^{(0)}$, are found by the usual method of linear least squares. The $\Delta R_k^{(0)}$ are then treated as corrections to the initial guesses, $R_k^{(0)}$, and the refined parameter estimates $R_k^{(1)} = R_k^{(0)} + \Delta R_k^{(0)}$ are computed. This process is repeated until a desired convergence criterion is met.

If the initial parameter estimates are not close enough, the linear approximation is no longer valid and a fit is not obtained. Alternatives to the procedure described above, which have wider regions of convergence, are discussed by Draper and Smith [16].

The computer programs discussed below, for various types of nickel spectra, were written in OMNITAB, a user-oriented programming package developed at NBS which facilitates communication with the electronic computer. A listing of one of the programs is included below, inasmuch as the instructions are basically English sentences and are largely self-explanatory. The OMNITAB package has been written in standard FORTRAN IV and is available from the NBS Statistical Engineering Laboratory upon request.

Case I - Magnetic Interaction

The equation for the magnetic nickel spectrum (see Ref. [2], p. 32) is given by

$$Y_i = B + Lv_i + Gv_i^2 - A \sum_{j=1}^{12} T_j^{(i)}$$

where the $T_j^{(i)}$ are the individual Lorentzians,

$$T_j^{(i)} = \frac{A_j}{1 + D(P_j - v_i)^2}$$

with the (known) relative peak amplitudes, A_j , given by (Ref. [2], p. 35)

$$[A_j] = [10, 3, 1, 6, 6, 3, 3, 6, 6, 1, 4, 10].$$

The peak positions, P_j , depend on the ground and excited state magnetic splittings, α and β , and the isomer shift, δ .

$$P_j = a_j \alpha + b_j \beta + \delta$$

$$[a_j] = \left[-\frac{3}{2}, -\frac{3}{2}, -\frac{3}{2}, -\frac{1}{2}, -\frac{1}{2}, -\frac{1}{2}, \frac{1}{2}, \frac{1}{2}, \frac{1}{2}, \frac{3}{2}, \frac{3}{2}, \frac{3}{2} \right]$$

$$[b_j] = \left[-\frac{5}{2}, -\frac{3}{2}, -\frac{1}{2}, -\frac{3}{2}, -\frac{1}{2}, \frac{1}{2}, -\frac{1}{2}, \frac{1}{2}, \frac{3}{2}, \frac{1}{2}, \frac{3}{2}, \frac{5}{2} \right]$$

The variable parameters to be fitted are listed below.

- B: Base line height (counts).
- L: Linear term of parabolic background.
- G: Quadratic term of parabolic background.
- D: $(1/H^2)$, where H is the half width at half maximum
- A: Overall amplitude factor
- α : Splitting of ground level magnetic substates (channels)
- β : Splitting of excited level magnetic substates (channels)
- δ : Chemical shift (channels)

The program was originally used to establish the ratio β/α in the high field alloy (1.5%)⁶¹Ni - Fe. In later applications, the ratio has been fixed at the value of .338 to lower the number of fitted variables from eight to seven.

The first three terms of (5) are common to all types of nickel spectra and have the obvious partial derivatives

$$\frac{\partial Y_i}{\partial B} = 1, \quad \frac{\partial Y_i}{\partial L} = v_i, \quad \frac{\partial Y_i}{\partial G} = v_i^2$$

The remaining partials are summarized in Table 12, along with those for the other cases.

Case II - Quadrupole Splitting with Zero Asymmetry Parameter

The quadrupole spectrum for the special case of $\eta = 0$ is given by

$$Y_i = B + Lv_i + Gv_i^2 - A \sum_{j=1}^3 S_j^{(i)}$$

where the Lorentzians are given by

$$S_j^{(i)} = \frac{1}{1 + \left(\frac{P_j - v_i}{H} \right)^2}, \quad P_j = g_j \gamma + \delta \quad j = 1, 2, 3$$

$$[g_j] = [-8, -2, 10]$$

The variable H is the half width at half maximum. The other new parameter, γ is given by

$$\gamma = eQV_{ZZ}/40$$

where eQ is the nuclear quadrupole moment and V_{ZZ} is the principal component of the electric field gradient tensor.

The pertinent partials again are listed in Table 12, and the program for this equation is listed in the appendix.

Table 12. Partial derivatives for linear approximation*

| Case | $\frac{\partial Y_i}{\partial \alpha}$ | $\frac{\partial Y_i}{\partial \beta}$ | $\frac{\partial Y_i}{\partial \delta}$ | $\frac{\partial Y_i}{\partial \gamma}$ | $\frac{\partial Y_i}{\partial D}$ | $\frac{\partial Y_i}{\partial H}$ |
|------|--|---------------------------------------|--|--|-----------------------------------|-----------------------------------|
| I | $\sum a_j U_j^i$ | $\sum b_j U_j^i$ | $\sum U_j^i$ | --- | $\sum U_j^i (P_j - v_i) / 2D$ | --- |
| II | --- | --- | $\sum W_j^i$ | $\sum g_j W_j^i$ | --- | $-\sum 2W_j^i (P_j - v_i) / H$ |
| III | $\sum a_j J_j^i$ | $\sum b_j U_j^i$ | $\sum J_j^i$ | $\sum c_j U_j^i$ | $\sum U_j^i (P_j - v_i) / 2D$ | --- |

*The following definitions are needed, in addition to those in Equations (6) through (14):

$$\Sigma = \sum_{j=1}^{12} \Sigma = \sum_{j=1}^3$$

$$U_j^i = 2AD(T_j^i) (P_j - v_i) / A_j$$

$$W_j^i = 2A(S_j^i) (P_j - v_i) / (H^2 A_j^i)$$

$$U_j^i = 2AD(T_j^i) (P_j - v_i) / A_j, T_j^i = A_j / (1 + D(P_j - v_i)^2)$$

Case III - Magnetic With Quadrupolar Perturbation

For a small, axially symmetric quadrupolar perturbation on a magnetic spectrum, only the line positions are affected significantly. Equations (5) through (7) are still valid, but the positions are now given by

$$P'_j = P_j + c_j \gamma$$

$$[c_j] = [10, -2, -8, -2, -8, -8, -8, -8, -2, -8, -2, 10]$$

where the P_j are given by (8). The partials are listed in Table 12.

3. Uncertainties of the Estimates

In the less well defined spectra no attempt has been made to approximate the uncertainties of the estimates, but in some of the better defined spectra, where the parameters are rather precisely determined, the Taylor series expansion has been used to provide rough approximations to the uncertainties. When the Taylor series approximation is very good in the neighborhood of the final solution, the approximate uncertainties should also be very nearly correct.

(J. C. Travis and B. L. Joiner)

I. The Application of Mössbauer Spectrometry to Quantitative Analysis

1. Introduction

During the past year Mössbauer spectrometry was investigated for use as a tool for quantitative analysis. This application could be important because the selectivity of this technique is such that no nuclei other than those of interest in the sample can be resonantly excited by the incident radiation and in this respect the method would be completely specific. Initial studies consisted of evaluating

the effects of variables such as drift in detector response, sample thickness, sample concentration, and time stability of the single channel analyzer, on the spectral parameters. Using $\text{Pd}_3^{119\text{m}}\text{Sn}$ as a source in conjunction with synthetic samples of SnO_2 in an Al_2O_3 matrix, the effects of these variables were systematically evaluated.

In the transmission mode, the magnitude of resonant absorption is related to concentration by the expression

$$\epsilon = \frac{I(\infty) - I(0)}{I(\infty)} = f_s \left[1 - e^{-T_A/2} J_0(iT_A/2) \right] \quad (1)$$

ϵ is called the Mössbauer fraction of resonant radiation absorbed, $I(\infty)$ and $I(0)$ refer to the transmitted intensities for non-resonant and resonant absorption, respectively. The effective absorber thickness is given by the expression $T_A = f_A \sigma_0 \alpha_A n_A t_A$ where f_s and f_A are the Debye-Waller factors for the source and absorber, respectively, σ_0 is the cross section for nuclear resonance absorption, and α_A is the isotopic abundance for n_A atoms per unit volume with a sample of thickness, t_A . J_0 is the zero-order Bessel function with an imaginary argument.

Because f_A depends on the lattice dynamic characteristics of the sample, an absolute determination of n_A based on equation 1 would be difficult even if the remaining parameters, i.e. f_s , σ_0 , α_A , and t_A could be measured with high accuracy. Therefore, the simplest approach for quantitative analysis would be the dissolution of the sample and incorporating the analate in a reproducible matrix. A series of standards in an identical matrix would then serve as the basis for a calibration curve.

To demonstrate this technique, a tin system was chosen. A stannic oxide sample was selected for study because of

previous experience with this compound [17] and the availability of a good single line tin source, i.e. $\text{Pd}_3^{119\text{m}}\text{Sn}$ [18]. An Al_2O_3 matrix was chosen because the photoelectric absorption of the 23.8 keV Mössbauer gamma photons is small and homogeneous samples are easily prepared. For application to real samples a series of standard reference materials (copper-base alloys) was analyzed for tin.

Preliminary studies on a series of tin-containing ore samples were undertaken in order to investigate the possibility for nondestructive analysis of the sample. Additional studies consisted of the evaluation of the source-sample-detector geometry, use of filters, a high resolution detector, and a resonant detector in an effort to optimize the ratio of the resonant absorption intensity to the total transmitted intensity.

2. Experimental

a. Apparatus

The NBS drift-free Mössbauer spectrometer was used in these experiments [19]. The aluminum sample holder was especially constructed for mounting powdered samples of varying thickness from 0.5 to 2.5 mm [20]. The area of the cell was 2.84 cm^2 . The moving absorber geometry was used throughout this work. The detector consisted of a NaI(Tl) crystal (2.5 cm in diameter \times 0.2 cm thick).

b. Reagents and Preparation of $\text{SnO}_2\text{-Al}_2\text{O}_3$ Mixtures.

Stock solutions of tin and aluminum were prepared by dissolving reagent grade tin metal in concentrated HCl and $\text{Al}(\text{NO}_3)_3 \cdot 9\text{H}_2\text{O}$ in distilled water. The aluminum solution was standardized by complexometric titration with the disodium salt of EDTA. The hydrous oxides were coprecipitated according to Kolthoff and Sandell [21], placed in Pt crucibles, and heated in an electric furnace to about 1200°C for complete conversion to the nonhygroscopic oxides. The SnO_2 content of these mixtures varied from 1 to 86%. In

constructing the calibration curves, the tin contents of three of the mixtures were verified by controlled-potential coulometry to an accuracy of better than 1%.

c. Mössbauer Experiments

Procedure A - Two values of sample thickness (0.5 and 2.5 mm), 5 values of sample composition from 7% to 86% of SnO_2 , and 5 single channel analyzer (SCA) widths were tested. The lower level discriminator of the SCA was set at about 20 keV and the upper level was varied in five steps from 30 to 60 keV. This permitted an energy range from 10 to 40 keV to be detected. A weighed sample of the mixture was placed in the cell and mounted. The spectra were accumulated until a total of approximately 9×10^5 counts/channel appeared in the baseline. This required from 2 to 6 hours per spectrum. All spectra were fitted as a singlet.

Procedure B - A 300-mg sample of mixture was placed in the 0.5 mm cell and mounted. The source-to-sample distance was 4.6 cm. This geometry was convenient since the sample could be mounted and removed without moving the detector, hence constant geometry is insured. The single channel was set to pass radiation from 20 keV to 30 keV. The spectra were accumulated until a baseline of 8×10^5 counts/channel appeared and required from 1.5 to 2 hours per spectrum. The uncertainty in the computer-estimated height of the Lorentzian function varied from 0.8% to 3% (relative standard deviation) whereas the uncertainty in the area varied from 2% to 7%.

d. Analysis of Copper-Base Alloys

From 2 to 10-gram samples were weighed and dissolved in 4:1 HNO_3 . After digestion on a hotplate for 24 hours, the metastannic acid precipitates were filtered and washed with hot 0.1M HNO_3 . The precipitates were then placed in beakers and enough aluminum solution added (see Section 2-b) so that about 1.8 g of Al_2O_3 would be present in the final mixture.

From this point on the procedure of Kolthoff and Sandell was followed. The tin content of these mixtures was obtained from comparison with a calibration curve (Section 2-c, Procedure B).

e. Tin Ores

Mössbauer spectra of seven ore samples were obtained. The tin content of these ores ranged from 0.3% to 0.9% as determined by emission spectroscopy. An approximately 1-gram sample was placed in the 2.5 mm cell and mounted. The source-sample-detector geometry and SCA settings used are described in Section 2-c, Procedure B. A 1.5 mil Pd foil was placed in back of the sample holder (side facing the detector). Spectra were accumulated until a difference of at least 4×10^4 counts appeared between the baseline counts and the counts in the peak channel. This required only a few hours for three of the samples (Nos. 9088, 9085, 9093) but 2 1/2 days for the remaining four (Nos. 9100, 9095, 9097, 9098).

3. Results and Discussion

In Figure 30 is a typical spectrum of SnO_2 in Al_2O_3 . The height (H) and the full-width at half-height (Γ) are computed from the fitting of a Lorentzian function for the absorption peak and a parabola for the baseline to the experimental points by an iterative least-squares procedure [22]. For the Lorentzian, the peak area (A) is then related to the peak height by the equation

$$A = 1/2 \pi H \Gamma$$

Experimentally, the transmission of nonresonant radiation ($I(\infty)$) through the sample is accompanied by background radiation (I') from the source which appears in the window of the SCA. Therefore, the total transmitted intensity ($I(\infty) + I'$) represents the baseline (B) of the Mössbauer spectrum.

The background radiation is comprised of other sources

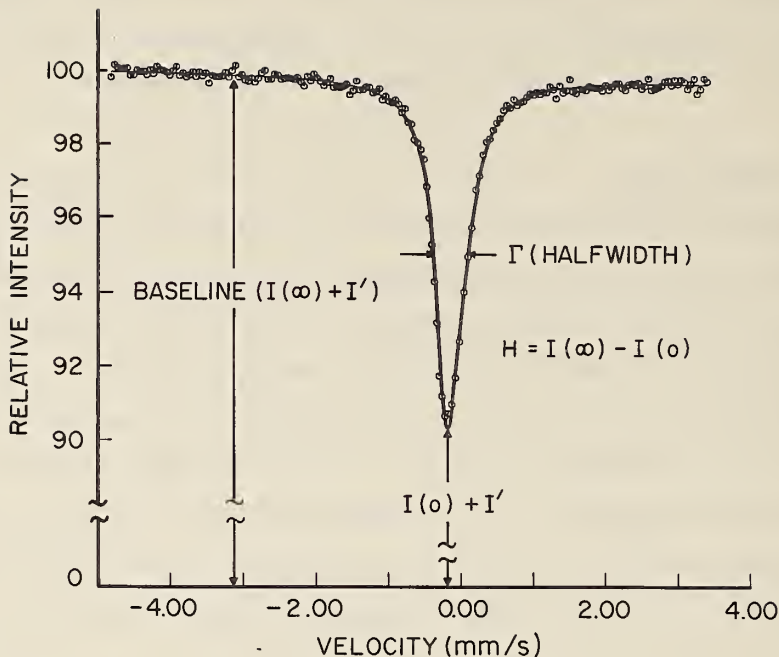


Figure 30. Typical Mössbauer spectrum of SnO_2 in Al_2O_3

of radiation even though pulse-height discrimination is used. The pulse-height spectrum of $\text{Pd}_3^{119\text{m}}\text{Sn}$ taken with a NaI(Tl) crystal consists of a broad single peak from approximately 18 to 35 keV. The energy of the gamma photons responsible for the resonance absorption is 23.8 keV. A number of x-rays are produced in this source, the most important being the 21, 25 and 28 keV x-rays. These cannot be resolved with the above detector, and therefore contribute to I' . In addition, photons of higher energy (180 to 1170 keV) have been identified in this source. These can be scattered into the detector by means of Compton processes and also contribute to I' .

In addition to the attenuation of the incident photons due to resonant absorption, there is an attenuation of the incident photons by the sample due primarily to the photoelectric absorption process. Since photoelectric absorption should affect the resonant and nonresonant portions of the

incident radiation in the same way, the absolute magnitude of the ratio of peak area or peak height to the baseline would not be affected. For this reason the ratios of A/B and H/B are used in these experiments.

An experiment using a modified Youden square was designed to test the effect of varying the window width, the amount of SnO₂, and the sample thickness on A/B and H/B (Procedure A). An analysis of variance did not give any evidence of an effect with variation in SCA over the indicated range. In addition, when either the amount of SnO₂ or thickness was increased, no effect on the portion of pulse-height spectrum passed by the SCA was detected other than a decrease in height because of the attenuation of the incident radiation. The increase in sample thickness from 0.5 to 2.5 mm resulted in a large increase in self-absorption by SnO₂. A significant broadening of the spectral line was also observed. Line broadening as a function of sample thickness has been discussed elsewhere [23]. Indeed, these authors have shown that this effect can be reduced by judicious selection of an "effective" sample thickness.

The results from this study showed that the reproducibility at the larger sample thickness was much poorer than anticipated. This suggested that a more rigid control over the source-sample-detector geometry was necessary.

Additional measurements were made (Procedure B) under carefully fixed geometry conditions. Figures 31 and 32 show the variation of H/B and A/B, respectively with increasing amount of SnO₂. The data are given in Table 13. As seen from Figure 31, H/B has nearly reached a maximum value at 50 mg of SnO₂. Above this value the peak continues to broaden, hence A/B increases as shown in Figure 32 over a much larger range of concentration. Of the variables studied, the critical one is the source-sample-detector geometry.

Table 13. Variation of spectral parameters with the amount of SnO₂.

SAMPLE THICKNESS: 0.5 mm

| SnO ₂ mg | A/B (Mean) ^a | (A/B) s ^b | H/B (Mean) ^a | (H/B) s ^b |
|---------------------|-------------------------|----------------------|-------------------------|----------------------|
| 3.50 | 0.1994 | 0.0105 | 0.0116 | 0.0006 |
| 9.04 | 0.4298 | 0.0082 | 0.0314 | 0.0016 |
| 16.28 | 0.6937 | 0.0015 | 0.0496 | 0.0015 |
| 28.82 | 1.064 | 0.017 | 0.0726 | 0.0015 |
| 38.22 | 1.286 | 0.028 | 0.0831 | 0.0017 |
| 52.84 | 1.534 | 0.053 | 0.0943 | 0.0016 |
| 56.85 | 1.648 | 0.032 | 0.1004 | 0.0012 |
| 76.35 | 1.961 | 0.040 | 0.1086 | 0.0006 |
| 97.11 | 2.249 | 0.034 | 0.1165 | 0.0006 |
| 121.9 | 2.422 | 0.086 | 0.1181 | 0.0005 |

^a Average of 3 replicates

^b Computed standard deviation of single measurement based on 2 degrees of freedom

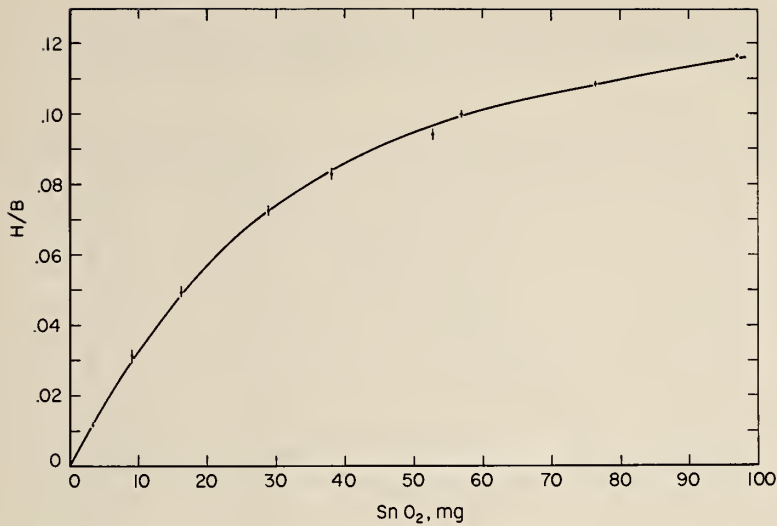


Figure 31. Plot of height of peak to baseline ratio vs mg of SnO₂

A least-squares fit of Equation 1 to the experimental data was performed. If I' is assumed constant, Equation 1 can be rewritten in the form

$$H/B = \frac{I(\infty) - I(0)}{I(\infty) + I'} = f \left(1 - e^{-Km/2} I_0(Km/2) \right) \quad (2)$$

where $f = \frac{I(\infty) f_s}{I(\infty) + I'}$, K includes the constants V, (volume) f_A , σ_o , α_A , t_A , and m is the mg of SnO₂ ($n_A V$). The Bessel function $J_0(iKm/2) = I_0(Km/2)$ see [24]. At low concentrations (e.g. low n_S) the function, $I_0(Km/2)$ is approximately one; therefore, Equation 3 can be rewritten as the familiar exponential relationship (similar to Beer's law)

$$H/B = f (1 - e^{-K'm/2}) \quad (3)$$

where f' and K' are empirical constants that approach the theoretical constants f and K, respectively as m approaches 0.

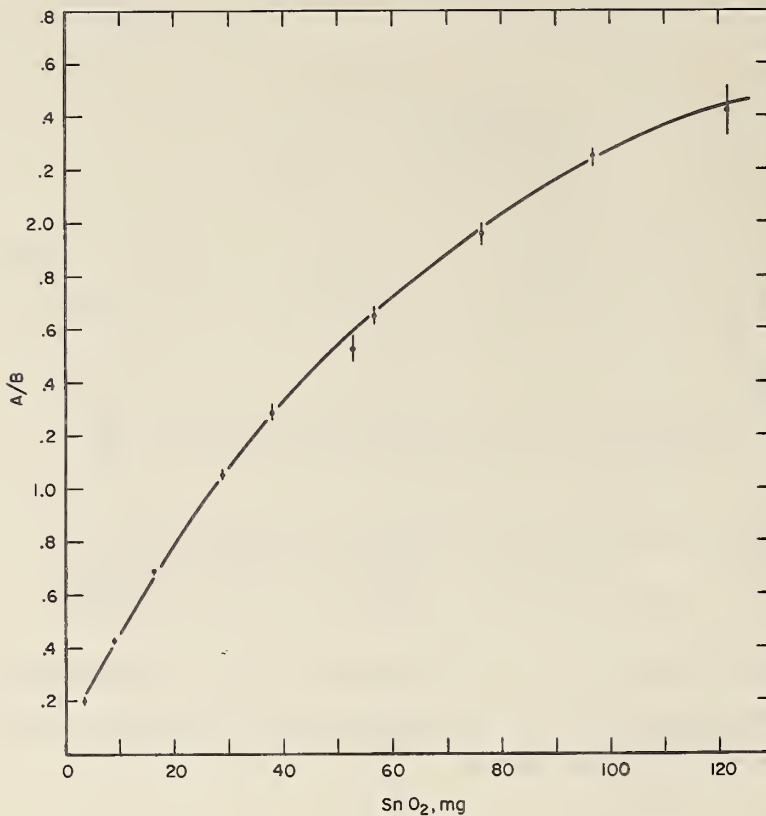


Figure 32. Plot of area of peak to baseline ratio vs mg of SnO₂

It can be seen from Table 14 that both Equations 2 and 3 both fit the data fairly well. This indicates that the presence of the Bessel function does not change the exponential form of Equation 3 appreciably over the concentration range studied. Thus either Equation 3 or Equation 2 can be used in this range although Equation 2 is preferable on theoretical grounds.

In Table 15 the results of the analysis of tin in the copper-base alloys are given.

The negative bias of the results from the certificate values can be attributed to losses in the separation of metastannic acid from the alloys. In addition there is non-

Table 14. Comparison of calculated values with the observed values of H/B

| SnO ₂ mg | Observed | Calc. ^a | Deviations,% ^c | Calc. ^b | Deviations,% ^c |
|---------------------|----------|--------------------|---------------------------|--------------------|---------------------------|
| 3.50 | .0116 | .0133 | -14.7 | .0125 | -7.2 |
| 9.04 | .0314 | .0311 | 0.9 | .0297 | 5.8 |
| 16.28 | .0496 | .0495 | 0.0 | .0481 | 3.1 |
| 28.82 | .0726 | .0719 | 0.9 | .0716 | 1.5 |
| 38.22 | .0831 | .0835 | - 0.5 | .0840 | -1.1 |
| 52.84 | .0943 | .0961 | - 1.9 | .0974 | -3.2 |
| 56.84 | .1004 | .0987 | 1.7 | .1001 | 0.3 |
| 76.35 | .0186 | .1083 | 0.3 | .1094 | -0.7 |
| 97.11 | .1165 | .1148 | 1.5 | .1146 | 1.7 |
| 121.9 | .1181 | .1199 | - 1.5 | .1177 | 0.3 |

$${}^a_{H/B} = f \left[1 - e^{-Km/2} I_0 (Km/2) \right]; \quad f = 0.1580; \quad k = 0.02595$$

$${}^b_{H/B} = f' \left(1 - e^{-K'm/2} \right); \quad f' = 0.1204; \quad K' = 0.03131$$

$${}^c_{\text{Deviation, \%}} = \frac{\text{Observed} - \text{Calc.} \times 100\%}{\text{Observed}}$$

agreement between the tin assay values calculated from H/B and A/B spectral parameters.

In order to maximize the ratios of H/B and A/B it is necessary to reduce I'. The source-sample-detector geometry was investigated for one sample concentration. Table 16 shows an increase in H/B and A/B as the source-to-detector distance was increased while keeping the source-to-sample distance constant. The decrease in I' is believed to be due to a reduction in the detected x-rays produced by fluorescence in the samples. Of course, this improvement was realized at the expense of a reduction in transmitted intensity, necessitating a much longer time to reach the same statistical precision in the baseline.

Table 15. Analysis of Sn in copper-base alloys

| SRM# | %Sn(H/B) ^a | %Sn(A/B) ^b | Cert. Value, % | %Dev.(H/B) ^c | %Dev.(A/B) ^d |
|--------|-----------------------|-----------------------|-------------------|-------------------------|-------------------------|
| 37e | 0.850 | 0.856 | 1.00 | -15.0 | -14.4 |
| 124d | 3.82 | 4.30 | 4.56 | -15.2 | - 5.7 |
| 52c | 6.66 | 6.95 | 7.85 | -15.2 | -11.5 |
| 184 | 4.91 | 5.97 | 6.38 | -23.0 | - 6.4 |
| C-1107 | 0.896 | 1.07 | 1.04 | -13.8 | + 2.9 |

^aSn determined using H/B as spectral parameter

^bSn determined using A/B as spectral parameter

^cDeviation of value calculated using H/B as spectral parameter from the certificate value

^dDeviation of value calculated using A/B as spectral parameter from the certificate value

Table 16. Effect of geometry on spectral parameters

| Source-to-Detector Dist., cm | A/B | H/B | Time, Min | Baseline Counts×10 ⁵ | Transmission Rate, cpm |
|---------------------------------|-------|--------|--------------|------------------------------------|---------------------------|
| 2.0 | 1.182 | 0.0743 | 57.0 | 8.751 | 1.54×10 ⁴ |
| 4.6 | 1.286 | 0.0831 | 97.4 | 7.897 | 0.81×10 ⁴ |
| 9.1 | 1.445 | 0.0947 | 345.8 | 7.852 | 0.23×10 ⁴ |

NOTE: Sample Content, 38.2 mg SnO₂
 Sample Thickness, 0.5 mm
 Source-to-Sample distance, 1.0 cm

Another way of decreasing I' is to reduce the 25 keV Sn x-rays by using a palladium foil which has a K-absorption edge at 24.3 keV. There is some reduction in the intensity of these x-rays due to the presence of palladium in the source itself. However, as shown in Table 17, there is a 25% increase in H/B when a 1.5 mil Pd foil was placed between the sample and detector. This increase is independent of the sample thickness over the range investigated. The same results were obtained when the foil was placed between the source and the sample.

Table 17. Effect of Pd filter on spectral parameters

| Sample Thickness, mm | SnO ₂ mg | NO Pd Foil | | 1.5 mil Pd foil | |
|----------------------|---------------------|------------|--------|--------------------|---------------------|
| | | A/B | H/B | A/B | H/B |
| 0.5 | 38.2 | 1.286 | 0.0831 | 1.654 | 0.1065 |
| 1.5 | 97.7 | 2.265 | 0.1166 | 2.795 | 0.1454 |
| 2.5 | 154.7 | 2.917 | 0.1294 | 3.566 | 0.1614 |
| 2.5 | 154.7 | | | 3.616 ^b | 0.1611 ^b |

^b1.5 mil Pd foil placed between source and sample

Increasing the resolution of the detector also reduces I'. In Figure 33 is a pulse-height spectrum of Pd₃^{119m}Sn taken with a Li-drifted silicon detector (sensitive area 80 mm²; sensitive depth 2 mm) which has a resolution between 1.2 and 1.3 keV FWHM for photon energies between 8 and 45 keV [2]. With this detector, the single channel can be set to pass only 23.8 and 25 keV photons. In conjunction with a Pd foil filter, the 25 keV Sn x-ray can virtually be eliminated and therefore permit only 23.8 gamma photons to

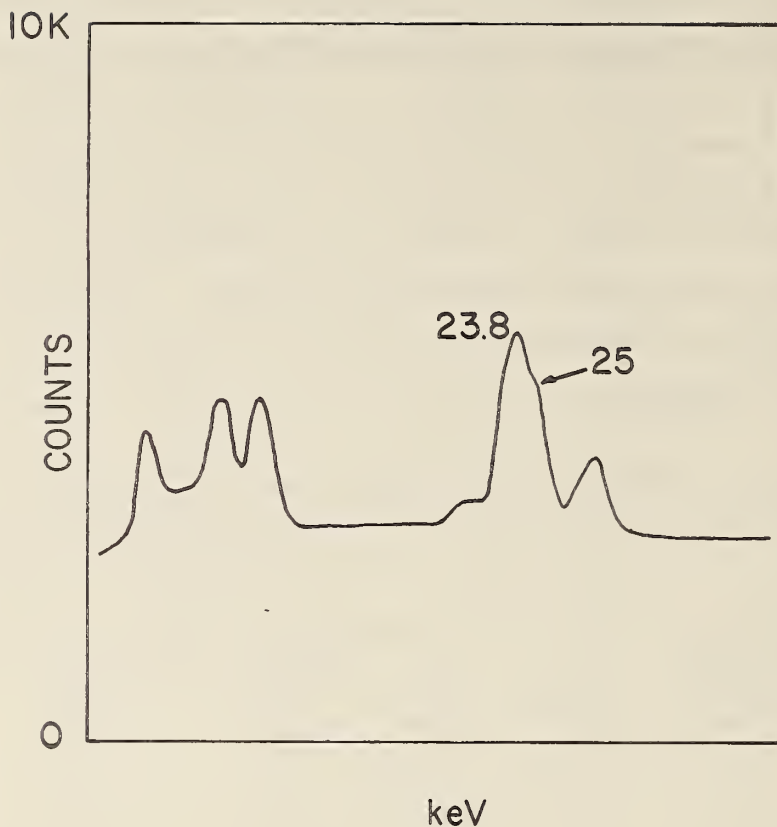


Figure 33. Pulse height spectrum of ^{119m}Sn with lithium drifted silicon detector

be detected. Again since the sensitive area is only 80 mm^2 , the counting efficiency is such that long counting times are required for the Mössbauer experiments. The tin source used has high energy gamma emitters as contaminants which produce Compton-scattering of the proper energy in the SCA to contribute to I'. Of course, this can be reduced by the production of a tin source with a minimum of contaminants.

Preliminary studies on a resonance detector for tin were initiated. The main advantage of such a detector is that it would virtually detect only the recoil-free Mössbauer gamma radiation from the source (via conversion electrons) and

hence eliminate the complications that arise in existing detection systems. Such a detection system would be of tantamount importance in quantitative analytical applications.

Counting efficiency studies using a scintillation gel with tritiated glucose showed that the highest count rate was obtained with the most rigid gel. In addition, when various amounts of SnO_2 were added to the rigid gel no significant decrease in count rate was observed which indicates that this compound is transparent to the light produced by the scintillator. It was also found that deaeration of the scintillator solution prior to forming the gel had no effect on the count rate.

First experiments with the detector using the E.M.I. tube consisted of observing the phototube noise with increasing applied voltage. Again using the E.M.I. tube J.J. Spijkerman investigated the optimum selection of the SCA settings in order to observe a Mössbauer emission spectrum due to the conversion electrons produced by the internal conversion of the 23.8 keV photons in the SnO_2 detector.

Additional studies consisted of using an RCA photomultiplier tube with much less dark current instead of the E.M.I. tube in an effort to decrease the tube noise. Also, in an effort to obtain a pulse-height spectrum of conversion electrons a number of radionuclides were investigated in a plastic scintillator using an anti-coincidence detection system. All spectra obtained thus far seem to indicate that conversion electron spectra are very similar in shape to beta particle spectra. This seems to preclude any capability for pulse-height discrimination. Since the photosensitive surface of these photomultiplier tubes are sensitive to gamma radiation, another source-detector geometry where the source is not directly in line with the phototube should be used. A number of these factors are currently being studied.

(P. A. Pella)

J. Tin Mössbauer Spectrometry Following the Decay of ^{119}Sb

The ^{119}Sb radioisotope has not been reported as a source for ^{119}Sn Mössbauer spectroscopy. The 38 hour half life and the difficulty of production of this radioisotope compared to the 245 day reactor-produced $^{119\text{m}}\text{Sn}$ source makes the Sb source undesirable for routine work. However, the ^{119}Sb radioisotope makes it possible to study the tin compounds formed by the decay of ^{119}Sb , and the possible formation of "charge states" during its decay. by electron capture. Sb is particularly attractive for this study since Sb and Sn have no common oxidation states, as is the case for the ^{57}Co - ^{57}Fe decay. Furthermore, the lifetime of the ^{119}Sn excited state is 1.8×10^{-8} sec, an order of magnitude shorter than that of ^{57}Fe .

The ^{119}Sb is produced by the $^{121}\text{Sb}(\gamma 2n)^{119}\text{Sb}$ nuclear reaction, using 100 MeV bremsstrahlung from the NBS Linac. Reagent grade Sb metal was irradiated for 8 hours, and used as a source with a 150 mg/cm^2 BaSnO_3 absorber at 80°K . The spectrum is shown in Figure 34, with a chemical shift of 1.65 ± 0.08 mm/sec, and a line width of 1.28 ± 0.16 mm/sec.*

Figure 35 shows the spectrum of a $^{119}\text{Sb}_2\text{O}_5$, prepared from the irradiated metal, with a 150 mg/cm^2 BaSnO_3 absorber. The chemical shift is -0.02 ± 0.10 mm/sec and the line width is 1.90 ± 0.18 mm/sec. This would indicate that ^{119}Sb decays to a Sn^{+4} oxidation state, since the spectral parameters are similar to those of SnO_2 [17]. Further work is in progress.

(P. A. Pella and J. J. Spijkerman)

*The uncertainty reported is approximately two standard deviations. The standard deviation was estimated from the last iteration of a non-linear fitting procedure on a Taylor series expansion about the estimated values.

BASELINE= 52303

SPECTRUM NO.PP0231

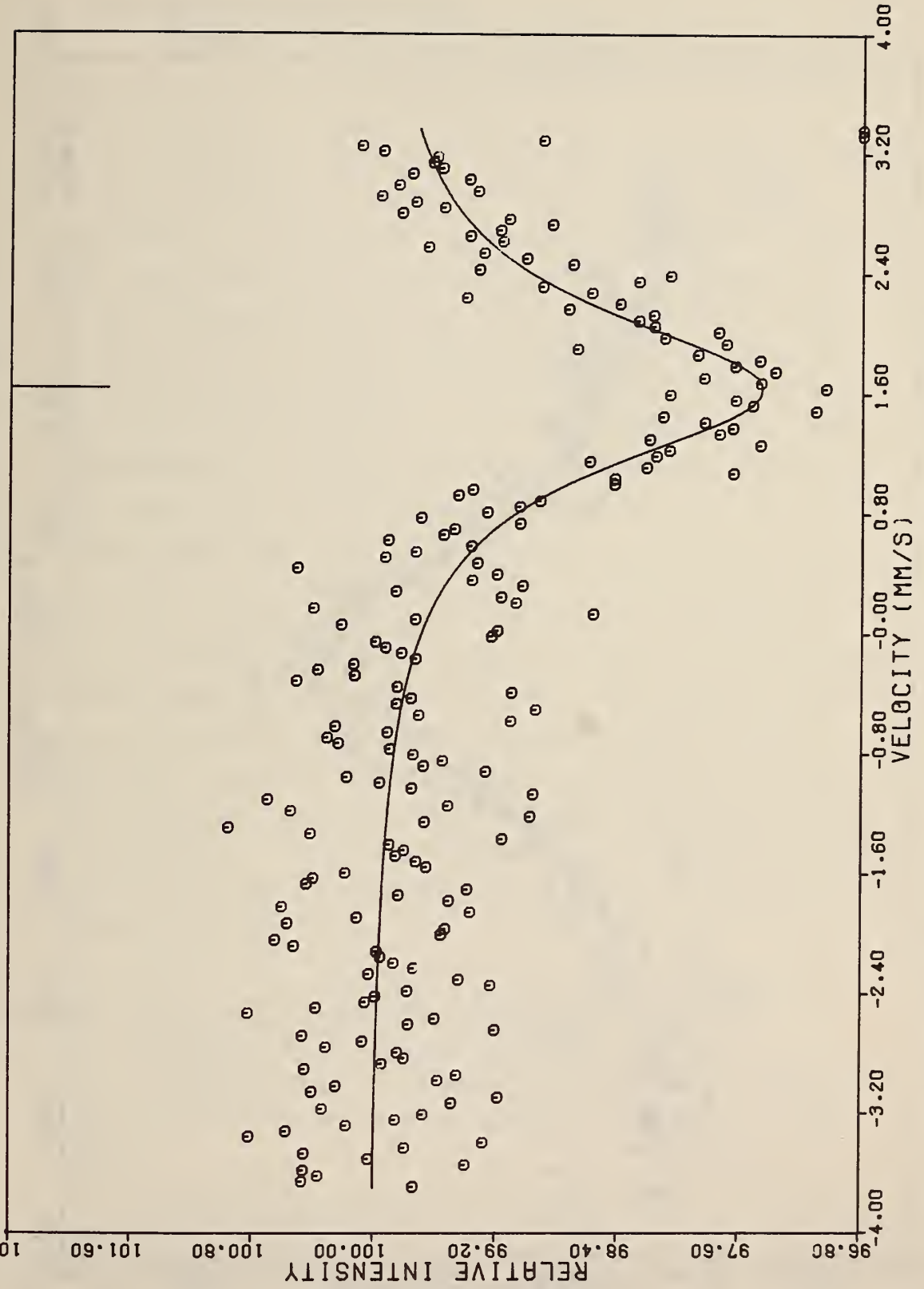


Figure 34. ^{119}Sb vs BaSnO_3 (thickness is 150 mg/cm^2)

SPECTRUM NO. PP0232

BASELINE= 155234

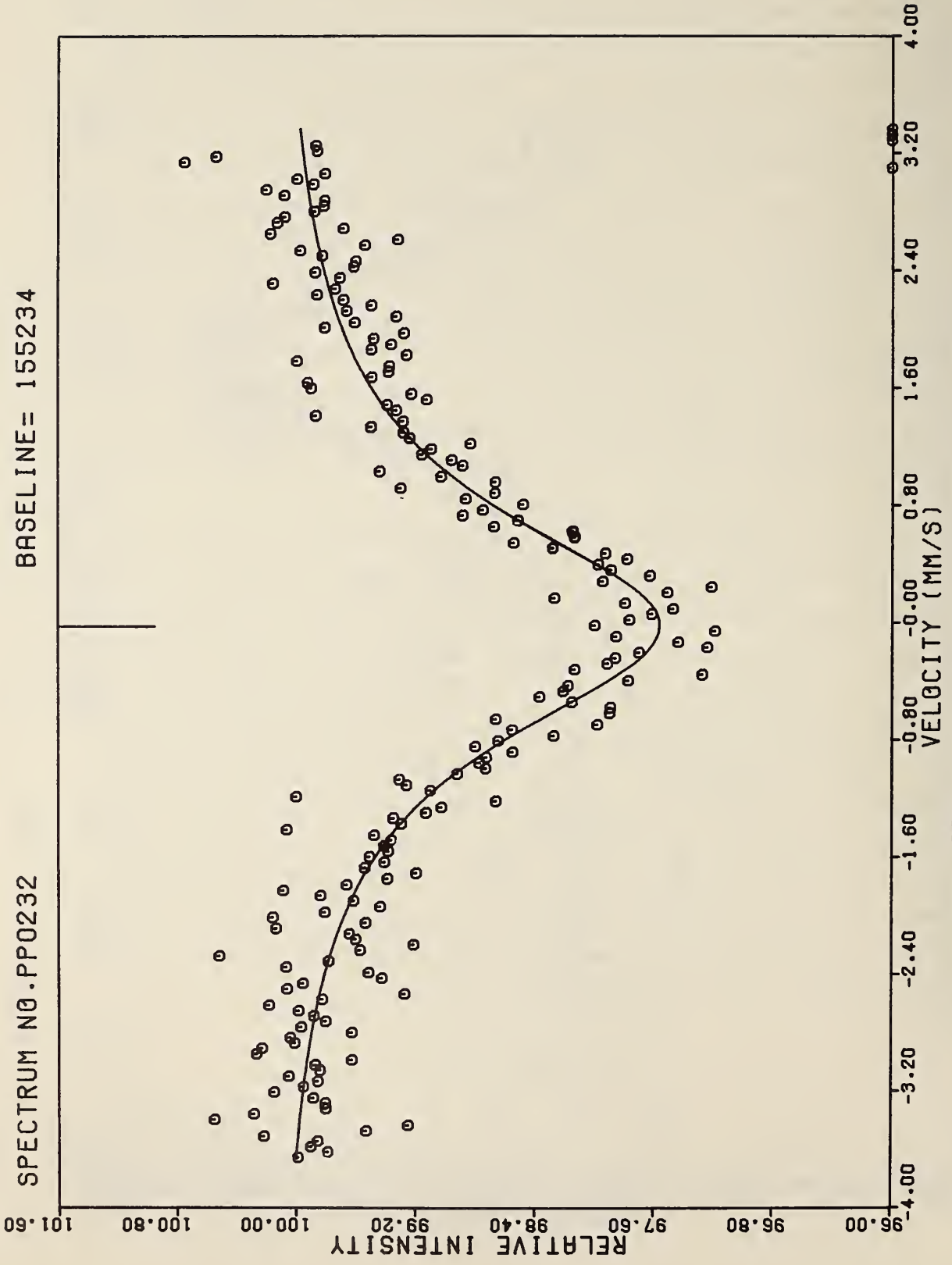


Figure 35. $^{119}\text{Sn}_2\text{O}_5$ vs BaSnO_3 (thickness is 150 mg/cm^2)

K. Abstracts of Publications

MÖSSBAUER SPECTROSCOPY OF ^{61}Ni

presented by J. J. Spijkerman to the Faraday Society, London, England, December 1967.

The Mössbauer effect of ^{61}Ni has been observed using a single line source prepared by a 30 minute LINAC irradiation. Of the many sources evaluated, the 85% Ni-Cr alloy gave the best result, with a f-factor of 0.1 and a linewidth of 0.097 cm/s at 80°K. The source was prepared by 100 MeV bremsstrahlung irradiation of the alloy, by the reaction $^{62}\text{Ni}(\gamma, p)^{61}\text{Co}$. The pulse height spectrum showed a single peak at 67.2 keV, with no interfering radiation. The 1.5 hours half life of the source required repeated irradiations, but no annealing was required.

Several alloys and compounds of nickel were examined, and showed partially resolved hyperfine interactions.

The magnetic moment of the 67.2 keV, 5/2 spin, first excited state is $+ 0.425 \pm 0.043 \text{ nm.}^*$ The magnetic field at the Ni nucleus in antiferromagnetic NiO is 96 ± 10 kilogauss. Quadrupole splitting was observed, but no value of the quadrupole moment of the 5/2 state could be determined. A tentative chemical shift-electron configuration diagram has been worked out, and gives a value of $\Delta R/R = 2.5 \times 10^{-4}$.

SOME ASPECTS OF THE INTERPRETATION OF THE MÖSSBAUER
CHEMICAL SHIFT IN TIN CHEMISTRY

by J. J. Spijkerman, published in the American Chemical Society, Advances in Chemistry Series No. 68, p. 105, (1967).

The Mössbauer spectra of a large number of organic

*The uncertainty reported is approximately two standard deviations. The standard deviation was estimated from the last iteration of a non-linear fitting procedure on a Taylor series expansion about the estimated values.

and inorganic tin compounds have been published. From these spectra, the oxidation state of tin in most compounds can be determined.

To interpret the Mössbauer spectra properly, the relationship between the chemical shift and the electron density at the Sn nucleus must be established. This requires that the magnitude and sign of $\Delta R/R$ (a factor that relates the change in the effective charge radius of the tin nucleus on passing from the excited to the ground state) must be known, in most instances, this factor can be determined from nuclear shell model calculation, but, for tin, it must be evaluated experimentally. The discussion includes the results of the various experiments that were designed to obtain this factor so that the chemical shift observed for tin compounds could be interpreted correctly.

MÖSSBAUER EXPERIMENTS WITH NICKEL-61

by J. C. Love, G. Czjek, J. J. Spijkerman and D. K. Snediker, published in U.S. Atomic Energy Commission Report No. ORNL-P-3251, Proceedings of Conference on Hyperfine Interactions, Pacific Grove, California (1967).

Using $^{61}\text{Mössbauer}$ effect, we have measured the ratio of the magnetic moments of ^{61}Ni nuclei in the first excited state and the ground state: $\mu(5/2)/\mu(3/2) = (-0.559 \pm 0.012)$. * Hyperfine fields at nickel nuclei in iron (241 ± 7 kilogauss) and in a Ni (85%) Cr (15%) alloy (~ 15 kilogauss) are determined. Very approximate values for isomer shifts of some nickel alloys, NiF_2 , and NiO are given.

*The uncertainty reported is approximately two standard deviations. The standard deviation was estimated from the last iteration of a non-linear fitting procedure on a Taylor series expansion about the estimated values.

DETERMINATION OF SURFACE COMPOUND FORMATION

BY BACKSCATTER MÖSSBAUER SPECTROSCOPY

presented by H. Terrell, R. H. Forsyth and J. J. Spijkerman at the Abstracts Symposium "Fundamental Corrosion Research in Progress" held March 12-21, Cleveland, Ohio.

The detection and identification of a surface compound formation on a steel surface was made using a backscatter Mössbauer effect technique. The compound was identified as β -FeOOH from Mössbauer effect parameters of iron oxide and oxy-hydroxide compounds. An estimate of the compound thickness is given based on a calculation of the backscatter amplitude versus distance into the sample. This technique can be used to identify corrosion products on the surface of iron bearing materials.

4. NUCLEAR INSTRUMENTATION

A. Introduction

This group is now comprised of two projects. One project is closely tied to other projects in the section and provides assistance on design and fabrication of equipment of specific use on a single task. In addition, a maintenance service is provided for all who wish it within or outside of the section. The other project in the nuclear instrumentation group devotes its efforts to special long term design and development problems. For example, this effort is now focused on a major data handling and computation system for the Mass Spectrometry Section, 310.06.

B. Overflow Counter

1. Introduction

In the taking of Mössbauer data, a large number of counts must be accumulated in order that the Mössbauer spectrum can be defined with high statistical precision. The spectra accumulated are contained in the 10^5 memories of our multi-channel analyzers but the counts in the base line of the spectra are frequently on the order of 10^7 counts/channel. For example, in Figure 36, a Mössbauer spectrum could be as shown with A overflows where A is frequently on the order of 100-200. Because of the large number of overflows, it is difficult to keep track of them accurately. Before the counter was designed and built, the method of computing the number of overflows was to measure approximately the count rate and then multiply it by the elapsed time. When this method was used and there were a large number of overflows (>100), one could not hope to calculate the correct number of overflows to better than ± 2 .

A counter has been designed which is gated on by one of the channels, channel 100, and this counts all of the overflows in either channel number 100, or in the second sub-group (200-399), channel 300.

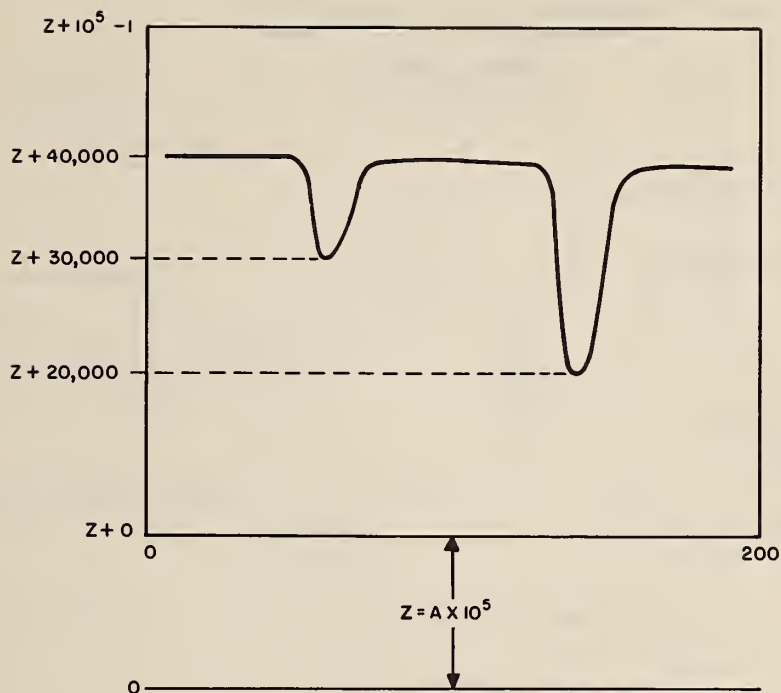


Figure 36. Diagram depicting overflow of memory for pulse height analyzer

2. Description of Logic

In Figures 37 and 38 are shown the logic signals which control the overflow counter and the logic diagram of the counter, respectively. The signals in Figure 37 represent the timing of the memory cycle of our multichannel analyzer and the timing of signals which affect the overflow counter. The first thing that occurs is the pulse from the time base oscillator (T.B.O.) which triggers the memory cycle. During the memory cycle the sequence of events is as follows:

- (1) Reset temporary store bistable (T.S.B.) if it had stored a count in the previous memory cycle.
- (2) If the T.S.B. had stored a count, add a count to the contents of the data scaler.
- (3) ADD-1 acts as a delay in the time mode so that the T.S.B. count could be added to the data scaler.

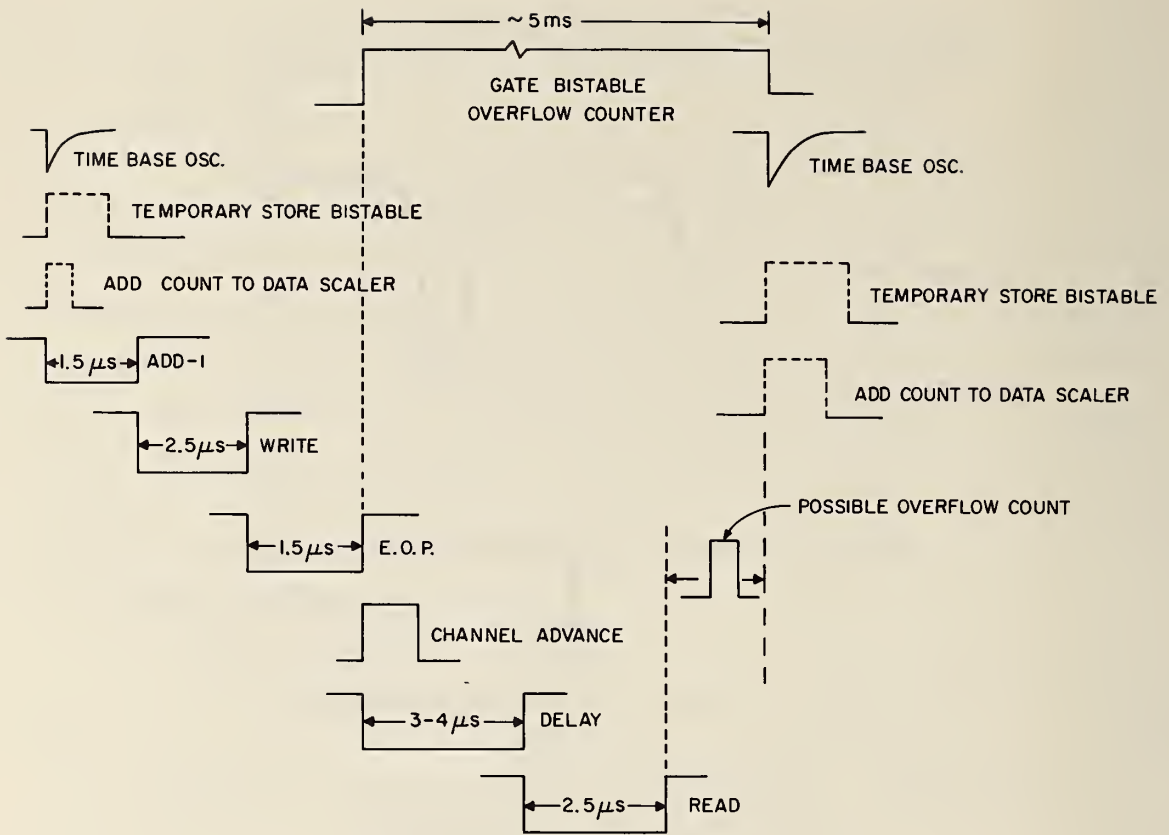


Figure 37. Timing of logic pulses in pulse height analyzer

- (4) WRITE enters contents of data scaler into memory.
- (5) END OF PROGRAM (E.O.P.) acts as a delay in the time mode; at end of delay it produces the channel advance pulse.
- (6) DELAY acts as a delay in time mode.
- (7) READ retrieves the contents of the new channel out of the memory into the data scaler.

The timing of the gate bistable in the overflow counting is shown in Figure 37. The gate bistable is set by the transition of the 100 bistable from the $\overline{100}$ to the 100 state. The bistable is triggered by the channel advance pulse when the address is in channel 99 (299). When the gate bistable is in

ALL DIODES DR435
 ALL CAP .001 μ F
 ALL RESISTORS 5.1K

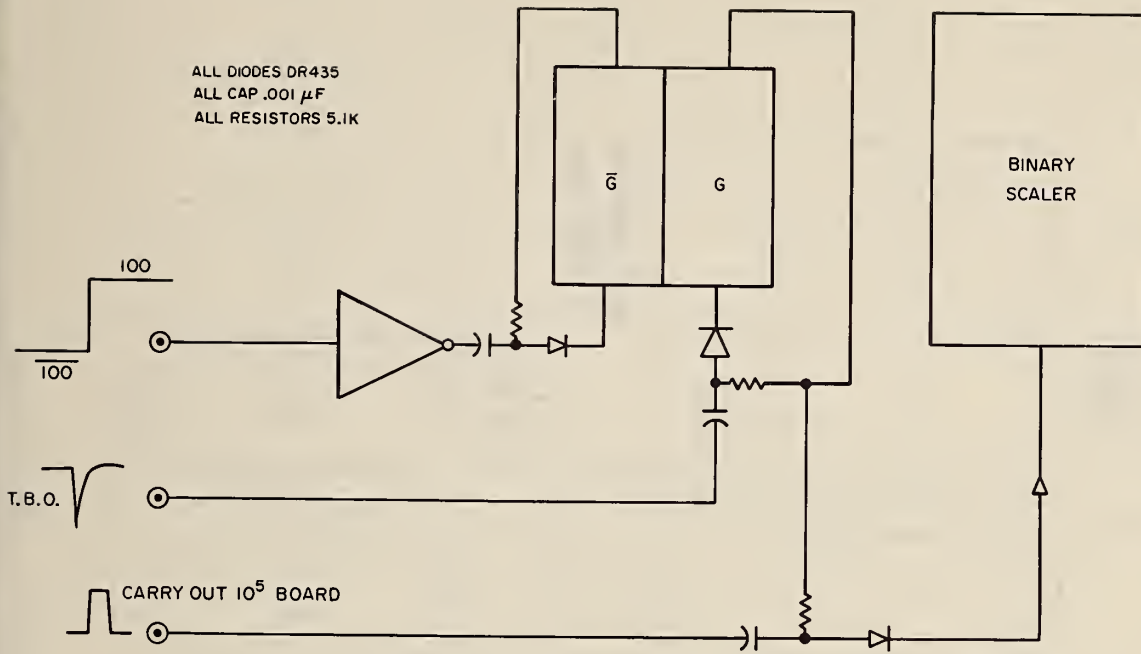


Figure 38. Logic diagram of overflow counter

its "set" state it allows pulses to reach the binary counter and it remains in its set state until the next T.B.O. pulse.

It can be seen in Figure 37 that the T.S.B. can add a count to the contents of channel 100 while the gate bistable is being reset. It is therefore necessary to delay the turn off of the gate to insure that a T.S.B. generated overflow would be counted. The type of gate being used has a time constant for shut off of 5 μ s, which meets the requirement that T.S.B.-generated overflow pulses will not be cancelled.

The binary scaler is shown in Figure 39. Each bistable is read out by a lamp on the front panel which is appropriately labeled with its binary designation. Also on the front panel is a switch to reset the scaler to zero.

(F. C. Ruegg)

C. Sequential Scanner to Control Frequency Synthesizer

1. Introduction

A special scanner has been designed to increment the

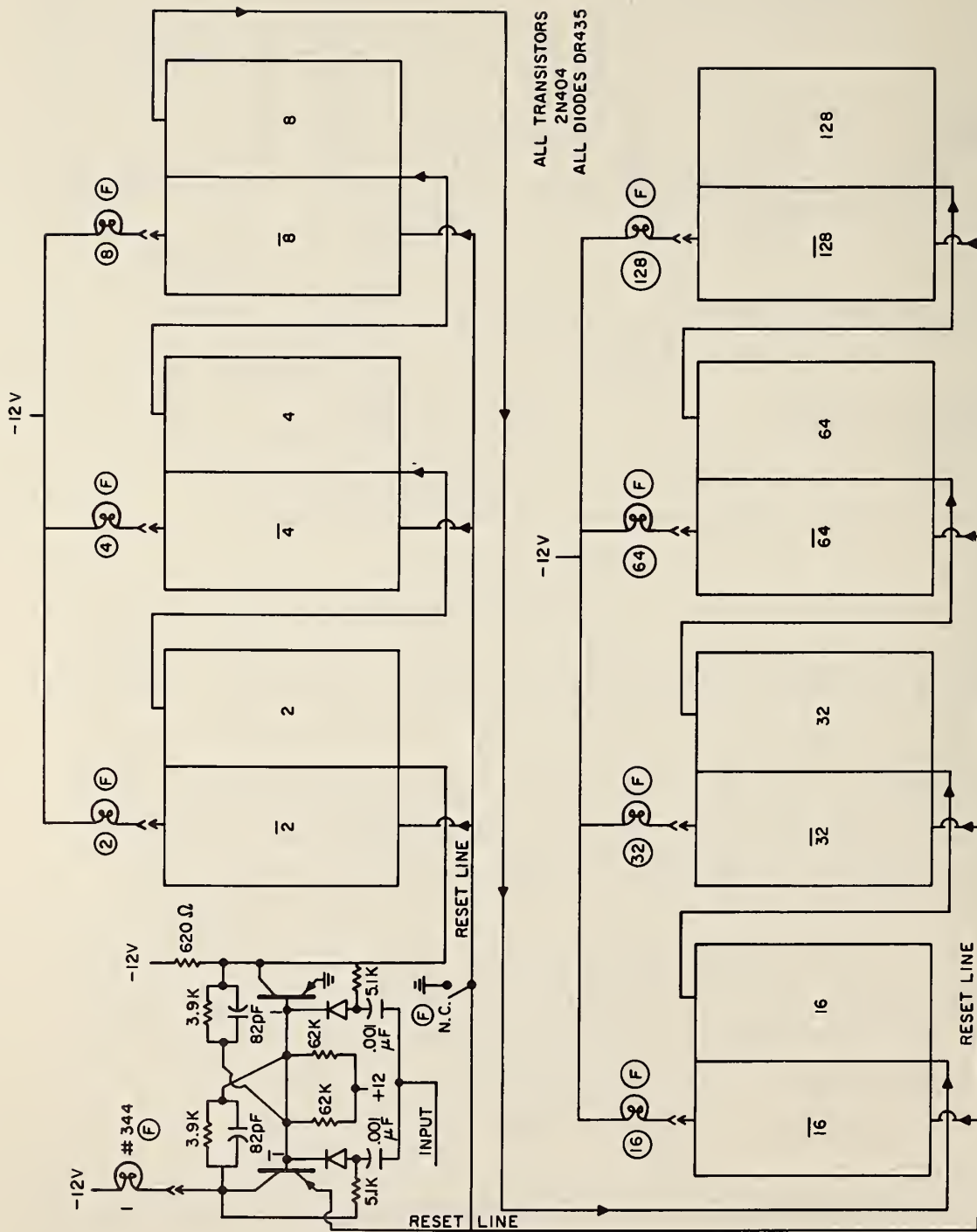


Figure 39. Binary scalers for counting overflows

frequency of General Radio frequency synthesizer in synchronization with the address advance of a R.I.D.L. 34-12B multichannel analyzer operating in the time mode. The synthesizer is an accurate source of frequency and it can be used with instruments which are frequency controlled. If the output of such an instrument is a frequency or if it can be converted to a frequency, then it can be counted by the analyzer obtaining a spectrum of output counts as a function of synthesizer frequency.

An example of an application for such a system is to control the velocity of the NBS optical Mössbauer spectrometer. The optical spectrometer uses a Michelson type interferometer to sense the velocity. The output of the fringe sensor is a frequency which is directly proportional to the velocity. This frequency is compared with the output of the synthesizer and the velocity of the spectrometer is corrected to make the two frequencies equal. Therefore, if the synthesizer's frequency is changed, the velocity of the spectrometer is correspondingly changed, i.e. the velocity is directly dependent on the synthesizer's output frequency. The output of the Mössbauer spectrometer detector system is counted by the analyzer resulting in a spectrum of γ -ray counts as a function of velocity (Mössbauer spectrum).

2. Description of System

A block diagram of the system is shown in Figure 40. The time base oscillator is used to increment the scaler and the multichannel address simultaneously. The number stored in the decades of the scaler is decoded from B.C.D. into decimal for its front panel display (see Figure 39). The ten line decimal information from the first two decades is brought out to the interface and transformed into the signals which are necessary to control the remotely programmable decades of the synthesizer, Figure 41.

(F. C. Ruegg)

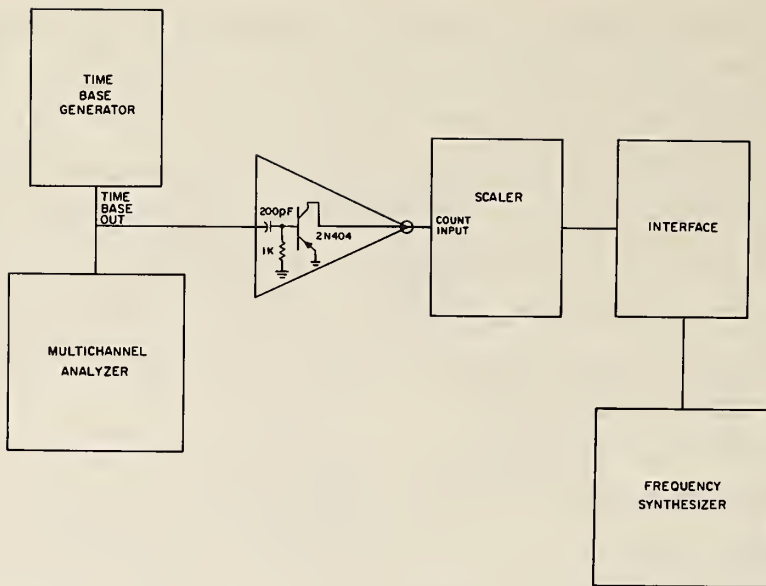


Figure 40. Block diagram of sequential scanner

D. Circuit Change to Improve Reliability of Interface Units

On the whole, the reliability of the interface units [2] has been quite good, but a failure mechanism occurred which required circuit modification. After the teletypes had been used for a substantial period of time, their commutators began to produce noise. The noise caused the gate control bistable to be set; this inhibits the datum in a channel from being printed and replaces it with spaces. To stop the gate control bistable from being triggered by the noise it was necessary to modify the circuit. The modified circuit is shown in Figure 42. Transistor Q6 is used to sense the signal coming from the commutator and its output triggers Q7 and Q8. To cancel the noise Q7 and Q8 have been converted into a monostable action with a direct coupled input. The monostable action has the effect of keeping the output of Q7 and Q8 constant for τ seconds after the input signal from

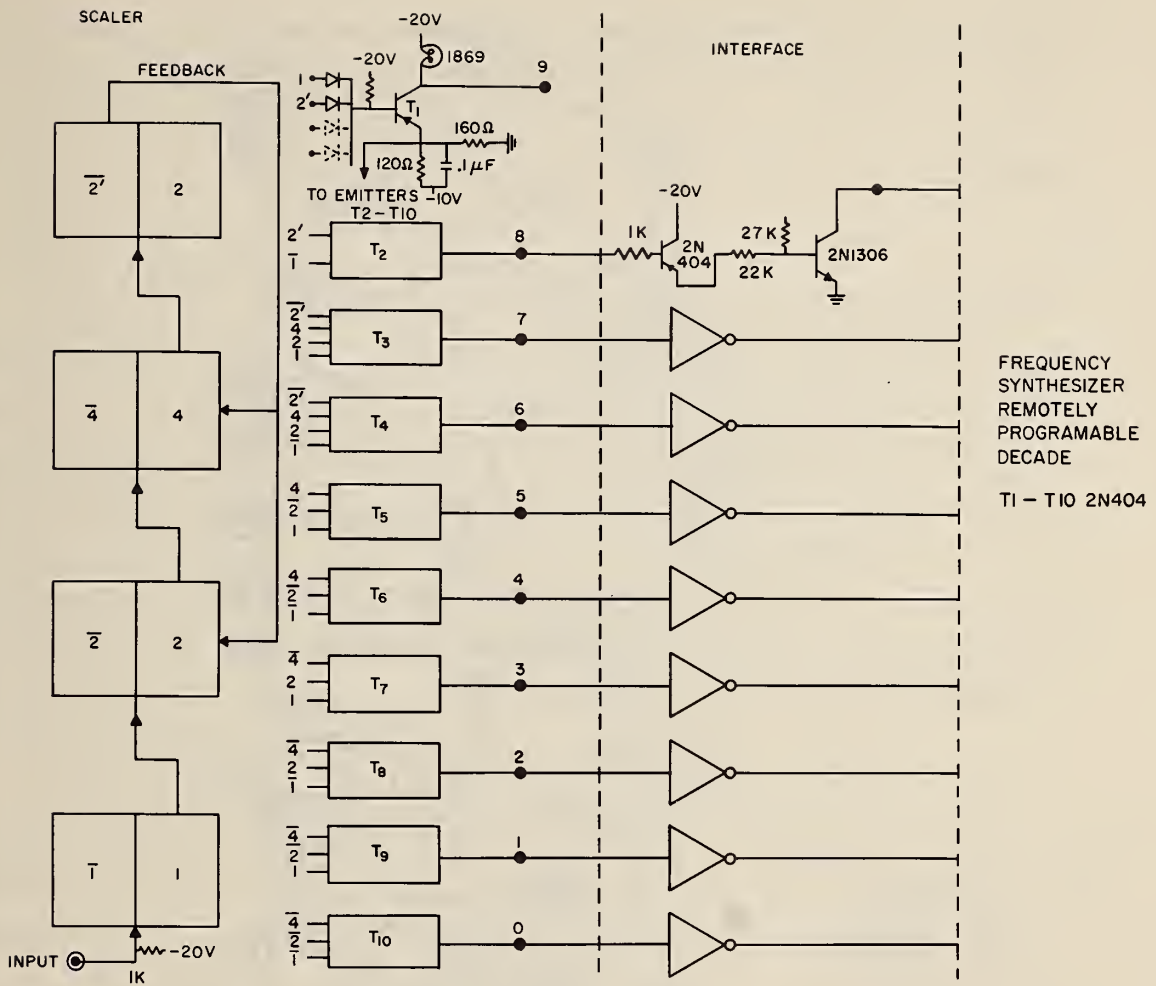
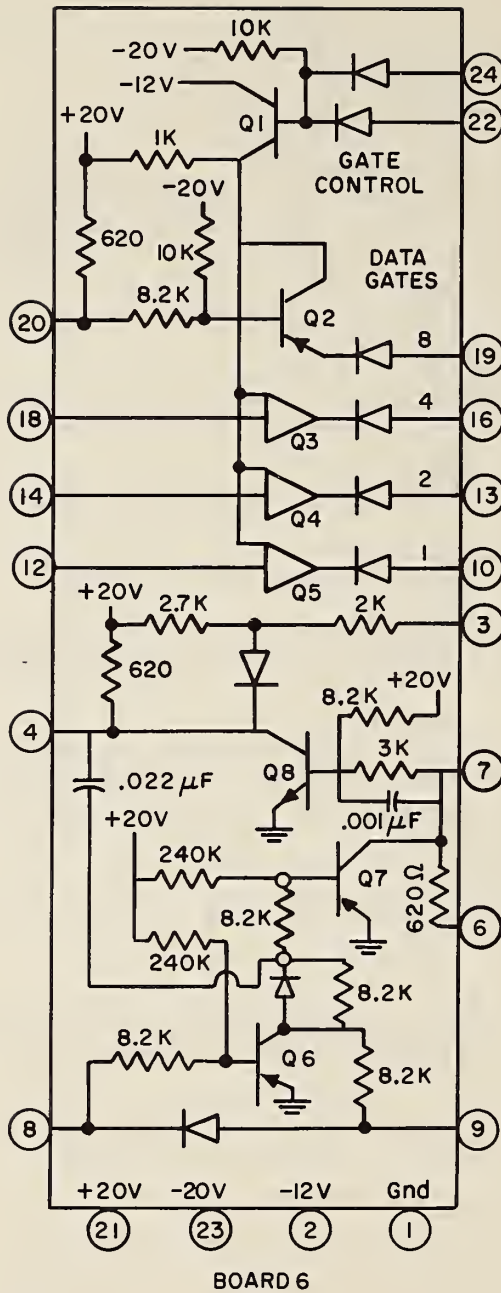


Figure 41. Logic diagram and schematic for interface of pulse height analyzer and frequency synthesizer



Q1 2N1384
 Q2-Q6 2N404
 Q7 2N1307
 Q8 2N1304
 ALL DIODES DR435

Figure 42. Board No. 6 of pulse height analyzer interface

Q6 changes state. Because the noise pulses have a duration of 1 millisecond, they are cancelled if τ is greater than one millisecond.

(F. C. Ruegg and R. W. Shideler)

E. Time of Year (TOY) System

1. Time of Year Clock

To provide time of year information to the interface-analyzer data readout system, a long term clock had to be obtained. Most of the clocks known to be available commercially which are capable of electronic readout with sufficient resolution had drawbacks. Decimal days were judged to be an inconvenient time form, and electronic scalers had a tendency to fail to change state in the digits that remained unchanged for long periods. Also, all of the clocks available are very expensive. A new design was made in order to overcome these deficiencies.

The design centers around an electromechanical digit counter having individual contacts for electrical readout and capable of very fast reset. Eight of these counters provide 999 days, 23 hours, and 59.9 minutes. A synchronous motor with a cam-operated switch provides impulses at six second (0.1 min) intervals driving the least significant digit (Figure 43). Each digit provides a "carry" after the nine, and relay logic performs the resets at 60 minutes and 24 hours. Provision is made to set the clock to any permitted state, and a warning light and circuit shut off the clock in the event of a power failure. Provisions were made in the clock to allow time manipulations as described below. An anticipated addition will increase the readout resolution to 0.01 minutes.

(R. W. Shideler)

2. Time of Year (TOY) Clock Controller

Complete timing information for a given spectrum is only obtained if one knows the start time, the stop time, and the

live time of the analyzer during the run. It is therefore necessary to synchronize either the clock with the analyzer or vice versa. A control circuit (Figure 44) was designed which sets the clock ahead 0.1 minute when the analyzer is manually set to "store" and prints this time only while holding the analyzer from storing. When the time pulse corresponding to the clock reading occurs, the analyzer is started synchronously while the clock resumes normal timing. At the end of the store cycle the analyzer automatically starts the readout cycle. The clock is stopped and held until the time has been read out and then restarted catching up by one time pulse if necessary. The logic for these operations is performed by a system of relays which is contained in the clock chassis.

(R. W. Shideler and F. C. Ruegg)

F. Maintenance of Teletypes and Paper Tape Punches

The Teletype (Model 33-C-ASR) is used as an input-output device for our digital multichannel pulse-height analyzers and also for the purpose of providing a data link with a computer.

A system of preventive maintenance was established which, through a scheduled examination of the equipment, will provide an opportunity to detect defective parts and thereby minimize on-line failures. While the machines are being examined, dust and dirt are removed, and new lubricant is applied.

It was observed that many of the failures which developed were caused by the improper replacement of paper tape, which resulted in jamming of the punch mechanism.

One other frequent problem is the rapid accumulation of dirt on the "dash pot" plunger, which causes the carriage to stick. The frequency of occurrence of this problem can be reduced considerably by frequent cleaning of the plunger.

Other failures were of a nonrecurrent nature, which does not reflect adversely on the equipment reliability.

The Teletype High Speed Tape Punch Set (BRPE) produces a punched tape at a high rate of speed, and its mechanical adjustments were found to be quite critical. The problem which developed was the need to accurately adjust the tension of the punch solenoid spring. This problem was overcome by the purchase of a very delicate gram scale enabling a precise adjustment of the tension. The only recurrent problem was the punch block becoming jammed due to improper replacement of new tape.

Since there are twelve Model 33 Teletypes and two High Speed Punches (BRPE) a substantial supply of parts have been ordered and stocked, so that the amount of equipment down time could be reduced.

(M. E. Stalbird)

G. Interface Between Mass Spectrometer and Small Electronic Computer

Design and fabrication of a system which causes a small electronic computer to control a mass spectrometer has been completed for the Mass Spectrometry Section. The system which is described in the progress report of that section is now operable.

(R. W. Shideler)

5. PERSONNEL AND ACTIVITIES*

A. Personnel Listing

Radiochemical Analysis Section

J. R. DeVoe, Section Chief (1)
L. A. Currie, Assistant Section Chief (1)
M. K. Oland, Secretary (1)

Instrumentation

F. C. Ruegg (1) Project Leader
M. E. Stalbird (1)
F. A. Lundgren (1/2)
R. W. Shideler (1) Project Leader

Mossbauer Spectrometry

J. J. Spijkerman (1) Project Leader
J. C. Travis (5/6)
P. A. Pella (3/4) One year leave of absence
K. R. Swanson (5/12) Bethlehem Steel Corporation,
(NBS Research Associate Industrial Cooperation
Program)
W. L. O'Neal (1)
L. J. Romanowski (1/4)

Nuclear Chemistry

L. A. Currie (1) Project Leader
G. Tassej (1/4)
M. C. Scheid (1/4) Summer Student
J. L. Burton (1/4) Summer Student

B. Publications

J. R. DeVoe and J. J. Spijkerman - "Mössbauer Spectrometry", Anal. Chem. 40, 472-489 (1968).

S. S. Nargolwalla, M. Crambes and J. R. DeVoe - "Techniques for Evaluation of Systematic Errors in the Activation Analysis for Oxygen With 14 MeV Neutrons, Anal. Chem. 40, 666-671 (1968).

L. A. Currie - "Limits for Qualitative Detection and Quantitative Determination; Application to Radiochemistry", Anal. Chem. 40, 586-593 (1968).

P. A. Pella, A. R. Landgrebe, J. R. DeVoe and W. C. Purdy - "Differential Controlled-Potential Coulometry Utilizing Substoichiometric Radioisotope Dilution", Anal. Chem. 39, 1781 (1967).

*Number in parenthesis indicates fraction of year on roster.

L. May and D. K. Snediker - "Criteria for Selection of Absorber Mounting Materials in Mössbauer Spectroscopy", Nuc. Instr. and Methods 55, 183-188 (1967).

A. R. Landgrebe, L. T. McClendon, J. R. DeVoe, P. A. Pella, and W. C. Purdy - "The Application of Substoichiometric Radioisotopic Dilution Principles to Controlled-Potential Coulometry and Solvent Extraction", Anal. Chim. Acta 39, 151-159 (1967).

F. C. Ruegg - "Multiplex for Dual-Spectrum Mössbauer Spectrometry", Proc. Second Symposium on Low Energy X- and Gamma Sources and Applications, Austin, Texas, 157-174 (1967).

M. G. Hollstein and J. R. DeVoe - "Determination of Medium Weight Elements by Gamma-Excited X-Ray Fluorescence", Proc. Second Symposium on Low Energy X- and Gamma Sources and Applications, Austin, Texas, U.S. Atomic Energy Comm. ORNL 11C-10, Vol. 1, 583-602 (1967).

J. J. Spijkerman - "Applications of Mössbauer Spectroscopy to Structure Analysis", Proc. Second Symposium on Low Energy X- and Gamma Sources and Applications, Austin, Texas, U.S. Atomic Energy Comm. ORNL 11C-10, Vol. 1, 85-100 (1967).

J. J. Spijkerman, D. K. Snediker, F. C. Ruegg and J. R. DeVoe - "Mössbauer Spectroscopy Standard for the Chemical Shift of Iron Compounds", NBS Misc. Publ. 260-13, July 1967.

C. I. Wynter, P. Hambright, C. H. Cheek and J. J. Spijkerman - "Mössbauer Spectroscopy of Some Iron Porphyrins", Nature 216, 105 (1967).

J. C. Love, G. Dzjzek, J. J. Spijkerman and D. K. Snediker - U.S. Atomic Energy Commission Report No. ORNL-P-3251 (1967).

R. R. Ruch and J. R. DeVoe - "Radiochemical Separations of Copper by Amalgam Exchange", Anal. Chem. 39, 1333-35 (1967).

G. W. Smith, D. A. Becker, G. J. Lutz, L. A. Currie and J. R. DeVoe - "Determination of Trace Elements in Standard Reference Materials by Neutron Activation Analysis", Anal. Chim. Acta 38, 333-340 (1967).

C. List of Talks

J. R. DeVoe - "The Future of Mössbauer Spectrometry in Chemistry" - Louisiana State University, New Orleans, May 1968.

J. R. DeVoe - "Modern Trends in Activation Analysis", Local Chapter of American Chemical Society, Louisiana State University, New Orleans, Louisiana, May 1968.

J. J. Spijkerman - "Aspects of Laboratory and Commercial Instrumentation; Mössbauer Spectra of Exotic Nuclei", a panel discussion Central Regional Meeting, American Chemical Society, May 1968.

J. J. Spijkerman - "The NBS Standard Reference Materials for the Chemical Shift of Iron and Tin Compounds", ASTM Committee Meeting, Chicago, Illinois, May 1968.

L. A. Currie - "Peak Height Method for Evaluating Nuclear Spectra", National ACS Meeting, San Francisco, California, April 1968.

L. A. Currie - Chairman of General Sessions on "Hot Atom and Radiation Chemistry" and "Activation Analysis", Division of Nuclear Chemistry and Technology, 155th National Meeting of the American Chemical Society, April 1968.

J. R. DeVoe - "Fluorine Analysis with 14 MeV Neutrons", National ACS Meeting, San Francisco, California, April 1968.

J. C. Travis - "The Mössbauer Effect in Nickel", Symposium, Mössbauer Effect Methodology, Chicago, Illinois, January 1968.

J. J. Spijkerman - "Mössbauer Spectroscopy of ^{61}Ni ", The Faraday Society, London, England, December 1967.

J. J. Spijkerman - "Spin Relaxation in ^{57}Fe Mössbauer Spectroscopy", Oxford University, Oxford, England, December 1967.

J. R. DeVoe - "Standard Reference Materials for Trace Analysis of Biological Materials", Bio-Assay Conference, Oak Ridge, Tennessee, November 1967.

F. A. Lundgren - "Non-reactor Methods of Activation Analysis", Conference Analytical Chemistry in Nuclear Technology, Gatlinburg, Tennessee, October 1967.

J. J. Spijkerman - "The NBS Standard Reference Materials for Chemical Shift", ASTM Committee Meeting, Boston, Massachusetts, 1967.

L. A. Currie - "High Accuracy Calibration and Control in Single-Channel Gamma Spectrometry", Pacific Conference on Chemistry and Spectroscopy sponsored by the Society of Applied Spectroscopy, Anaheim, California, October 1967.

L. A. Currie - "Criteria for Reporting Trace Amounts of Radioactivity", 11th Conference on Analytical Chemistry in Nuclear Technology sponsored by Oak Ridge National Laboratory, Gatlinburg, Tennessee, October 1967.

6. ACKNOWLEDGMENTS

We wish to express our thanks to Dr. C. O. Muehlhause and his staff for their cooperation in making arrangements for our use of the facilities in the NBS Reactor Building. Further, the assistance of Dr. J. E. Leiss and staff of the Radiation Physics Division for arrangements to use the LINAC facilities is greatly appreciated. Use of the mass spectrometer of the Photonuclear Physics Section and the assistance of H. M. Gerstenberg are gratefully acknowledged. Cooperation with R. B. Schwartz of the Radiation Physics Division in assisting with the 45° room irradiations is gratefully acknowledged.

The assistance of Mr. J. D. Waggoner and Mrs. Gloria Holmes for their part in modifying various parts of our computer programs is greatly appreciated.

We wish to thank the Statistical Engineering Laboratory and in particular, Dr. Brian Joiner, who has provided excellent consultation and who set up the OMNITAB routine for resolving Mössbauer spectra.

Special appreciation is expressed to Mrs. M. Oland who has assumed the almost overwhelming burden of section secretary and in spite of it all still managed to type this entire report.

7. REFERENCES

1. DeVoe, J. R., editor, NBS Technical Note 428 (1967).
2. DeVoe, J. R., editor, NBS Technical Note 421 (1967).
3. Extended abstract of a paper presented at the 11th Conference on Analytical Chemistry in Nuclear Technology, Gatlinburg, Tennessee, October 1967.
4. Currie, L. A., Anal. Chem. 40, 586 (1968).
5. Extended abstract of a paper presented at The Pacific Conference on Chemistry and Spectroscopy, Anaheim, California, October 1967.
6. Extended abstract of a paper presented at the 155th National Meeting of the American Chemical Society, San Francisco, California, April 1968.
7. Natrella, M. G., "Experimental Statistics", National Bureau of Standards Handbook No. 91, U.S. Gov't. Printing Office (1959).
8. Muir, A. H., Jr., Aido, K. S., Coogan, H. M., "Mössbauer Effect Data Index (1958-1965)", Interscience, New York, 1966.
9. Muller, James G. and Hang Nam, O. K., "Mössbauer Effect Methodology", Vol. 4, Plenum Press, New York, N. Y., (to be published).
10. Hershkowitz, N. and Walker, J. C., Phys. Rev. 156, 391 (1967).
11. Stevens, K. W. H., Proc. Phys. Soc. A65, 209 (1952).
12. Griffith, J. S., "The Theory of Transition-Metal Ions", (Cambridge University Press, Cambridge, England, 1961).
13. Locher, P. R., and Geschwind, S., Phys. Rev. Letters 11, 333 (1963).
14. Collins, R. L., and Travis, J. C., "Mössbauer Effect Methodology", Vol. 3, Plenum Press, N. Y., 1967, pp. 123-162.
15. Travis, J. C., and Spijkerman, J. J., "Mössbauer Effect Methodology", Vol. 4, Plenum Press, New York (to be published).

16. Draper, N. R., and Smith, H., "Applied Regression Analysis", John Wiley, New York, N.Y. (1966).
17. Herber, R. H., and Spijkerman, J. J., J. Chem. Phys. 42, 4312 (1965).
18. Snediker, D. K., "Mössbauer Effect Methodology", Vol. 2, Plenum Press, New York, 1966, pp. 161-170.
19. Ruegg, F. C., Spijkerman, J. J., and DeVoe, J. R., Rev. Sci. Instr. 36, 356 (1965).
20. May, L., and Snediker, D. K., Nucl. Instr. Methods 55, 183 (1967).
21. Kolthoff, I. M., and Sandell, E. B., "Textbook of Quantitative Inorganic Analysis", The Macmillan Company, New York, N. Y., 3rd ed., 1952, p. 318.
22. DeVoe, J. R., editor, NBS Technical Note 404 (1966), p. 108-115.
23. Marguelies, S., and Ehrman, J. R., Nucl. Instr. Methods 12, 131 (1961).
24. Abramowitz, M. and Stegun, I. A., eds., "Handbook of Mathematical Functions", AMS 55, U.S. Gov't. Printing Office, Washington, D.C., 1966, p. 378.

| | | | | | | | | | |
|-------|-------|-------|-------|-------|-------|-------|-------|-------|-------|
| 05434 | 05188 | 04548 | 04998 | 04183 | 04965 | 04691 | 05417 | 05619 | 04386 |
| 04881 | 04665 | 04961 | 02864 | 05594 | 04856 | 04973 | 05118 | 05856 | 04420 |
| 04704 | 04736 | 05283 | 04368 | 05965 | 05241 | 04833 | 05400 | 05166 | 04813 |
| 05091 | 04836 | 04537 | 04097 | 04352 | 05407 | 03702 | 04635 | 04851 | 04306 |
| 03747 | 03825 | 02859 | 03823 | 04625 | 03661 | 03903 | 02072 | 04157 | 03511 |
| 02682 | 02844 | 02828 | 02391 | 02048 | 02176 | 01989 | 02236 | 01006 | 02114 |
| 01841 | 01347 | 01930 | 02312 | 01802 | 02848 | 03511 | 04009 | 03163 | 04602 |
| 04933 | 03788 | 03958 | 03501 | 03642 | 05195 | 04373 | 05271 | 04501 | 04621 |
| 04864 | 04729 | 03954 | 05478 | 04832 | 03775 | 04159 | 05582 | 03649 | 04510 |
| 04447 | 05606 | 04901 | 05854 | 04950 | 04369 | 04372 | 05084 | 04638 | 03984 |
| 05241 | 05145 | 05705 | 03893 | 05533 | 04910 | 04609 | 04549 | 04252 | 04021 |
| 04469 | 05057 | 04670 | 05259 | 04146 | 05257 | 04415 | 04310 | 05262 | 04311 |
| 04089 | 04739 | 04698 | 04424 | 05304 | 05516 | 05304 | 04707 | 06454 | 04985 |
| 05031 | 05357 | 04845 | 05360 | 04732 | 06107 | 04831 | 04258 | 05350 | 05131 |
| 04301 | 04918 | 05244 | 04294 | 05518 | 04516 | | | | |

```

PLOT          5      VS      2
ADD          0.0    1.0    7
DEFINE      1.E20      1,4
10/ MULT      *1,1*  G(J)  BY  *6,4*  GAMMA INTO 8
11/ INCREM    10      *1,0*  *0,0*      0
12/ ADD      *7,4*  DELTA  TO 8  IN 8
13/ SUB       2      8      8
14/ DIV       8      *8,4*  8      (P(J)-X)/H
15/ MULT      8      8      9      T(J)
16/ ADD      1.0    9      10
17/ DIV      1.0    10     10
18/ MULT     10     10     11
19/ MULT      8     11     2.0    12      PARTIAL (DELTA)
20/ MULT      *1,1*  G(J)  BY  2.0    20
21/ INCREM   20     *1,0*  0.0    0
22/ MULT     20     8      11     13      PARTIAL (GAMMA)
23/ DIV      9      *8,4*  20
24/ MULT     20     -2.0    11     14
25/ SUB      11     15     15
30/ ERASE    12     13     14     15
31/ EXECUTE  10     25     3
32/ RESTORE  10     *1,1*  *6,4*  8
33/ RESTORE  20     *1,1*  2.0    20
34/ MULT     15     *5,4  16
35/ MULT     14     *5,4*  14
36/ MULT     13     *5,4*  13
36.5/ DIV   13     *8,4*  13
37/ MULT     12     *5,4*  12
37.5/ DIV   12     *8,4*  12
40/ SUB      *2,4*  5      6
41/ MULT      *3,4*  2     -1.0  6
42/ MULT      *4,4*  3     -1.0  6
43/ SUB      16     6      17
44/ PLOT     16     6      VS      2

```

```

45/ PLOT      17      VS      2
60/ SFIT     17      7      7      2      3      15      13      12      14      18      19
61/ MTRANS   1,4     20,1     200,1
62/ ABRIDGE  A      200      1 **** 8
63/ DEFINE   0.0     1,4
64/ ADD      18      4      4
65/ MTRANS   1,4     20,1     199,1
66/ ABRIDGE  A      199      1 **** 8
79/ MULT     *199,1*  1.00002  20
80/ IFGT     IF *1,20* IS GREATER THAN *200,1* STOP
    
```

```

EXECUTE      30      80      5      TIMES
    
```

```

60/ FIT      17      7      7      2      3      15      13      12      14      18      19
EXECUTE      30      80      1
    
```

```

FIXED      1
PRINT      2      6      16      17      5
PUNCH      2      6      16      17
SUB        19      17      20
FIT        20      7      7      2      3      15      13      12      14      18      19
STOP
    
```


NBS TECHNICAL PUBLICATIONS

PERIODICALS

JOURNAL OF RESEARCH reports National Bureau of Standards research and development in physics, mathematics, chemistry, and engineering. Comprehensive scientific papers give complete details of the work, including laboratory data, experimental procedures, and theoretical and mathematical analyses. Illustrated with photographs, drawings, and charts.

Published in three sections, available separately:

● Physics and Chemistry

Papers of interest primarily to scientists working in these fields. This section covers a broad range of physical and chemical research, with major emphasis on standards of physical measurement, fundamental constants, and properties of matter. Issued six times a year. Annual subscription: Domestic, \$6.00; foreign, \$7.25*.

● Mathematical Sciences

Studies and compilations designed mainly for the mathematician and theoretical physicist. Topics in mathematical statistics, theory of experiment design, numerical analysis, theoretical physics and chemistry, logical design and programming of computers and computer systems. Short numerical tables. Issued quarterly. Annual subscription: Domestic, \$2.25; foreign, \$2.75*.

● Engineering and Instrumentation

Reporting results of interest chiefly to the engineer and the applied scientist. This section includes many of the new developments in instrumentation resulting from the Bureau's work in physical measurement, data processing, and development of test methods. It will also cover some of the work in acoustics, applied mechanics, building research, and cryogenic engineering. Issued quarterly. Annual subscription: Domestic, \$2.75; foreign, \$3.50*.

TECHNICAL NEWS BULLETIN

The best single source of information concerning the Bureau's research, developmental, cooperative and publication activities, this monthly publication is designed for the industry-oriented individual whose daily work involves intimate contact with science and technology—for engineers, chemists, physicists, research managers, product-development managers, and company executives. Annual subscription: Domestic, \$3.00; foreign, \$4.00*.

*Difference in price is due to extra cost of foreign mailing.

Order NBS publications from:

Superintendent of Documents
Government Printing Office
Washington, D.C. 20402

NONPERIODICALS

Applied Mathematics Series. Mathematical tables, manuals, and studies.

Building Science Series. Research results, test methods, and performance criteria of building materials, components, systems, and structures.

Handbooks. Recommended codes of engineering and industrial practice (including safety codes) developed in cooperation with interested industries, professional organizations, and regulatory bodies.

Special Publications. Proceedings of NBS conferences, bibliographies, annual reports, wall charts, pamphlets, etc.

Monographs. Major contributions to the technical literature on various subjects related to the Bureau's scientific and technical activities.

National Standard Reference Data Series. NSRDS provides quantitative data on the physical and chemical properties of materials, compiled from the world's literature and critically evaluated.

Product Standards. Provide requirements for sizes, types, quality and methods for testing various industrial products. These standards are developed cooperatively with interested Government and industry groups and provide the basis for common understanding of product characteristics for both buyers and sellers. Their use is voluntary.

Technical Notes. This series consists of communications and reports (covering both other agency and NBS-sponsored work) of limited or transitory interest.

Federal Information Processing Standards Publications. This series is the official publication within the Federal Government for information on standards adopted and promulgated under the Public Law 89-306, and Bureau of the Budget Circular A-86 entitled, Standardization of Data Elements and Codes in Data Systems.

CLEARINGHOUSE

The Clearinghouse for Federal Scientific and Technical Information, operated by NBS, supplies unclassified information related to Government-generated science and technology in defense, space, atomic energy, and other national programs. For further information on Clearinghouse services, write:

Clearinghouse
U.S. Department of Commerce
Springfield, Virginia 22151

U.S. DEPARTMENT OF COMMERCE
WASHINGTON, D.C. 20230

POSTAGE AND FEES PAID
U.S. DEPARTMENT OF COMMERCE

OFFICIAL BUSINESS
